# LOW-CALCIUM FLY ASH-BASED GEOPOLYMER CONCRETE: REINFORCED BEAMS AND COLUMNS

**By**

**M. D.J. Sumajouw and B. V. Rangan**

**Research Report GC 3**
**Faculty of Engineering**
**Curtin University of Technology**
**Perth, Australia**

**2006**

# PREFACE

From 2001, we have conducted some important research on the development, manufacture, behaviour, and applications of **Low-Calcium Fly Ash-Based Geopolymer Concrete**. This concrete uses no Portland cement; instead, we use the low-calcium fly ash from a local coal burning power station as a source material to make the binder necessary to manufacture concrete.

Concrete usage around the globe is second only to water. An important ingredient in the conventional concrete is the Portland cement. The production of one ton of cement emits approximately one ton of carbon dioxide to the atmosphere. Moreover, cement production is not only highly energy-intensive, next to steel and aluminium, but also consumes significant amount of natural resources. In order to meet infrastructure developments, the usage of concrete is on the increase. Do we build additional cement plants to meet this increase in demand for concrete, or find alternative binders to make concrete?

On the other hand, already huge volumes of fly ash are generated around the world; most of the fly ash is not effectively used, and a large part of it is disposed in landfills. As the need for power increases, the volume of fly ash would increase.

Both the above issues are addressed in our work. We have covered significant area in our work, and developed the know-how to manufacture low-calcium fly ash-based geopolymer concrete. Our research has already been published in more than 30 technical papers in various international venues.

This Research Report describes the behaviour and strength of reinforced low-calcium fly ash-based geopolymer concrete structural beams and columns. Earlier, Research Reports GC1 and GC2 covered the development, the mixture proportions, the short-term properties, and the long-term properties of low-calcium fly ash-based geopolymer concrete.

Heat-cured low-calcium fly ash-based geopolymer concrete has excellent compressive strength, suffers very little drying shrinkage and low creep, excellent resistance to sulfate attack, and good acid resistance. It can be used in many infrastructure applications. One ton of low-calcium fly ash can be utilised to produce about 2.5 cubic metres of high quality geopolymer concrete, and the bulk price of chemicals needed to manufacture this concrete is cheaper than the bulk price of one ton of Portland cement. Given the fact that fly ash is considered as a waste material, the low-calcium fly ash-based geopolymer concrete is, therefore, cheaper than the Portland cement concrete. The special properties of geopolymer concrete can further enhance the economic benefits. Moreover, reduction of one ton of carbon dioxide yields one carbon credit and, the monetary value of that one credit is approximately 20 Euros. This carbon credit significantly adds to the economy offered by the geopolymer concrete. In all, there is so much to be gained by using geopolymer concrete.

We are happy to participate and assist the industries to take the geopolymer concrete technology to the communities in infrastructure applications. We passionately believe that our work is a small step towards a broad vision to serve the communities for a better future.

For further information, please contact: Professor B. Vijaya Rangan BE PhD FIE Aust FACI CPEng, Emeritus Professor of Civil Engineering, Faculty of Engineering, Curtin University of Technology, Perth, WA 6845, Australia; Telephone: 61 8 9266 1376, Email: V.Rangan@curtin.edu.au

# ACKNOWLEDGEMENTS

The authors are grateful to Emeritus Professor Joseph Davidovits, Director, Geopolymer Institute, Saint-Quentin, France, and to Dr Terry Gourley, Rocla Australia for their advice and encouragement during the conduct of the research.

The first author was financially supported by the Technological and Professional Skills Development Sector Project (TPSDP) of the University of Sam Ratulangi, Indonesia. The authors are grateful to Mr Djwantoro Hardjito and Mr. Steenie Wallah, the other members of the research team, for their contributions.

The experimental work was carried out in the laboratories of the Faculty of Engineering at Curtin University of Technology. The authors are grateful to the support and assistance provided by the team of talented and dedicated technical staff comprising Mr. Roy Lewis, Mr. John Murray, Mr. Dave Edwards, Mr. Rob Cutter, and Mr. Mike Ellis.

# TABLE OF CONTENTS

# CHAPTER 1

# INTRODUCTION

This Chapter describes the background, research objectives and scope of work. An overview of the Report arrangement is also presented.

## 1.1 Background

Portland cement concrete is a mixture of Portland cement, aggregates, and water. Concrete is the most often-used construction material. The worldwide consumption of concrete was estimated to be about 8.8 billion tons per year (Metha 2001). Due to increase in infrastructure developments, the demand for concrete would increase in the future.

The manufacture of Portland cement releases carbon dioxide ($CO_2$) that is a significant contributor of the greenhouse gas emissions to the atmosphere. The production of every tonne of Portland cement contributes about one tonne of $CO_2$. Globally, the world's Portland cement production contributes about 1.6 billion tons of $CO_2$ or about 7% of the global loading of carbon dioxide into the atmosphere (Metha 2001, Malhotra 1999; 2002). By the year 2010, the world cement consumption rate is expected to reach about 2 billion tonnes, meaning that about 2 billion tons $CO_2$ will be released. In order to address the environmental effect associated with Portland cement, there is a need to use other binders to make concrete.

One of the efforts to produce more environmentally friendly concrete is to replace the amount of Portland cement in concrete with by-product materials such as fly ash. An important achievement in this regard is the development of high volume fly ash (HVFA) concrete that utilizes up to 60 percent of fly ash, and yet possesses excellent mechanical properties with enhanced durability performance. The test results show that HVFA concrete is more durable than Portland cement concrete (Malhotra 2002).

Another effort to make environmentally friendly concrete is the development of inorganic alumina-silicate polymer, called Geopolymer, synthesized from materials of geological origin or by-product materials such as fly ash that are rich in silicon and aluminium (Davidovits 1994, 1999).

Fly ash, one of the source materials for geopolymer binders, is available abundantly world wide, but to date its utilization is limited. From 1998 estimation, the global coal ash production was more than 390 million tons annually, but its utilization was less than 15% (Malhotra 1999). In the USA, the annual production of fly ash is approximately 63 million tons, and only 18 to 20% of that total is used by the concrete industries (ACI 232.2R-03 2003).

In the future, fly ash production will increase, especially in countries such as China and India. Just from these two countries, it is estimated that by the year 2010 the production of the fly ash will be about 780 million tones annually (Malhotra 2002). Accordingly, efforts to utilize this by-product material in concrete manufacture are important to make concrete more environmentally friendly. For instance, every million tons of fly ash that replaces Portland cement helps to conserve one million tons of lime stone, 0.25 million tons of coal and over 80 million units of power, not withstanding the abatement of 1.5 million tons of CO2 to atmosphere (Bhanumathidas and Kalidas 2004).

In the light of the above, a comprehensive research program was commenced in 2001 on **Low-Calcium Fly Ash-Based Geopolymer Concrete**. Earlier Research Reports GC1 and GC2 described the development and manufacture, short-term properties, and long-term properties of geopolymer concrete (Hardjito and Rangan 2005, Wallah and Rangan 2006). It was found that heat-cured low-calcium fly ash-based geopolymer concrete possesses high compressive strength, undergoes very little drying shrinkage and moderately low creep, and shows excellent resistance to sulphate and acid attack. Other researchers have reported that geopolymers do not suffer from alkali-aggregate reaction (Davidovits, 1999), and possess excellent fire resistant (Cheng and Chiu, 2003).

The work described in this Report compliments the research reported in Research Reports GC1 and GC2, and demonstrates the application of heat-cured low-calcium fly ash-based geopolymer concrete in large-scale reinforced concrete beams and columns.

## 1.2 Research Objectives

The primary objectives of this research are to conduct experimental and analytical studies to establish the following:

a) The flexural behaviour of reinforced geopolymer concrete beams including flexural strength, crack pattern, deflection, and ductility.

b) The behaviour and strength of reinforced geopolymer concrete slender columns subjected to axial load and bending moment.

c) The correlation of experimental results with prediction methods currently used for reinforced Portland cement concrete structural members.

## 1.3 Scope of Work

The scope of work involved the following:

a) Based on the research described in Research Reports GC1 and GC2 (Hardjito and Rangan 2005, Wallah and Rangan 2006), select appropriate geopolymer concrete mixtures needed to fabricate the reinforced test beams and columns.

b) Manufacture and test twelve simply supported reinforced geopolymer concrete rectangular beams under monotonically increasing load with the longitudinal tensile reinforcement ratio and the concrete compressive strength as test variables.

c) Manufacture and test twelve reinforced geopolymer concrete square columns under short-term eccentric loading with the longitudinal reinforcement ratio, the load eccentricity and the concrete compressive strength as test variables.

d) Perform calculations to predict the strength and the deflection of geopolymer concrete test beams and columns using the methods currently available for Portland cement concrete members.

e) Study the correlation of test and calculated results, and demonstrate the application of heat-cured low-calcium fly ash-based geopolymer concrete in reinforced concrete beams and columns.

## 1.4 Report Arrangement

The Report comprises six Chapters. Chapter 2 presents a brief review of literature on geopolymers. The manufacture of test specimens and the conduct of tests are described in Chapter 3. Chapter 4 presents and discusses the test results. The correlations of analytical results with the test results are given in Chapter 5. The conclusions of this work are given in Chapter 6. The Report ends with a list of References and Appendices containing the details of experimental data.

# CHAPTER 2

# LITERATURE REVIEW

## 2.1 Introduction

This Chapter presents a brief review of geopolymers and geopolymer concrete. This review compliments similar reviews given in Research Reports GC1 and GC2 (Hardjito and Rangan 2005, Wallah and Rangan 2006).

## 2.2 Geopolymer Materials

Davidovits (1988) introduced the term 'geopolymer' in 1978 to represent the mineral polymers resulting from geochemistry. Geopolymer, an inorganic alumina-silicate polymer, is synthesized from predominantly silicon (Si) and aluminium (Al) material of geological origin or by-product material. The chemical composition of geopolymer materials is similar to zeolite, but they reveal an amorphous microstructure (Davidovits 1999). During the synthesized process, silicon and aluminium atoms are combined to form the building blocks that are chemically and structurally comparable to those binding the natural rocks.

Most of the literature available on this material deals with geopolymer pastes. Davidovits and Sawyer (1985) used ground blast furnace slag to produce geopolymer binders. This type of binders patented in the USA under the title Early High-Strength Mineral Polymer was used as a supplementary cementing material in the production of precast concrete products. In addition, a ready-made mortar package that required only the addition of mixing water to produce a durable and very rapid strength-gaining material was produced and utilised in restoration of concrete airport runways, aprons and taxiways, highway and bridge decks, and for several new constructions when high early strength was needed.

Geopolymer has also been used to replace organic polymer as an adhesive in strengthening structural members. Geopolymers were found to be fire resistant and durable under UV light (Balaguru et al 1997)

van Jaarsveld, van Deventer, and Schwartzman (1999) carried out experiments on geopolymers using two types of fly ash. They found that the compressive strength after 14 days was in the range of 5 – 51 MPa. The factors affecting the compressive strength were the mixing process and the chemical composition of the fly ash. A higher CaO content decreased the microstructure porosity and, in turn, increased the compressive strength. Besides, the water-to-fly ash ratio also influenced the strength. It was found that as the water-to-fly ash ratio decreased the compressive strength of the binder increased.

Palomo, Grutzeck, and Blanco (1999) studied the influence of curing temperature, curing time and alkaline solution-to-fly ash ratio on the compressive strength. It was reported that both the curing temperature and the curing time influenced the compressive strength. The utilization of sodium hydroxide (NaOH) combined with sodium silicate ($Na_2Si_3$) solution produced the highest strength. Compressive strength up to 60 MPa was obtained when cured at 85$^{o}$C for 5 hours.

Xu and van Deventer (2000) investigated the geopolymerization of 15 natural Al-Si minerals. It was found that the minerals with a higher extent of dissolution demonstrated better compressive strength after polymerisation. The percentage of calcium oxide (CaO), potassium oxide ($K_2O$), the molar ratio of Si-Al in the source material, the type of alkali and the molar ratio of Si/Al in the solution during dissolution had significant effect on the compressive strength.

Swanepoel and Strydom (2002) conducted a study on geopolymers produced by mixing fly ash, kaolinite, sodium silica solution, NaOH and water. Both the curing time and the curing temperature affected the compressive strength, and the optimum strength occurred when specimens were cured at 60$^{o}$C for a period of 48 hours.

van Jaarsveld, van Deventer and Lukey (2002) studied the interrelationship of certain parameters that affected the properties of fly ash-based geopolymer. They reported that the properties of geopolymer were influenced by the incomplete dissolution of the materials involved in geopolymerization. The water content, curing time and curing temperature affected the properties of geopolymer; specifically the curing condition and calcining temperature influenced the compressive strength. When the samples were cured at 70$^{o}$C for 24 hours a substantial increase in the compressive

strength was observed. Curing for a longer period of time reduced the compressive strength.

## 2.3 Use of Fly Ash in Concrete

Fly ash has been used in the past to partially replace Portland cement to produce concretes. An important achievement in this regard is the development of high volume fly ash (HVFA) concrete that utilizes up to 60 percent of fly ash, and yet possesses excellent mechanical properties with enhanced durability performance. The test results show that HVFA concrete is more durable than Portland cement concrete (Malhotra 2002).

Recently, a research group at Montana State University in the USA has demonstrated through field trials of using 100% high-calcium (ASTM Class C) fly ash to replace Portland cement to make concrete. Ready mix concrete equipment was used to produce the fly ash concrete on a large scale. The field trials showed that the fresh concrete can be easily mixed, transported, discharge, placed, and finished (Cross et al 2005).

## 2.4 Fly Ash-Based Geopolymer Concrete

Past studies on reinforced fly ash-based geopolymer concrete members are extremely limited. Palomo et.al (2004) investigated the mechanical characteristics of fly ash-based geopolymer concrete. It was found that the characteristics of the material were mostly determined by curing methods especially the curing time and curing temperature. Their study also reported some limited number of tests carried out on reinforced geopolymer concrete sleeper specimens. Another study related to the application of geopolymer concrete to structural members was conducted by Brooke et al. al (2005). It was reported that the behaviour of geopolymer concrete beam-column joints was similar to that of members made of Portland cement concrete.

Curtin research on fly ash-based geopolymer concrete is described in Research Reports GC1 and GC2 (Hardjito and Rangan 2005, Wallah and Rangan 2006), and other publications listed in References at the end of this Report.

# CHAPTER 3

# SPECIMEN MANUFACTURE AND TEST PROGRAM

## 3.1 Introduction

This Chapter describes the manufacture of test specimens, and presents the detail of the test program. Twelve reinforced geopolymer concrete beams and twelve reinforced geopolymer concrete columns were manufactured and tested. The test parameters covered a range of values encountered in practice. The sizes of test specimens were selected to suit the capacity of test equipment available in the laboratory. The compressive strength of concrete and the tensile reinforcement ratio were the test parameters for beam specimens. In the case of column specimens, the compressive strength of concrete, the longitudinal reinforcement ratio, and the load eccentricity were the test parameters.

## 3.2 Beams

### 3.2.1 Materials in Geopolymer Concrete

#### *3.2.1.1 Fly Ash*

In this study, the low-calcium (ASTM Class F) dry fly ash obtained from Collie Power Station in Western Australia was used as the base material.

The chemical composition of the fly ash as determined by X-Ray Fluorescence (XRF) test is given in Table 3.1. The Department of Applied Chemistry, Curtin University of Technology, conducted the XRF test.

**Table 3.1 Chemical Composition of Fly Ash (mass %)**

| $SiO_2$ | $Al_2O_3$ | $Fe_2O_3$ | CaO | $Na_2O$ | $K_2O$ | $TiO_2$ | MgO | $P_2O_5$ | $SO_3$ | $H_2O$ | LOI*) |
|---|---|---|---|---|---|---|---|---|---|---|---|
| 48.0 | 29.0 | 12.7 | 1.76 | 0.39 | 0.55 | 1.67 | 0.89 | 1.69 | 0.5 | - | 1.61 |

*) *Loss on ignition*

The particle size distribution of the fly ash is given in Figure 3.1. In Fig 3.1, graph A shows the size distribution in percentage by volume, and graph B shows the size

distribution in percentage by volume cumulative (passing size). The CSIRO-Division of Minerals (Particle Analysis Services) in Perth, Western Australia, conducted the particle size analysis of the fly ash.

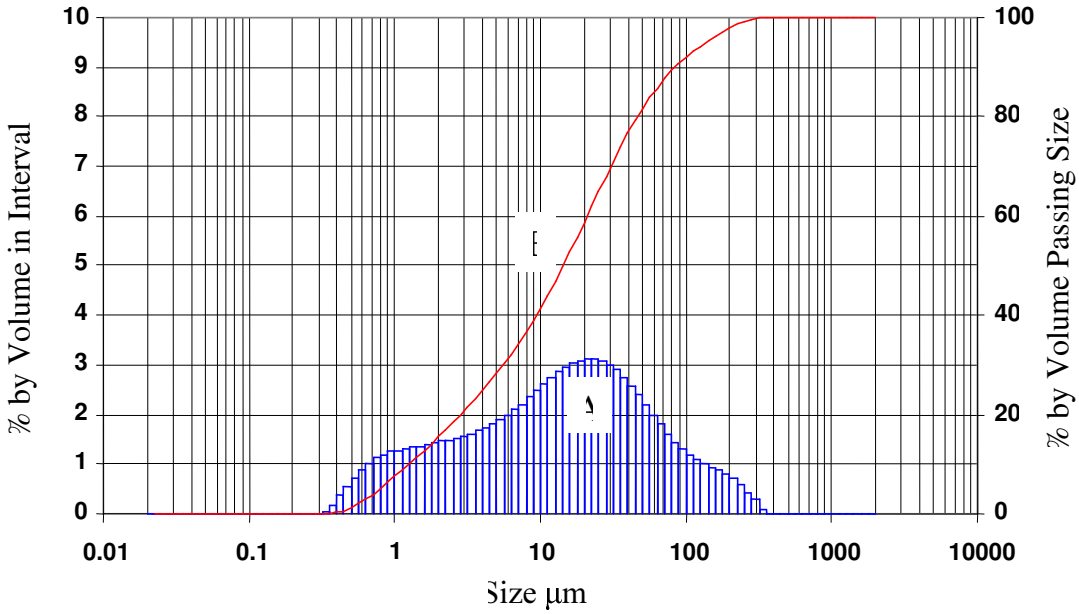


**Figure 3.1 Particle Size Distribution of Fly Ash**

### *3.2.1.2 Alkaline Solutions*

A combination of sodium silicate solution and sodium hydroxide solution was used to react with the aluminium and the silica in the fly ash.

The sodium silicate solution comprised $Na_2O$=14.7%, $SiO_2$=29.4%, and water=55.9% by mass; it was purchased in bulk from a local supplier. Sodium hydroxide (commercial grade with 97% purity) pellets, bought in bulk from a local supplier, were dissolved in water to make the solution. In the case of beams, the concentration of the sodium hydroxide solution was 14 Molars. In order to yield this concentration, one litre of the solution contained 14x40 = 560 grams of sodium hydroxide pellets. Laboratory measurements have shown that the solution comprised 40.4% sodium hydroxide pellets and 59.6% water by mass. The alkaline solutions were prepared and mixed together at least one day prior to use.

#### *3.2.1.3 Super Plasticiser*

To improve the workability of the fresh concrete, a sulphonated-naphthalene based super plasticiser supplied by MBT Australia was used.

#### *3.2.1.4 Aggregates*

Three types of locally available aggregates, i.e. 10mm aggregate, 7mm aggregate, and fine sand were used. All aggregates were in saturated surface dry (SSD) condition, and were prepared to meet the requirements given by the relevant Australian Standards AS 1141.5-2000 and AS 1141.6-2000.

The grading combination of the aggregates is in accordance with the British Standard BS 882:1992. The fineness modulus of the combined aggregates was 4.5. Table 3.2 shows the grading combination of the aggregates.

**Table 3.2 Grading Combination of Aggregates**

| Sieve Size | Aggregates | | | Combination[*)] | BS 882:1992 |
|---|---|---|---|---|---|
| | 10mm | 7mm | Fine sand | | |
| 14 | 100 | 100 | 100 | 100.00 | 100 |
| 10 | 74.86 | 99.9 | 100 | 92.42 | 95-100 |
| 5 | 9.32 | 20.1 | 100 | 44.83 | 30-65 |
| 2.36 | 3.68 | 3.66 | 100 | 37.39 | 20-50 |
| 1.18 | 2.08 | 2.05 | 99.99 | 36.34 | 15-40 |
| No. 600 | 1.47 | 1.52 | 79.58 | 28.83 | 10-30 |
| No. 300 | 1.01 | 1.08 | 16.53 | 6.47 | 5-15 |
| No. 150 | 0.55 | 0.62 | 1.11 | 0.77 | 0-18 |

*[*)] 30% (10 mm) + 35% (7 mm) + 35%( fine sand)*

### 3.2.2 Mixture Proportions of Geopolymer Concrete

The mixture proportions were developed based on the test results given in Research Report GC1 (Hardjito and Rangan 2005). Several trial mixtures were manufactured and tested in order to ensure consistency of results prior to casting of the beam specimens.

Three mixtures, designated as GBI, GBII, and GBIII, were selected to yield nominal compressive strengths of 40, 50, or 75 MPa respectively. The details of the mixtures

are given in Table 3.3. It can be seen that the only difference between the three mixtures is the mass of extra water added.

**Table 3.3 Mixture Proportions of Geopolymer Concrete for Beams**

| Material | Mass (kg/m$^3$) |
|---|---|
| 10mm aggregates | 550 |
| 7mm aggregates | 640 |
| Fine Sand | 640 |
| Fly ash | 404 |
| Sodium hydroxide solution | 41 (14M) |
| Sodium silicate solution | 102 |
| Super plasticizer | 6 |
| Extra water | 25.5 (GBI), 17.0 (GBII), 13.5(GBIII) |

### 3.2.3 Reinforcing Bars

Four different sizes of deformed steel bars (N-bars) were used as the longitudinal reinforcement. Samples of steel bars were tested in the laboratory. The results of these tests are given in Table 3.4.

**Table 3.4 Steel Reinforcement Properties**

| Diameter (mm) | Nominal area (mm$^2$) | Yield Strength (MPa) | Ultimate Strength (MPa) |
|---|---|---|---|
| 12 | 110 | 550 | 680 |
| 16 | 200 | 560 | 690 |
| 20 | 310 | 560 | 675 |
| 24 | 450 | 557 | 660 |

### 3.2.4 Geometry and Reinforcement Configuration

All beams were 200mm wide by 300mm deep in cross-section; they were 3300mm in length and simply-supported over a span of 3000mm. The beams were designed to fail in a flexural mode. Four different tensile reinforcement ratios were used. The clear cover to reinforcement was 25 mm on all faces. The geometry and

reinforcement details of beams are shown in Figure 3.2, and the specimen details are given in Table 3.5.

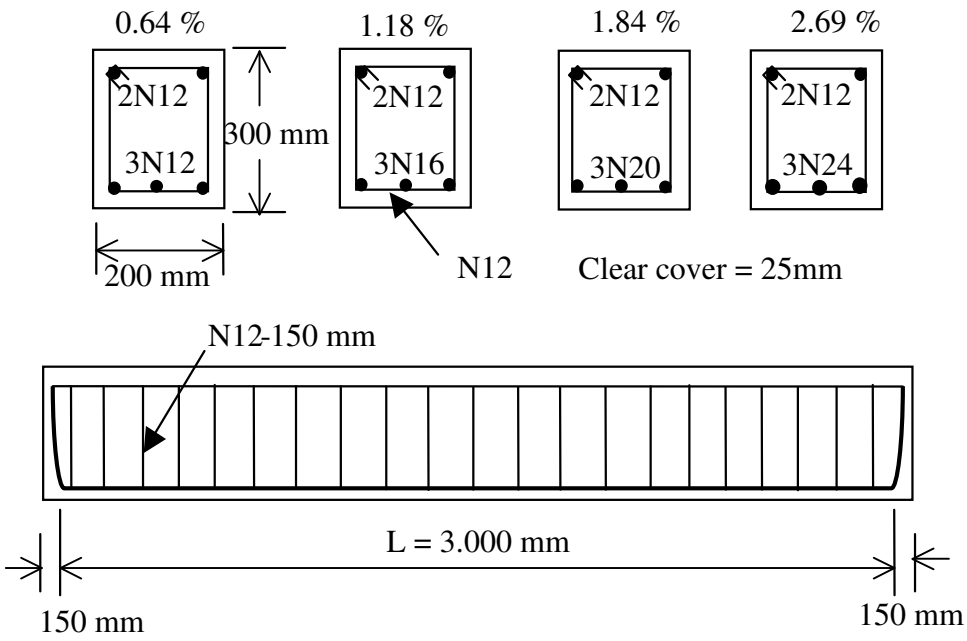


**Figure 3.2 Beam Geometry and Reinforcement Details**

**Table 3.5 Beam Details**

| Series | Beam | Beam Dimensions (mm) | Reinforcement | | Tensile Reinforcement ratio (%) |
|---|---|---|---|---|---|
| | | | **Compression** | **Tension** | |
| 1 | GBI-1 | 200x300x3300 | 2N12 | 3N12 | 0.64 |
| | GBI-2 | 200x300x3300 | 2N12 | 3N16 | 1.18 |
| | GBI-3 | 200x300x3300 | 2N12 | 3N20 | 1.84 |
| | GBI-4 | 200x300x3300 | 2N12 | 3N24 | 2.69 |
| 2 | GBII-1 | 200x300x3300 | 2N12 | 3N12 | 0.64 |
| | GBII-2 | 200x300x3300 | 2N12 | 3N16 | 1.18 |
| | GBII-3 | 200x300x3300 | 2N12 | 3N20 | 1.84 |
| | GBII-4 | 200x300x3300 | 2N12 | 3N24 | 2.69 |
| 3 | GBIII-1 | 200x300x3300 | 2N12 | 3N12 | 0.64 |
| | GBIII-2 | 200x300x3300 | 2N12 | 3N16 | 1.18 |
| | GBIII-3 | 200x300x3300 | 2N12 | 3N20 | 1.84 |
| | GBIII-4 | 200x300x3300 | 2N12 | 3N24 | 2.69 |

### 3.2.5 Specimen Manufacture and Curing Process

The coarse aggregates and the sand in saturated surface dry condition were first mixed in 80-litre capacity laboratory pan mixer with the fly ash for about three minutes. At the end of this mixing, the alkaline solutions together with the super plasticizer and the extra water were added to the dry materials and the mixing continued for another four minutes.

**Figure 3.3 Moulds with Reinforcement Cages**

Immediately after mixing, the fresh concrete was cast into the moulds. All beams were cast horizontally in wooden moulds in two layers. Each layer was compacted using a stick internal compacter. Due to the limited capacity of the laboratory mixer, six batches were needed to cast two beams. With each batch, a number of 100mm diameters by 200mm high cylinders were also cast. These cylinders were tested in compression on the same day as the beam tests. The slump of every batch of fresh concrete was also measured in order to observe the consistency of the mixtures. Figure 3.3 shows the moulds with reinforcement cages, and Figure 3.4 shows the compaction process.

**Figure 3.4 Beam Compaction**

After casting, all specimens were kept at room temperature for three days. It was found that postponing the curing for periods of time causes an increase in the compressive strength of concrete (Hardjito and Rangan, 2005). At the end of three days, the specimens were placed inside the steam-curing chamber (Figure 3.5), and cured at 60$^{o}$C for 24 hours.


**Figure 3.5 Curing Chamber**

To maintain the temperature inside the steam-curing chamber, the solenoid valve complete with digital temperature controller and thermocouple were attached to the boiler installation system (Figure 3.6). The digital controller automatically opened the solenoid valve to deliver the steam, and closed after desired temperature inside the chamber was reached. To avoid condensation over the concrete, a sheet of plastic was used to cover the concrete surface.

After curing, the beams and the cylinders were removed from the chamber and left to air-dry at room temperature for another 24 hours before demoulding. The test specimens (Figure 3.7) were then left in the laboratory ambient conditions until the day of testing. The laboratory temperature varied between 25$^{o}$ and 35$^{o}$C during that period.

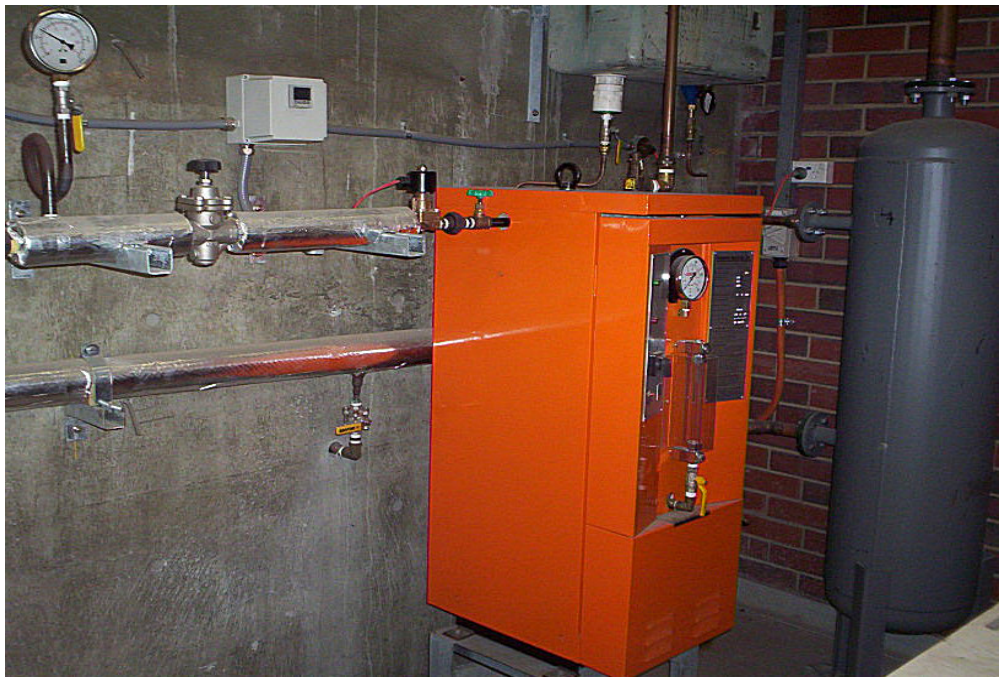

**Figure 3.6 Steam Boiler System**


**Figure 3.7 Beams after Demoulding**

### 3.2.6 Test Set-up and Instrumentation

All beams were simply supported over a span of 3000 mm and tested in a Universal test machine with a capacity of 2500 kN. Two concentrated loads placed symmetrically over the span loaded the beams. The distance between the loads was 1000 mm. The test configuration is shown in Figure 3.8 and Figure 3.9.

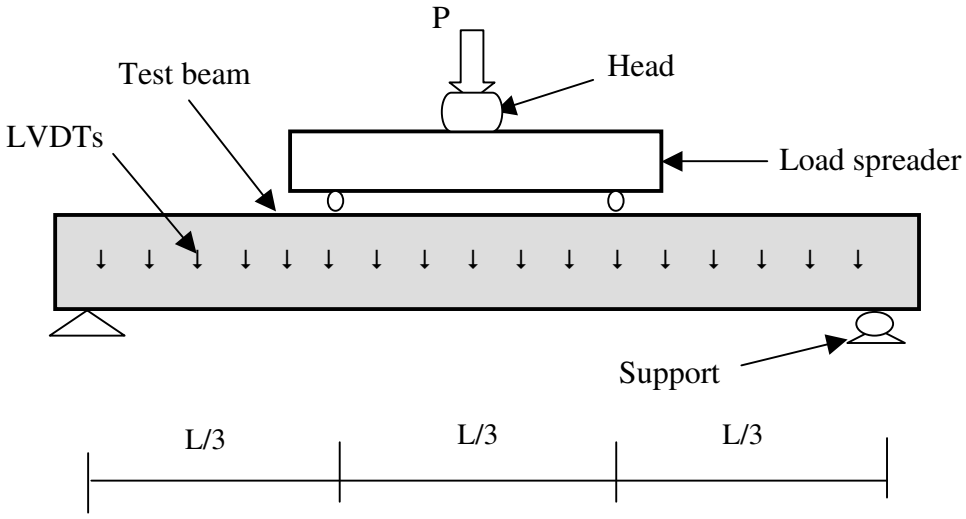


**Figure 3.8 Arrangement for Beam Tests**

Digital data acquisition unit was used to collect the data during the test. Linear Variable Data Transformers (LVDTs) were used to measure the deflections at selected locations along the span of the beam. All LVDTs were calibrated prior to tests. The relationship between output of the LVDTs in milli-volts (*mV*) and real movement in millimetres (*mm*) was determined to be linear.

The LVDTs were calibrated by using a milling machine. The LVDTs were attached to the milling machine, and a dial gauge measured their movement. The output of the LVDTs movement was expressed in *mV* and correlated to measured change of the dial gauge in *mm*. These data were used to transform the LVDTs reading from *mV* to *mm*.

### 3.2.7 Test Procedure

Prior to placing the specimens in the machine, the beam surfaces at the locations of supports and loads were smoothly ground to eliminate unevenness. All the specimens were white washed in order to facilitate marking of cracks.

The tests were conducted by maintaining the movement of test machine platen at a rate of 0.5mm/minute. The rate of data capture varied from 10 to 100 samples per second. Higher rate was used when the test beam was approaching the expected peak load to ensure that enough data were captured to trace the load-deflection curve near failure.

LVDTs were positioned at selected locations along the span of the beam to monitor the deflection. Prior to loading, the entire data acquisition system was checked and the initial readings were set to zero.

Both the ascending and descending (softening) parts of the load-deflections curve were recorded for each test beam. The measurement of softening part (after peak load) was continued until either the limit of LVDT travel at mid-span was reached or no further information was recorded by data logger due to the complete failure of the specimen.


**Figure 3.9 Beam Test Set-up**

### 3.2.8 Properties of Concrete

Samples of fresh concrete were collected from each batch to conduct the slump test (Figure 3.10) and to cast 100mmx200mm cylinders for compressive strength test. The data from the slump tests indicated that the different batches of concrete from each mixture were consistent. The average slump values for each series are presented on Table 3.6.

**Figure 3.10 Slump Test of Fresh Concrete**

All test cylinders were compacted and cured in the same manner as the beams, and tested for compressive strength when the beams were tested. At least three cylinders were made from each batch of fresh concrete. The test data indicated that the compressive strength of cylinders from various batches of concrete were consistent. The average cylinder compressive strengths of concrete are given in Table 3.6, together with the average density of hardened concrete.

**Table 3.6 Properties of Concrete**

| Series | Beam | Slump (mm) | Concrete compressive strength (MPa) | Density ($kg/m^3$) |
|---|---|---|---|---|
| I | GBI-1 | 255 | 37 | 2237 |
| | GBI-2 | 254 | 42 | 2257 |
| | GBI-3 | 254 | 42 | 2257 |
| | GBI-4 | 255 | 37 | 2237 |
| II | GBII-1 | 235 | 46 | 2213 |
| | GBII-2 | 220 | 53 | 2226 |
| | GBII-3 | 220 | 53 | 2226 |
| | GBII-4 | 235 | 46 | 2213 |
| III | GBIII-1 | 175 | 76 | 2333 |
| | GBIII-2 | 185 | 72 | 2276 |
| | GBIII-3 | 185 | 72 | 2276 |
| | GBIII-4 | 175 | 76 | 2333 |

## 3.3 Columns

### 3.3.1 Materials in Geopolymer Concrete

#### *3.3.1.1 Fly Ash*

Similar to the beams, low-calcium (ASTM Class F) dry fly ash obtained from Colli Power Plant in Western Australia was used as the base material. The fly ash used for columns was from a different batch to the one used for beams. The chemical composition of the fly ash as determined by X-ray Fluorescence (XRF) analysis is given in Table 3.7, and the particle size distribution is shown in Figure 3.11.

**Table 3.7 Chemical Composition of Fly Ash (mass %)**

| $SiO_2$ | $Al_2O_3$ | $Fe_2O_3$ | CaO | $Na_2O$ | $K_2O$ | $TiO_2$ | MgO | $P_2O_5$ | $SO_3$ | $H_2O$ | LOI[*)] |
|---|---|---|---|---|---|---|---|---|---|---|---|
| 47.8 | 24.4 | 17.4 | 2.42 | 0.31 | 0.55 | 1.328 | 1.19 | 2.0 | 0.29 | - | 1.1 |

[*)] *Loss on ignition*

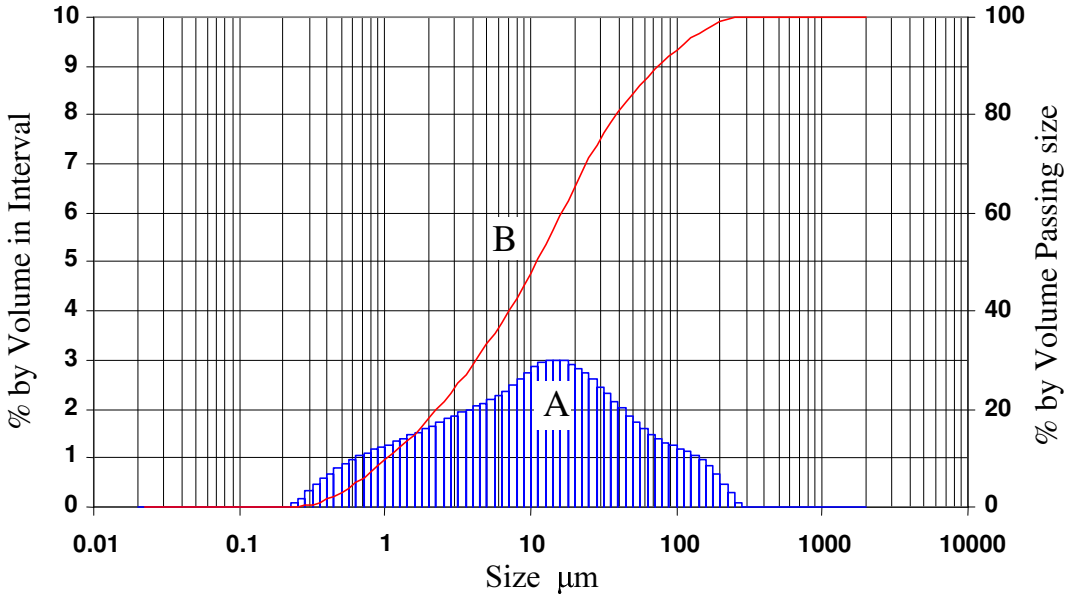


**Figure 3.11 Particle Size Distribution of Fly Ash**

### *3.3.1.2 Alkaline Solutions*

As in the case of beams (Section 3.2.1.2), sodium hydroxide solution and sodium silicate solution were used as alkaline solutions. Analytical grade sodium hydroxide (NaOH) in flake form with 98% purity was dissolved in water to produce a solution with a concentration of 16 or 14 Molars. One litre of sodium hydroxide solution with a concentration of 16 Molars contained 16x40=640 grams of NaOH flakes. Laboratory measurements have shown that this solution comprised 44.4% of NaOH flakes and 55.6% water by mass. The details of the solution with a concentration of 14 Molars are the same as given earlier in Section 3.2.1.2. The sodium silicate solution ($Na_2O$=14.7%, $SiO_2$=29.4% and water=55.9% by mass) was mixed with NaOH solution at least one day prior to use.

### *3.3.1.3 Super Plasticiser*

As for the beams (Section 3.2.1.3), a sulphonated-naphthalene based super plasticiser was used.

### *3.3.1.4 Aggregates*

Three types of locally available aggregates comprising 10mm and 7mm coarse aggregates, and fine sand were used. The fineness modulus of combined aggregates was 4.50. The aggregate grading combination is shown in Table 3.8

**Table 3.8 Grading Combination of Aggregates**

| Sieve Size | Aggregates | | | Combination*) | BS 882:1992 |
|---|---|---|---|---|---|
| | **10mm (all-in)** | **7mm** | **Fine sand** | | |
| 14 | 100.00 | 100 | 100 | 100.00 | 100 |
| 10 | 84.94 | 99.9 | 100 | 92.45 | 95-100 |
| 5 | 17.27 | 20.1 | 100 | 46.65 | 30-65 |
| 2.36 | 4.43 | 3.66 | 100 | 37.76 | 20-50 |
| 1.18 | 2.74 | 2.05 | 99.99 | 36.68 | 15-40 |
| No. 600 | 1.96 | 1.52 | 79.58 | 29.06 | 10-30 |
| No. 300 | 1.50 | 1.08 | 16.53 | 6.70 | 5-15 |
| No. 150 | 1.19 | 0.62 | 1.11 | 1.08 | 0-18 |

*) *50% (10 mm) + 15% (7 mm) + 35% (Fine sand)*

### 3.3.2 Mixture Proportions of Geopolymer Concrete

The mixture proportions of geopolymer concrete used to manufacture column specimens are given in Table 3.9. The mixtures were designed to achieve an average compressive strength of 40 MPa for GCI and GCII, and 60 MPa for GCIII and GCIV.

**Table 3.9 Mixture Proportions of Geopolymer Concrete for Columns**

| **Material** | **Column series** | |
|---|---|---|
| | **GCI & GCII (kg/m$^3$)** | **GCIII & GCIV (kg/m$^3$)** |
| 10mm aggregates | 555 | 550 |
| 7mm aggregates | 647 | 640 |
| Find sand | 647 | 640 |
| Fly ash | 408 | 404 |
| Sodium hydroxide solution | 41 *(16M)* | 41 *(14M)* |
| Sodium silicate solution | 103 | 102 |
| Extra added water | 26 | 16.5 |
| Super plasticizer | 6 | 6 |

### 3.3.3 Reinforcing Bars

The columns were longitudinally reinforced with N12 deformed bars. Plain 6 mm diameter hard-drawn wires were used as lateral reinforcement. Three samples of bars were tested in tension in a universal test machine. The steel reinforcement properties are given in Table 3.10

**Table 3.10 Steel Reinforcement Properties**

| Diameter (mm) | Nominal area ($mm^2$) | Yield Strength (MPa) | Ultimate Strength (MPa) |
|---|---|---|---|
| 6 | 28 | 570 | 660 |
| 12 | 110 | 519 | 665 |

### 3.3.4 Geometry and Reinforcement Configuration

All columns were 175 mm square and 1500 mm in length. Six columns contained four 12mm deformed bars, and the other six were reinforced with eight 12mm deformed bars as longitudinal reinforcement. These arrangements gave reinforcement ratios of 1.47% and 2.95% respectively. A concrete cover of 15mm was provided between the longitudinal bars and all faces of the column. The column geometry and reinforcement details are shown in Figure 3.12. The column details are given in Table 3.11.

Due to the use of end assemblages at both ends of test columns (Section 3.3.6), the effective length of the columns measured from centre-to-centre of the load knife-edges was 1684mm.

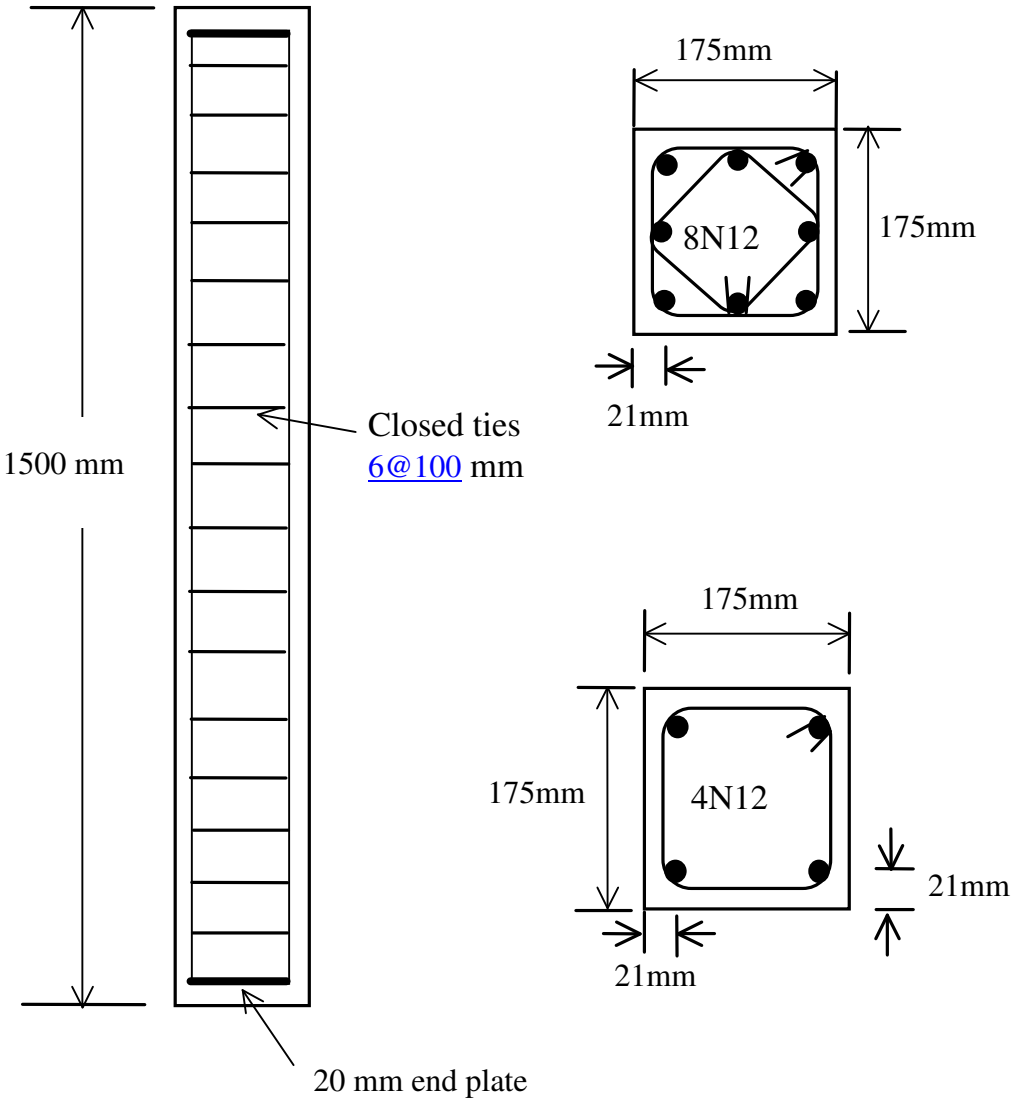


**Figure 3.12 Column Geometry and Reinforcement Details**

**Table 3.11 Column Details**

| Column No. | Column Dimensions (mm) | Lateral Reinforce-ment | Long. Reinforce-ment | Long. Reinforce-ment Ratio (%) |
|---|---|---|---|---|
| GCI-1 | 175x175x1500 | 6@100mm | 4N12 | 1.47 |
| GCI-2 | 175x175x1500 | 6@100mm | 4N12 | 1.47 |
| GCI-3 | 175x175x1500 | 6@100mm | 4N12 | 1.47 |
| GCII-1 | 175x175x1500 | 6@100mm | 8N12 | 2.95 |
| GCII-2 | 175x175x1500 | 6@100mm | 8N12 | 2.95 |
| GCII-3 | 175x175x1500 | 6@100mm | 8N12 | 2.95 |
| GCIII-1 | 175x175x1500 | 6@100mm | 4N12 | 1.47 |
| GCIII-2 | 175x175x1500 | 6@100mm | 4N12 | 1.47 |
| GCIII-3 | 175x175x1500 | 6@100mm | 4N12 | 1.47 |
| GCIV-1 | 175x175x1500 | 6@100mm | 8N12 | 2.95 |
| GCIV-2 | 175x175x1500 | 6@100mm | 8N12 | 2.95 |
| GCIV-3 | 175x175x1500 | 6@100mm | 8N12 | 2.95 |

### 3.3.5 Specimen Manufacture and Curing Process

The coarse aggregates and sand were in saturated surface dry condition. The aggregates and the dry fly ash were first mixed in a pan mixer for about three minutes. While mixing, the alkaline solutions and the extra water were mixed together and added to the solid particles. The mixing of the wet mixture continued for another four minutes.

The fresh concrete was cast into the moulds immediately after mixing. All columns were cast horizontally in wooden moulds in three layers. Each layer was manually compacted using a rod bar, and then vibrated for 30 seconds on a vibrating table. With each mixture, a number of 100mm diameters by 200mm high cylinders were also cast. Figure 3.13 shows the moulds and column cages seating on the vibrating table.

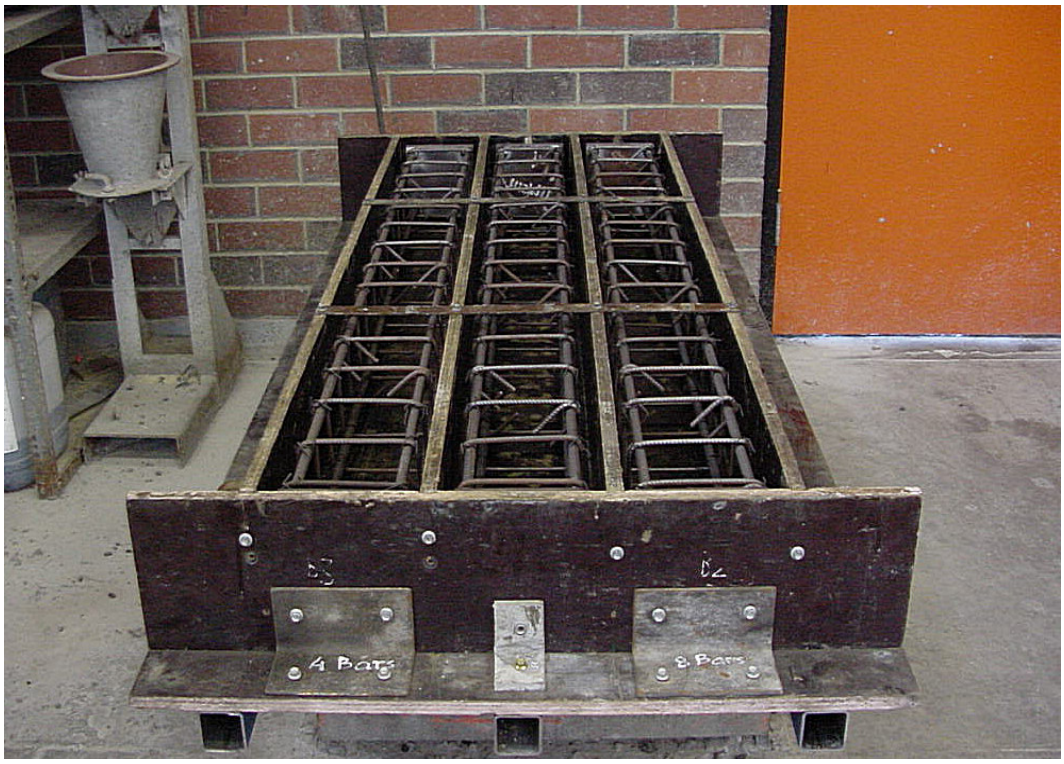


**Figure 3.13 Moulds and Column Cages**

Immediately after casting, the GC-I and GC-II column series and the cylinders were cured in a steam-curing chamber at a temperature of 60°C for 24 hours. The specimens of GC-III and GC-IV series were kept in room temperature for three days and then cured in the steam-curing chamber at a temperature of 60°C for 24 hours. The curing procedure was similar to that used in the case of beams. To avoid condensation over the concrete, a sheet of plastic was used to cover the concrete surface.

After curing, the columns and the cylinders were removed from the chamber and left to air-dry at room temperature for another 24 hours before demoulding. The test specimens were then left in the laboratory ambient conditions until the day of testing (Figure 3.14). The laboratory temperature varied between 25° and 35°C during that period.


**Figure 3.14 Columns after Demoulding**

### 3.3.6 Test Set-up and Instrumentation

All columns were tested in a Universal test machine with a capacity of 2500 kN. Two specially built end assemblages were used at the ends of the columns. The end assemblages were designed to accurately position the column to the specified load eccentricity at all stages of loading during testing (Kilpatrick, 1996).

Each of the end assemblage consisted of three 40mm thick steel plates. The end assemblages were attached to the test machine by rigidly bolted base plates at the top and bottom platens of the machine. The male plates had a male knife-edge that was fitted to female knife-edge slotted into a female plate. The tips of the knife-edges were smooth and curved in shape in order to minimize friction between them. The adaptor plate had a number of holes to accommodate different load eccentricity ranging from 0 to 65mm with 5mm intervals. Once the end assemblage positioned on the test machine, the male and female plates remained fixed in the position relative to

the platen of test machine. The details of end assemblage are shown in Figure 3.15 and Figure 3.16 (Kilpatrick 1996).

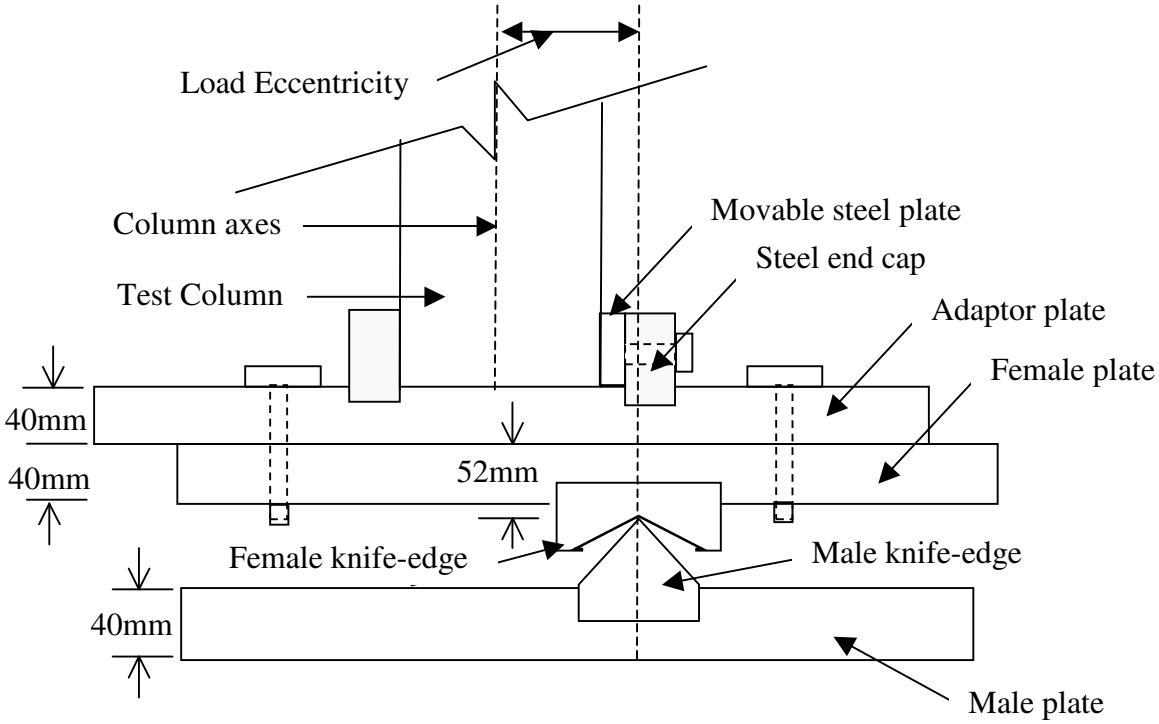


**Figure 3.15 Section View of the End Assemblage**

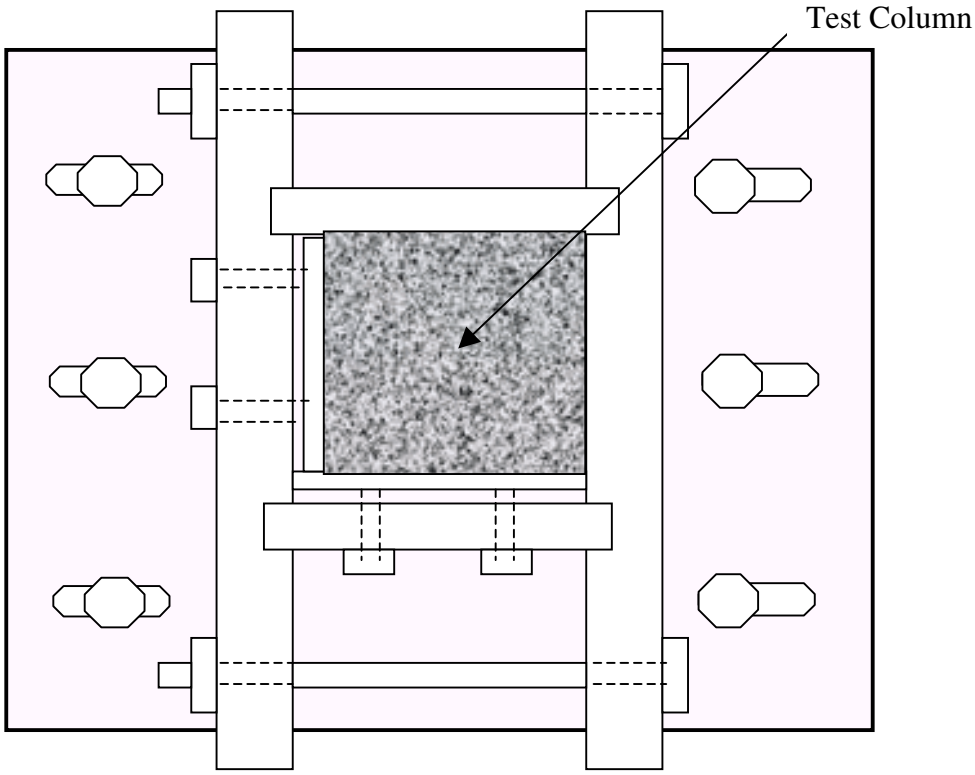


**Figure 3.16 Plan View of the End Assemblage**

The end assemblage simulated hinge support conditions at column ends, and has been successfully used in previous column tests at Curtin. The steel end caps attached at end assemblage units and located at all sides of the test column prevented failure of the end zones of the column. The complete end assemblage arrangement is shown in Figure 3.17.

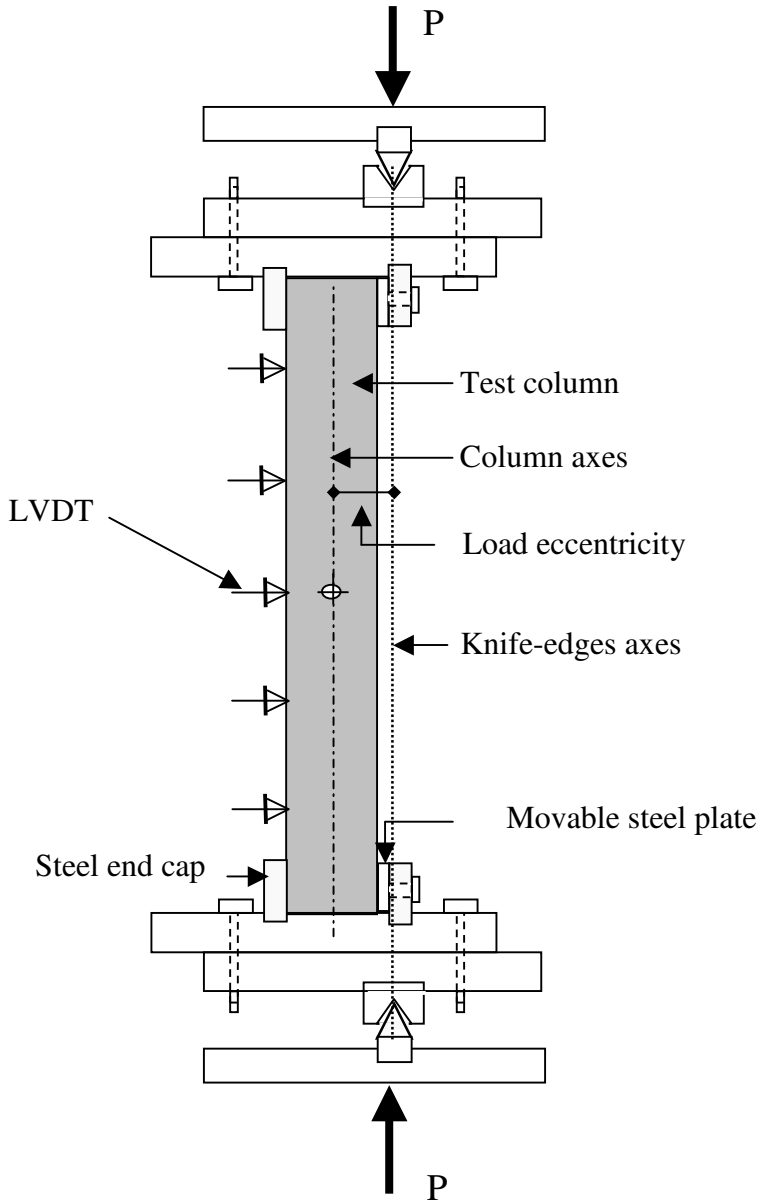


**Figure 3.17 End Assemblage Arrangement for Column Tests**

An automatic data acquisition unit was used to collect the data during the test. Six calibrated Linear Variable Differential Transformers (LVDTs) were used. Five LVDTs measured the deflections along the column length, and were placed at selected locations of the tension face of test columns. One LVDT was placed on the perpendicular face to check the out of plane movement of columns during testing.

### 3.3.7 Test Procedure

In order to eliminate loading non-uniformity due to uneven surfaces, the column ends were smoothly ground before placing the specimen into the end assemblages. Prior to placing the column in the machine, the end assemblages were adjusted to the desired load eccentricity. The line through the axes of the knife-edges represented the load eccentricity (Figure 3.17).

The base plates were first attached to the top and bottom platen of the machine. The female plate, with female knife-edge, was attached to base plate and fitted to male knife-edge. The specimen was then placed into the bottom end cap. Having the specimen properly positioned into the bottom end assemblage, the test machine platens were moved upward until the top of the column was into the top end cap. To secure the column axes parallel to the axes of the knife-edges, a 20 kN preload was applied to the specimen. When the column was correctly positioned, the appropriate movable steel plates were inserted, and firmly bolted between column and steel end cap.

LVDTs were positioned at selected locations to monitor the lateral deflection of the column. The specimens were tested under monotonically increasing axial compression with specified load eccentricity. The movement of the bottom platen of the test machine was controlled at a rate of 0.3mm/minute. Figure 3.18 shows a column ready for testing.

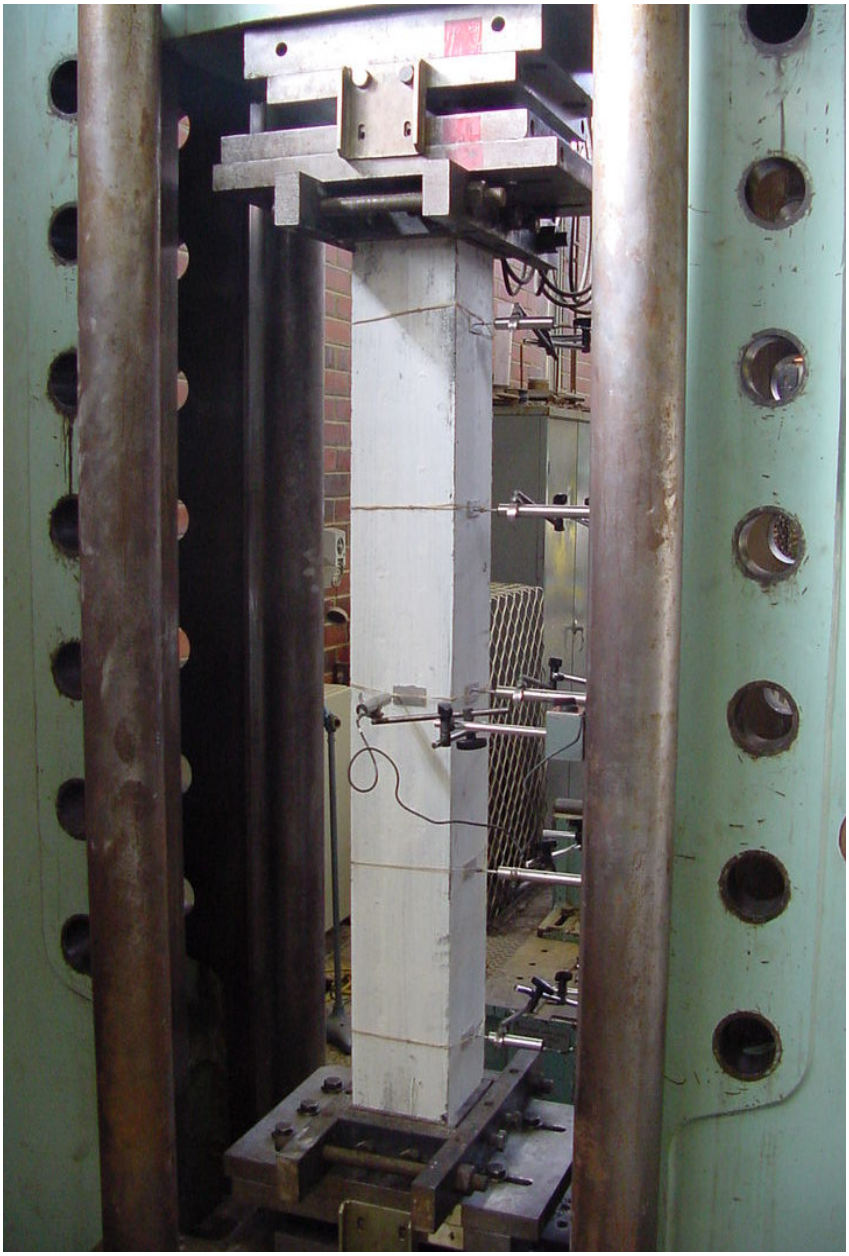

**Figure 3.18 Column in the Test Machine**

The rate of data capture varied from 10 to 100 samples per second. Higher rate was used when the test column was approaching the expected peak load to ensure that enough data were captured to trace the load-deflection curve near the peak load. Both the ascending and descending (softening) parts of the load-deflections curve were obtained for each test column.

The measurement of softening part (after peak load) continued until either the limit of LVDT travel at mid-height was attained or the deflected column approached the rotation limit of knife-edges.

### 3.3.8 Concrete Properties and Load Eccentricities

As the columns were cast, representative samples of concrete were taken from the mixer to conduct slump test, and to cast 100mmx200mm cylinders for compressive strength test. The casting, compacting, and curing process of the cylinders were the same as the test columns. They were tested on the same day when the columns were tested. The average values of slump of fresh concrete and, the compressive strength and density of hardened concrete are given in Table 3.12.

The load eccentricities were achieved by setting the adopter plates of the end assemblages to the desired values. These data are also given in Table 3.12.

**Table 3.12 Load Eccentricity and Concrete Properties**

| Series | Column | Load Eccentricity (mm) | Slump (mm) | Concrete Compressive Strength (MPa) | Density ($kg/m^3$) |
|---|---|---|---|---|---|
| I | GCI-1 | 15 | 240 | 42 | 2243 |
| | GCI-2 | 35 | 240 | 42 | 2243 |
| | GCI-3 | 50 | 240 | 42 | 2243 |
| II | GCII-1 | 15 | 240 | 43 | 2295 |
| | GCII-2 | 35 | 240 | 43 | 2295 |
| | GCII-3 | 50 | 240 | 43 | 2295 |
| III | GCIII-1 | 15 | 219 | 66 | 2342 |
| | GCIII-2 | 35 | 219 | 66 | 2342 |
| | GCIII-3 | 50 | 219 | 66 | 2342 |
| IV | GCIV-1 | 15 | 212 | 59 | 2313 |
| | GCIV-2 | 35 | 212 | 59 | 2313 |
| | GCIV-3 | 50 | 212 | 59 | 2313 |

# CHAPTER 4

# PRESENTATION AND DISCUSSION OF TEST RESULTS

## 4.1 Introduction

This Chapter presents the results of the experimental program on geopolymer reinforced concrete beams and columns. The behaviour, the crack patterns, the failure modes, and the load-deflection characteristics are described. The effects of different parameters on the strength of beams and columns are also presented.

## 4.2 Beams

### 4.2.1 General Behaviour of Beams

The specimens were tested under monotonically increasing load until failure. As the load increased, beam started to deflect and flexural cracks developed along the span of the beams. Eventually, all beams failed in a typical flexure mode.

Figure 4.1 shows an idealized load-deflection curve at mid-span of beams. The progressive increase of deflection at mid-span is shown as a function of increasing load. The load-deflection curves indicate distinct events that were taking place during the test. These events are identified as first cracking (A), yield of the tensile reinforcement (B), crushing of concrete at the compression face associated with spalling of concrete cover (C), a slight drop in the load following the ultimate load (C'), and disintegration of the compression zone concrete as a consequence of buckling of the longitudinal steel in the compression zone (D). These features are typical of flexure behaviour of reinforced concrete beams (Warner et al 1998).

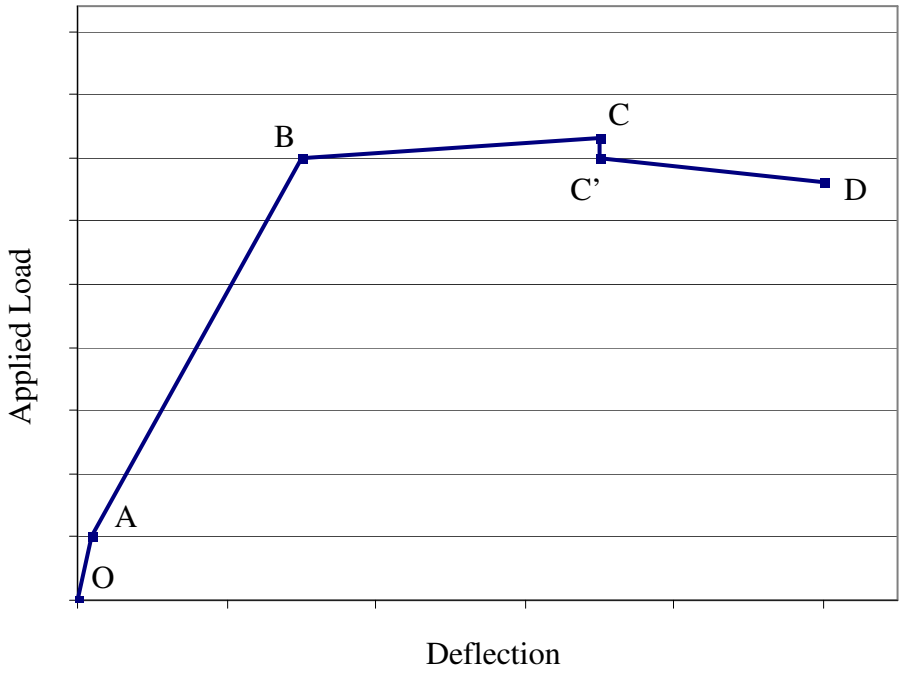


**Figure 4.1 Idealized load-deflection Curve at Mid-span**

All beams behaved in a similar manner, although the distinct events shown in Figure 4.1 were not clearly identified in all cases. All test beams were designed as under-reinforced beams; therefore the tensile steel must have reached its yield strength before failure. The effects of different parameters on the flexural behaviour of the test beams are presented latter in this Chapter.

### 4.2.2 Crack Patterns and Failure Mode

As expected, flexure cracks initiated in the pure bending zone. As the load increased, existing cracks propagated and new cracks developed along the span. In the case of beams with larger tensile reinforcement ratio some of the flexural cracks in the shear span turned into inclined cracks due to the effect of shear force. The width and the spacing of cracks varied along the span. In all, the crack patterns observed for reinforced geopolymer concrete beams were similar to those reported in the literature for reinforced Portland cement concrete beams.

The cracks at the mid-span opened widely near failure. Near peak load, the beams deflected significantly, thus indicating that the tensile steel must have yielded at failure. The final failure of the beams occurred when the concrete in the compression zone crushed, accompanied by buckling of the compressive steel bars. The failure mode was typical of that of an under-reinforced concrete beam.

The crack patterns and failure mode of several test beams are shown in Figure 4.2.

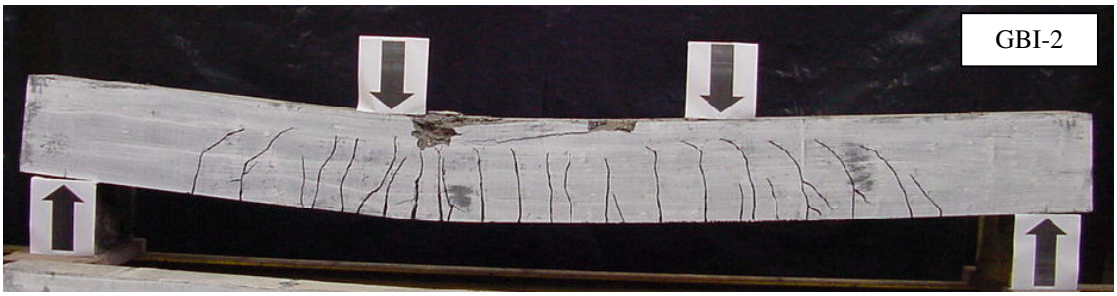


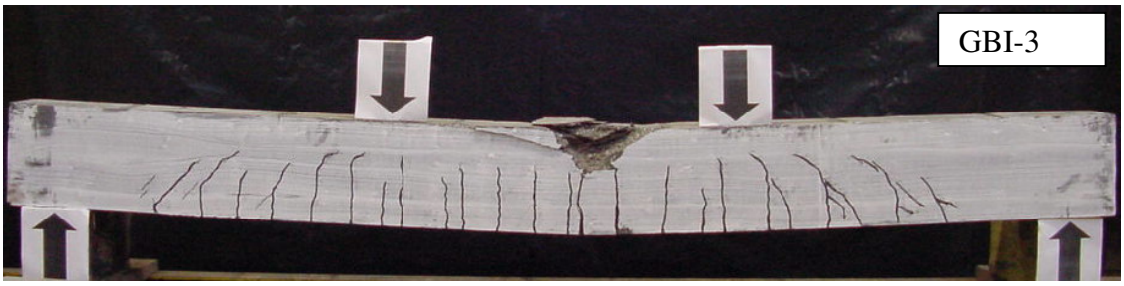


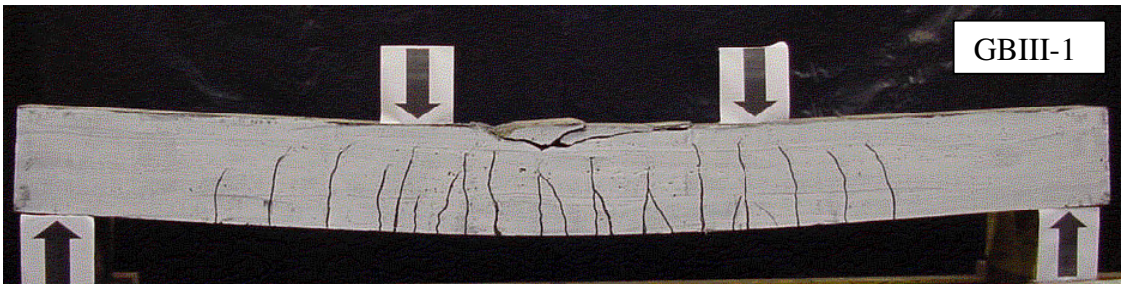


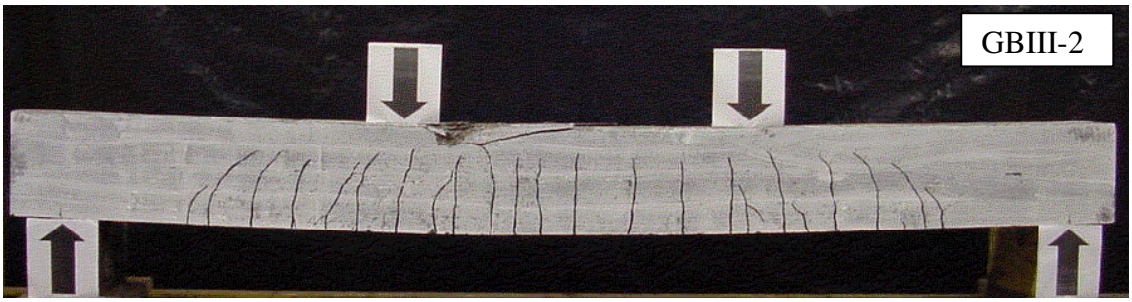


**Figure 4.2 Crack Patterns and Failure Mode of Test Beams**

### 4.2.3 Cracking Moment

The load at which the first flexural crack was visibly observed was recorded. From these test data, the cracking moments were determined. The results are given in Table 4.1.

**Table 4.1 Cracking Moment of Test Beams**

| Beam | Concrete compressive strength (MPa) | Tensile Reinforce-ment ratio (%) | Cracking Moment $M_{cr}$ (kNm) |
|---|---|---|---|
| GBI-1 | 37 | 0.64 | 13.40 |
| GBI-2 | 42 | 1.18 | 13.55 |
| GBI-3 | 42 | 1.84 | 13.50 |
| GBI-4 | 37 | 2.69 | 14.30 |
| GBII-1 | 46 | 0.64 | 15.00 |
| GBII-2 | 53 | 1.18 | 16.20 |
| GBII-3 | 53 | 1.84 | 16.65 |
| GBII-4 | 46 | 2.69 | 16.05 |
| GBIII-1 | 76 | 0.64 | 19.00 |
| GBIII-2 | 72 | 1.18 | 20.00 |
| GBIII-3 | 72 | 1.84 | 21.00 |
| GBIII-4 | 76 | 2.69 | 19.90 |

Figure 4.3 and Figure 4.4 show the variation of cracking moment with the concrete compressive strength. As to be expected, the cracking moment increased as the concrete compressive strength increased. The test data also indicated that the effect of longitudinal steel on the cracking moment is marginal (Table 4.1).

These test trends are similar to those observed in the case of reinforced Portland cement concrete beams.

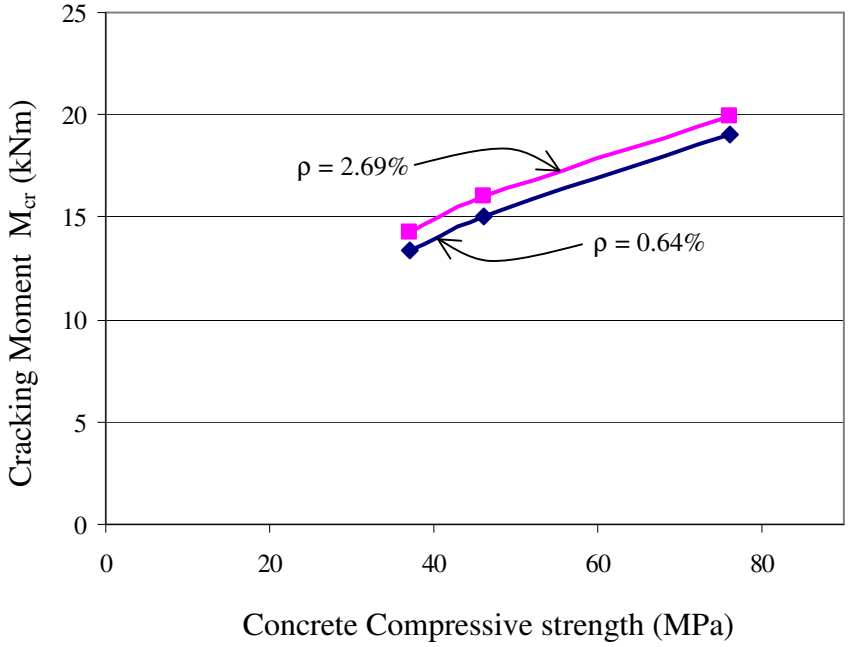


**Figure 4.3 Effect of Concrete Compressive Strength on Cracking Moment ($\rho$ = 0.64% and $\rho$ = 2.69%)**

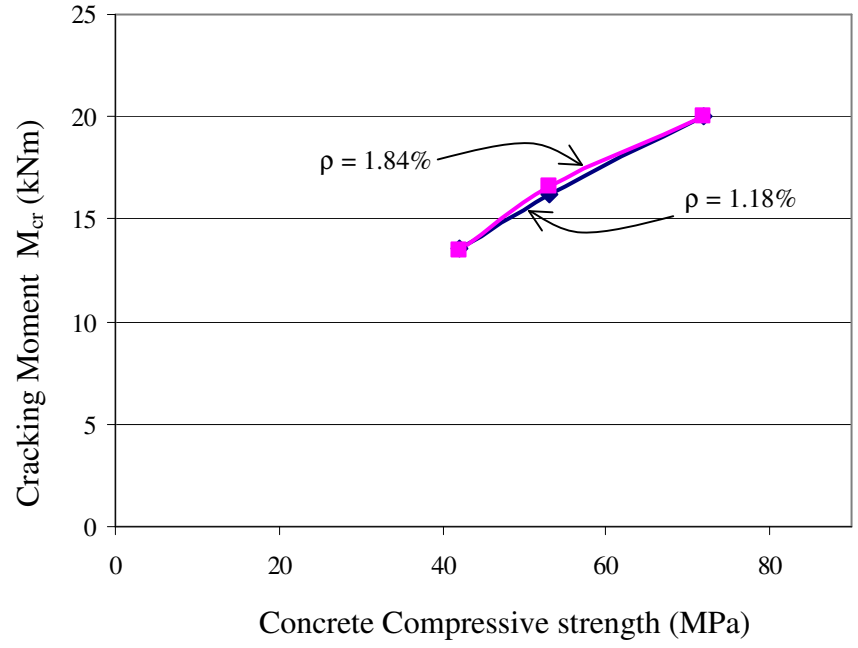


**Figure 4.4 Effect of Concrete Compressive Strength on Cracking Moment ($\rho$ = 1.18% and $\rho$ = 1.84%)**

### 4.2.4 Flexural Capacity

The ultimate moment and the corresponding mid-span deflection of test beams are given in Table 4.2.

**Table 4.2 Flexural Capacity of Test beams**

| Beam | Tensile Reinforce-ment ratio (%) | Concrete compressive strength (MPa) | Mid-span Deflection at Failure Load (mm) | Experimental Ultimate Moment (kNm) |
|---|---|---|---|---|
| GBI-1 | 0.64 | 37 | 56.63 | 56.30 |
| GBI-2 | 1.18 | 42 | 46.01 | 87.65 |
| GBI-3 | 1.84 | 42 | 27.87 | 116.85 |
| GBI-4 | 2.69 | 37 | 29.22 | 162.50 |
| GBII-1 | 0.64 | 46 | 54.27 | 58.35 |
| GBII-2 | 1.18 | 53 | 47.20 | 90.55 |
| GBII-3 | 1.84 | 53 | 30.01 | 119.0 |
| GBII-4 | 2.69 | 46 | 27.47 | 168.7 |
| GBIII-1 | 0.64 | 76 | 69.75 | 64.90 |
| GBIII-2 | 1.18 | 72 | 40.69 | 92.90 |
| GBIII-3 | 1.84 | 72 | 34.02 | 126.80 |
| GBIII-4 | 2.69 | 76 | 35.85 | 179.95 |

Figure 4.5 to Figure 4.7 show the effect of tensile reinforcement on the flexural capacity of each series of beams. These test trends show that, as expected, the flexural capacity of beams increased significantly with the increase in the tensile reinforcement ratio. Because all beams are under-reinforced, the observed increase in flexural strength is approximately proportional to the increase in the tensile reinforcement ratio.

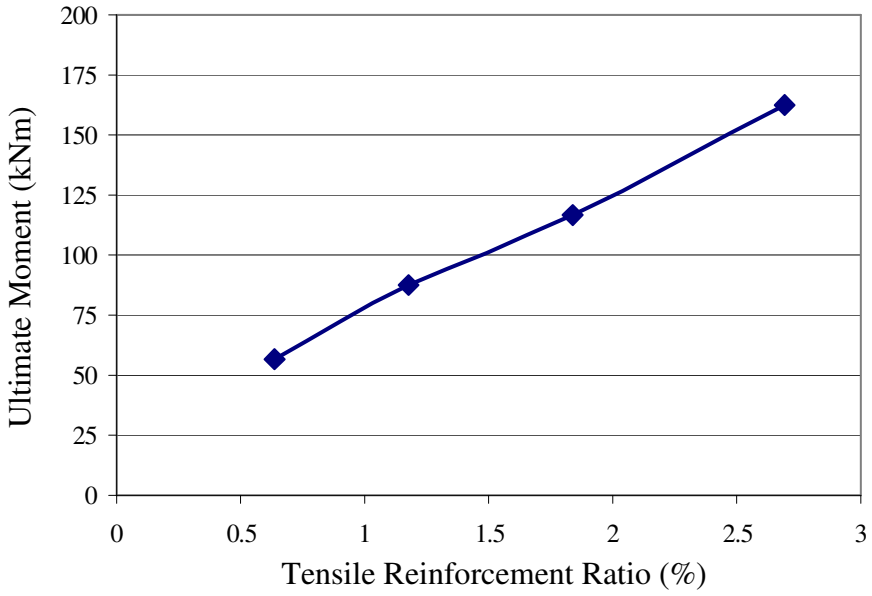


**Figure 4.5 Effect of Tensile Reinforcement Ratio on the Flexural Capacity of Beams (GBI Series)**

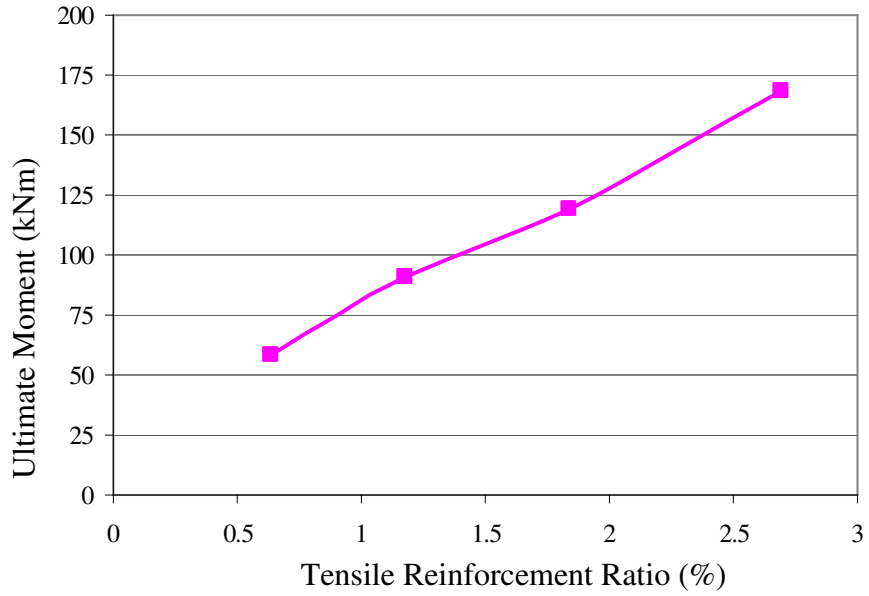


**Figure 4.6 Effect of Tensile Reinforcement Ratio on the Flexural Capacity of Beams (GBII Series)**

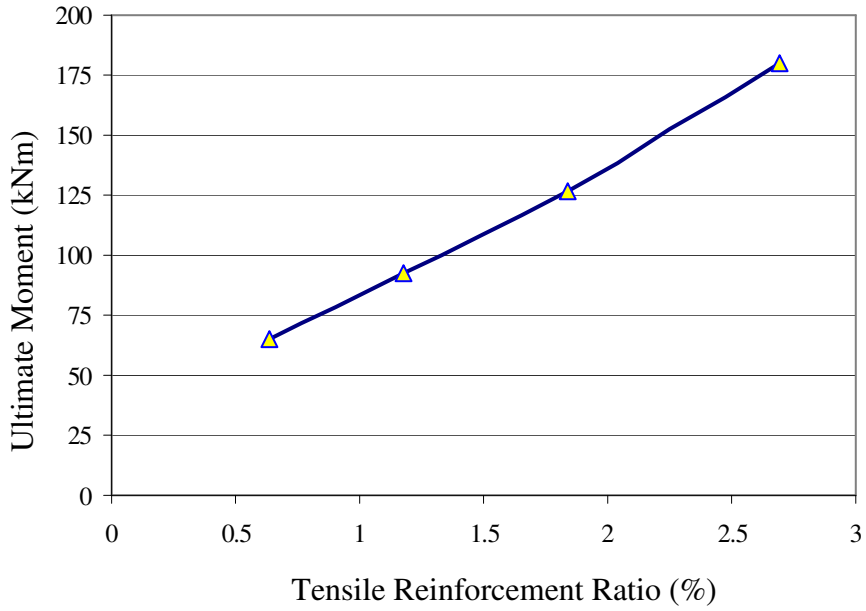


**Figure 4.7 Effect of Tensile Reinforcement Ratio on the Flexural Capacity of Beams (GBIII Series)**

The flexural capacity of beams is also influenced by the concrete compressive strength, as shown by the test data plotted in Figure 4.8. Because the beams are under-reinforced, the effect of concrete compressive strength on the flexural capacity is only marginal.

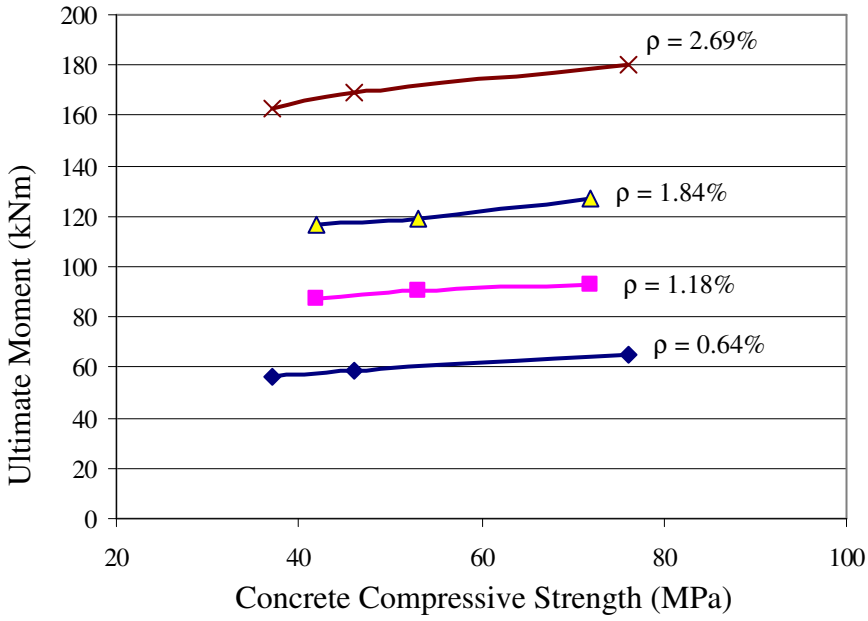


**Figure 4.8 Effect of Concrete Compressive Strength on Flexural Capacity of Beams**

### 4.2.5 Beam Deflection

The load versus mid-span deflection curves of the test beams are presented in Figure 4.9 to Figure 4.20. Complete test data are given in Appendix A to Appendix C. The distinct events indicated in Figure 4.1 are marked on the load-deflection curves.

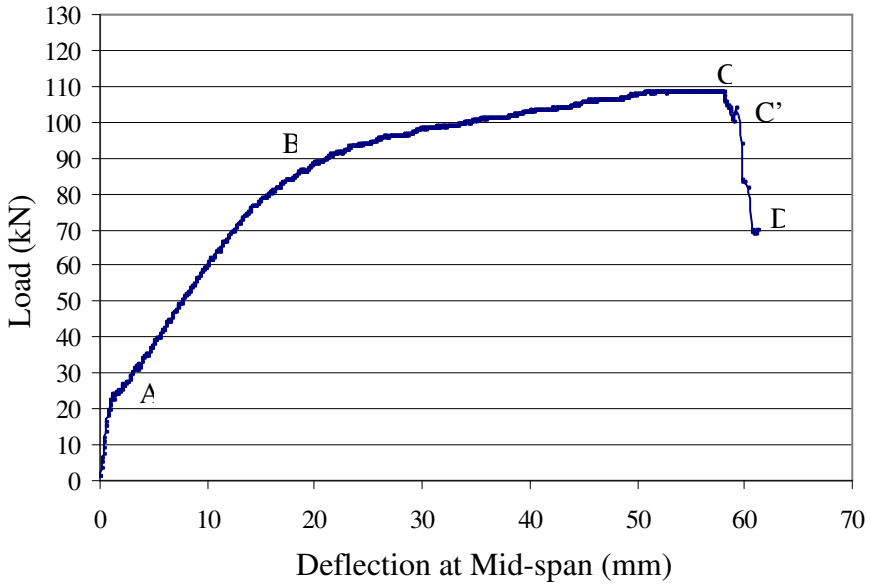


**Figure 4.9 Load versus Mid-span Deflection of Beam GBI-1**

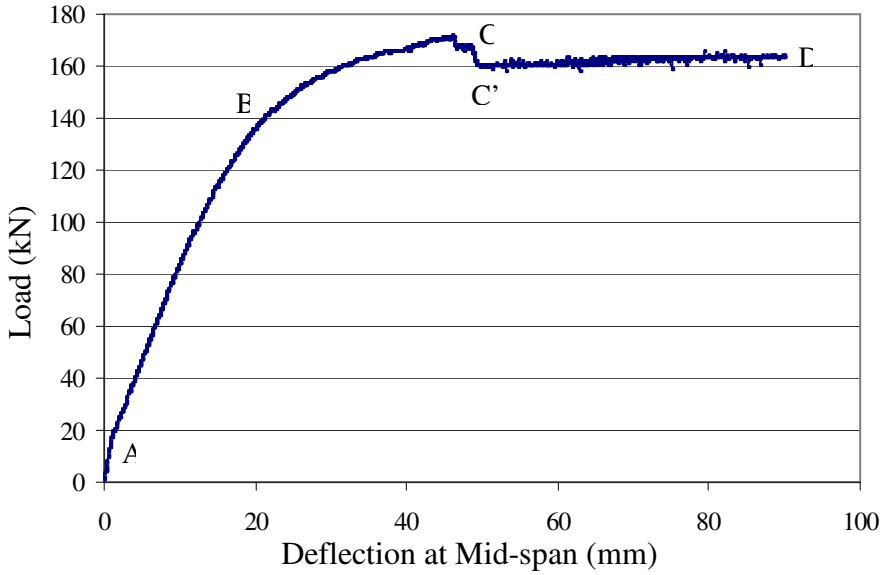


**Figure 4.10 Load versus Mid-span Deflection of Beam GBI-2**

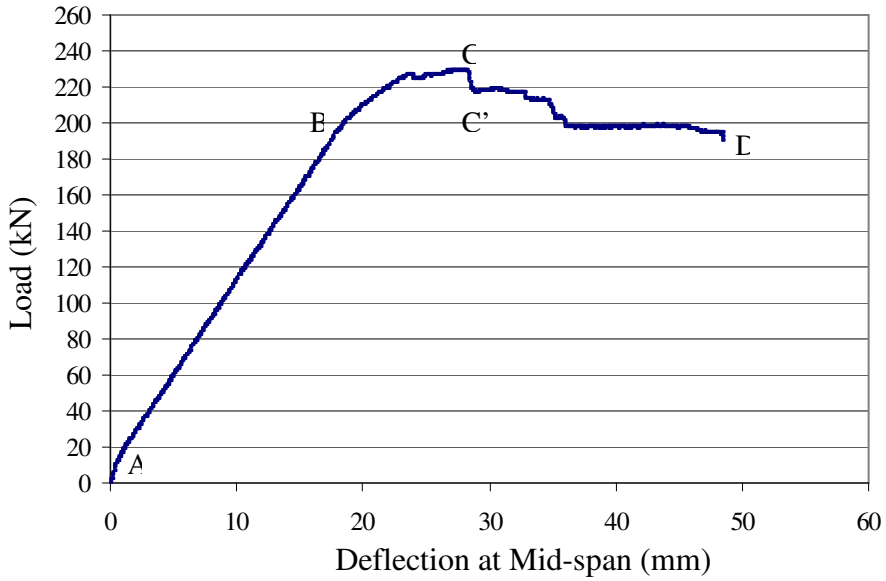


**Figure 4.11 Load versus Mid-span Deflection of Beam GBI-3**

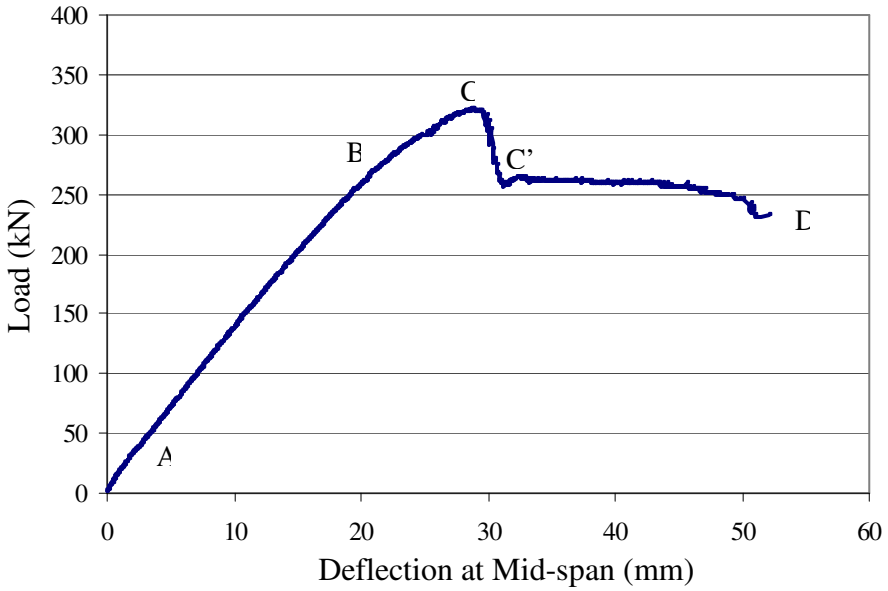


**Figure 4.12 Load versus Mid-span Deflection of Beam GBI-4**

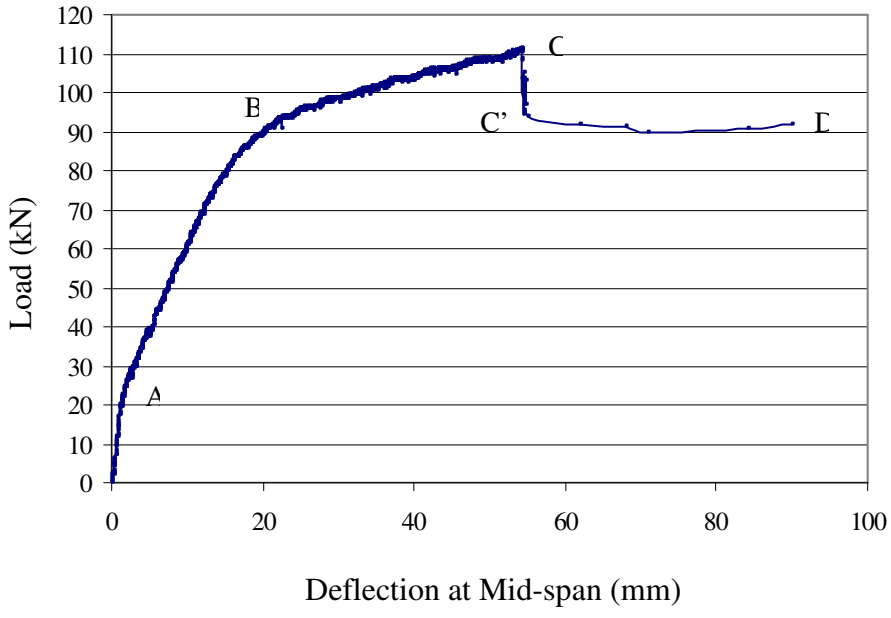


**Figure 4.13 Load versus Mid-span Deflection of Beam GBII-1**

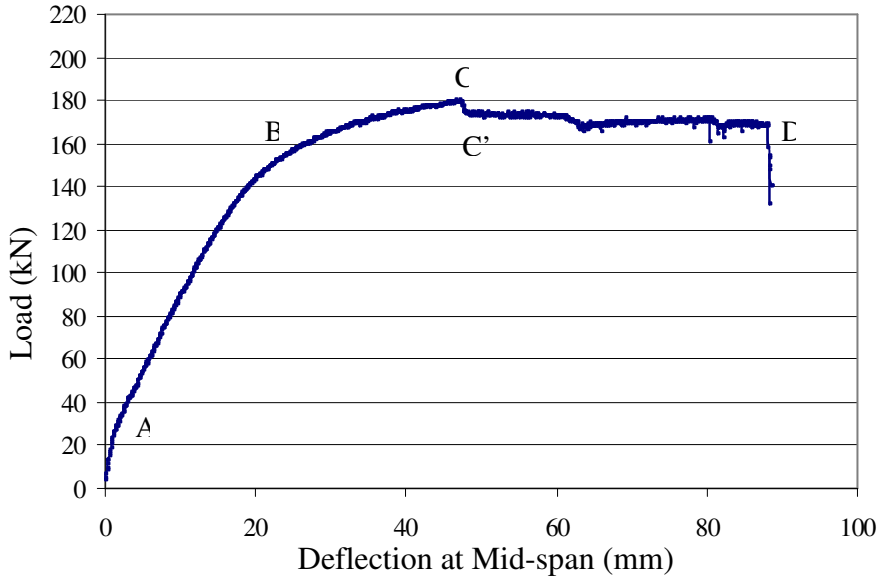


**Figure 4.14 Load versus Mid-span Deflection of Beam GBII-2**

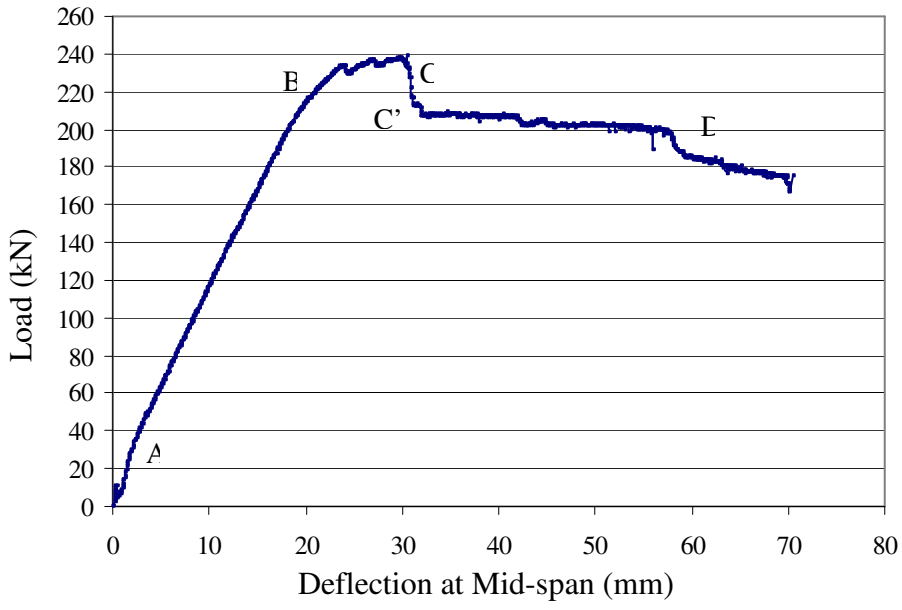


**Figure 4.15 Load versus Mid-span Deflection of Beam GBII-3**

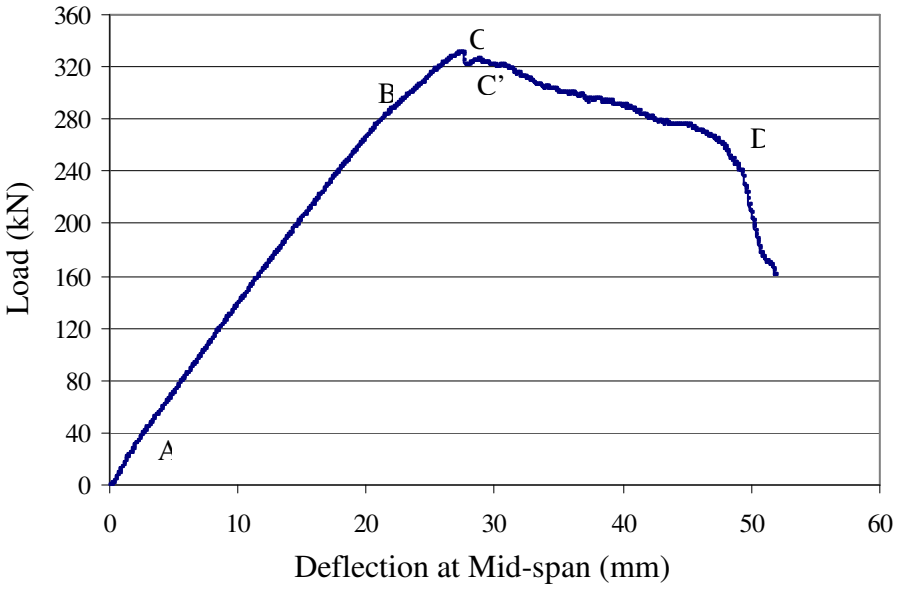


**Figure 4.16 Load versus Mid-span Deflection of Beam GBII-4**

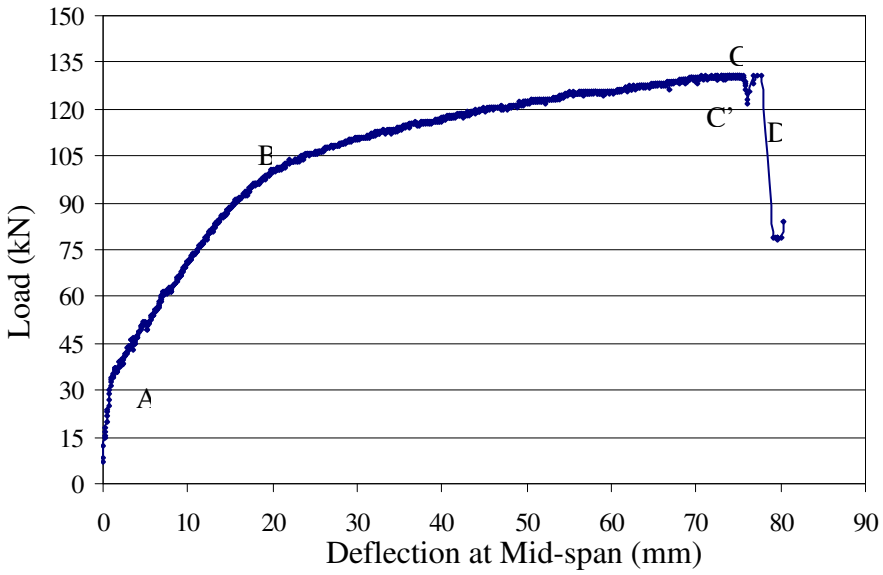


**Figure 4.17 Load versus Mid-span Deflection of Beam GBIII-1**

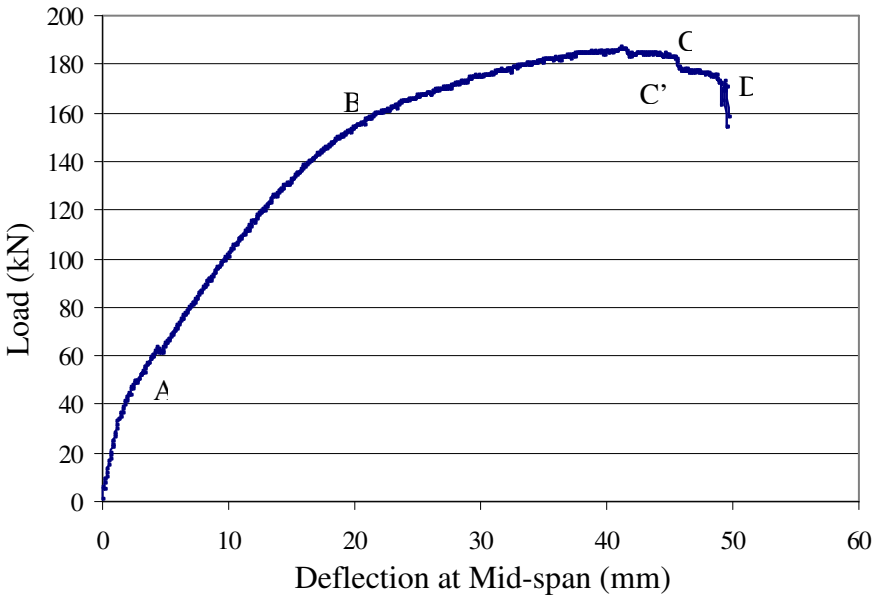


**Figure 4.18 Load versus Mid-span Deflection of Beam GBIII-2**

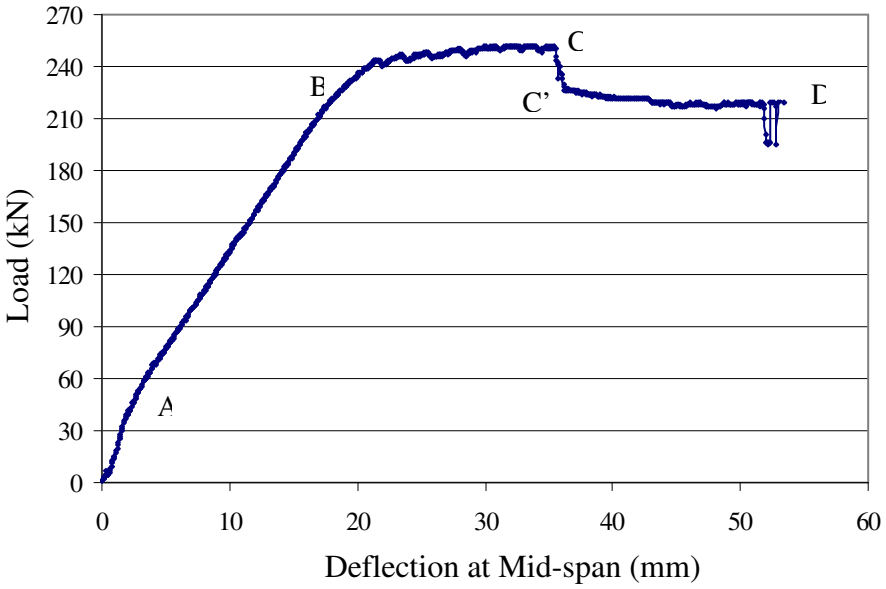


**Figure 4.19 Load versus Mid-span Deflection of Beam GBIII-3**

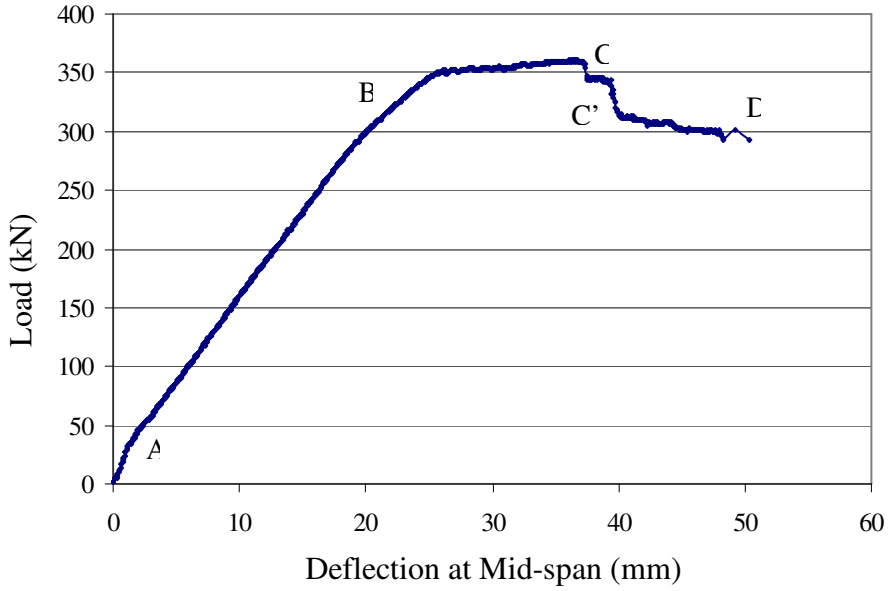


**Figure 4.20 Load versus Mid-span Deflection of Beam GBIII-4**

The test data plotted in Figures 4.9 to 4.20 were used to obtain the deflections at the service load ($P_s$) and the failure load ($P_u$). For this purpose, the service load was taken as $P_u/1.5$. The results are summarised in Table 4.3.

**Table 4.3 Deflection of Beams at Various Load Levels**

| Beam | Tensile Reinforce-ment ratio (%) | Concrete Compressive Strength (MPa) | Service Load -$P_s$ (kN) | $\Delta_s$ (mm) | Failure Load - $P_u$ (kN) | $\Delta_u$ (mm) |
|---|---|---|---|---|---|---|
| GBI-1 | 0.64 | 37 | 75 | 13.49 | 112.6 | 56.63 |
| GBI-2 | 1.18 | 42 | 117 | 15.27 | 175.3 | 46.01 |
| GBI-3 | 1.84 | 42 | 156 | 13.71 | 233.7 | 27.87 |
| GBI-4 | 2.69 | 37 | 217 | 15.60 | 325.0 | 29.22 |
| GBII-1 | 0.64 | 46 | 78 | 14.25 | 116.7 | 54.27 |
| GBII-2 | 1.18 | 53 | 121 | 14.38 | 181.1 | 47.20 |
| GBII-3 | 1.84 | 53 | 159 | 13.33 | 238.0 | 30.01 |
| GBII-4 | 2.69 | 46 | 225 | 16.16 | 337.4 | 27.47 |
| GBIII-1 | 0.64 | 76 | 87 | 14.10 | 129.8 | 69.75 |
| GBIII-2 | 1.18 | 72 | 124 | 12.55 | 185.8 | 40.69 |
| GBIII-3 | 1.84 | 72 | 169 | 12.38 | 253.6 | 34.02 |
| GBIII-4 | 2.69 | 76 | 240 | 14.88 | 359.89 | 35.85 |

### 4.2.6 Ductility

In this study, the ductility of the test beams was observed by calculating the ratio of deflection at ultimate moment, $\Delta_u$ to the deflection at yield moment, $\Delta_y$. For this purpose, the elastic theory was used to calculate the yield moment $M_y$ (Warner et al 1998). The deflections corresponding to $M_y$ and $M_u$ were determined from the load-deflection test curves shown in Figures 4.9 to 4.20. The ductility index $\mu_d$ is then calculated as the ratio of deflection at ultimate moment-to-deflection at yield moment. Table 4.4 gives the ductility index of test beams.

**Table 4.4 Deflection Ductility of Test Beams**

| Beam | Concrete Compressive Strength (MPa) | $\Delta_y$ (mm) | $\Delta_u$ (mm) | Ductility Index $\mu_d = \Delta_u/\Delta_y$ |
|---|---|---|---|---|
| GBI-1 | 37 | 13.49 | 56.63 | 4.20 |
| GBI-2 | 42 | 15.27 | 46.01 | 3.01 |
| GBI-3 | 42 | 13.71 | 27.87 | 2.03 |
| GBI-4 | 37 | 15.60 | 29.22 | 1.87 |
| GBII-1 | 46 | 14.25 | 54.27 | 3.80 |
| GBII-2 | 53 | 14.38 | 47.20 | 3.28 |
| GBII-3 | 53 | 13.33 | 30.01 | 2.25 |
| GBII-4 | 46 | 16.16 | 27.47 | 1.70 |
| GBIII-1 | 76 | 14.10 | 69.75 | 4.95 |
| GBIII-2 | 72 | 12.55 | 40.69 | 3.24 |
| GBIII-3 | 72 | 12.38 | 34.02 | 2.74 |
| GBIII-4 | 76 | 14.88 | 35.85 | 2.41 |

Figures 4.21 to 4.23 show the influence of tensile reinforcement on ductility index. These Figures show that the ductility index decreased as the tensile reinforcement is increased. The deflection ductility significantly increased for beams with tensile reinforcement ratio less than 2%, whereas the deflection ductility is moderately unaffected for beams with tensile reinforcement ratio greater than 2%. These test trends are similar to those observed in the case of reinforced Portland cement concrete beams (Warner et al 1998).

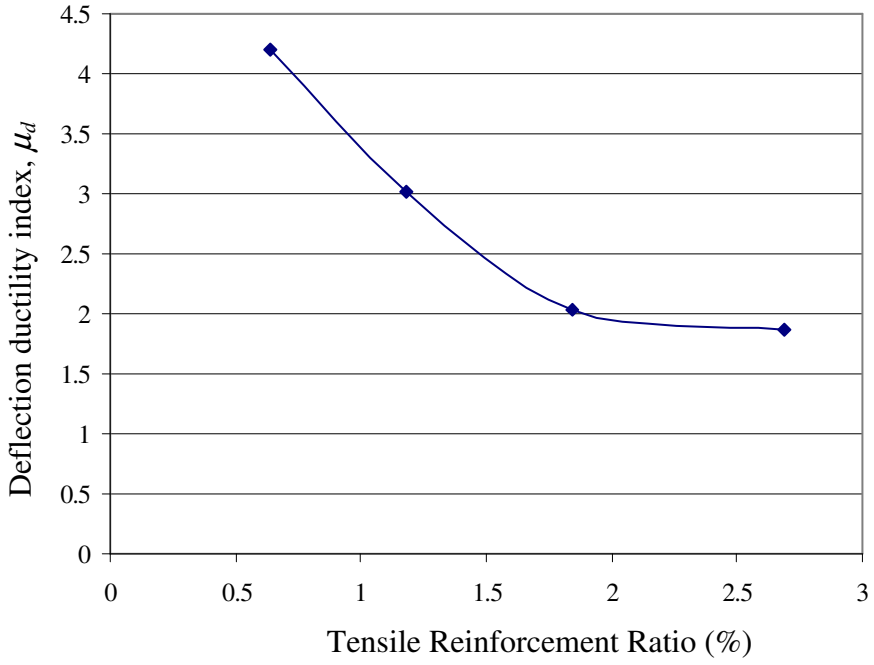


**Figure 4.21 Effect of Tensile Reinforcement Ratio on Ductility (GBI Series)**

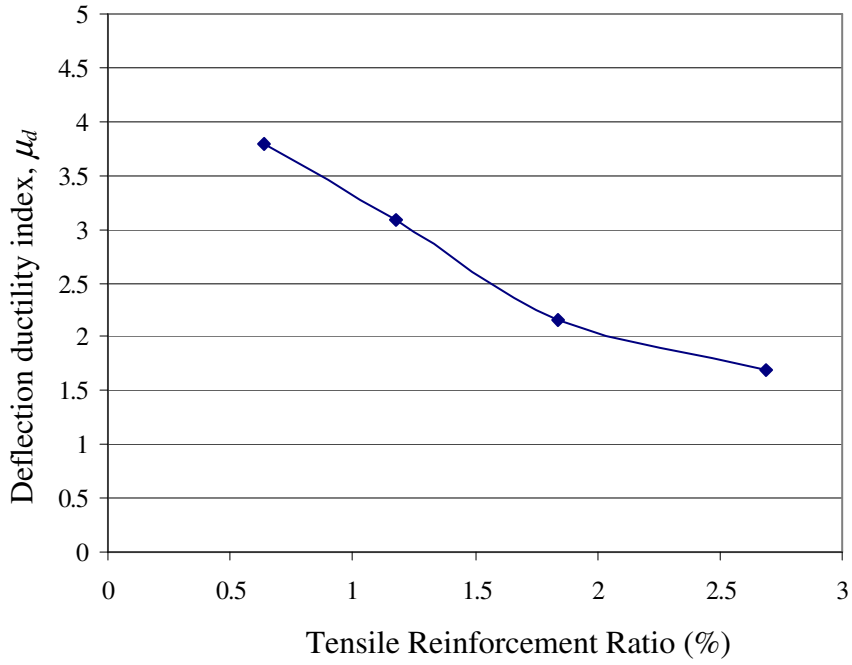


**Figure 4.22 Effect of Tensile Reinforcement Ratio on Ductility (GBII Series)**

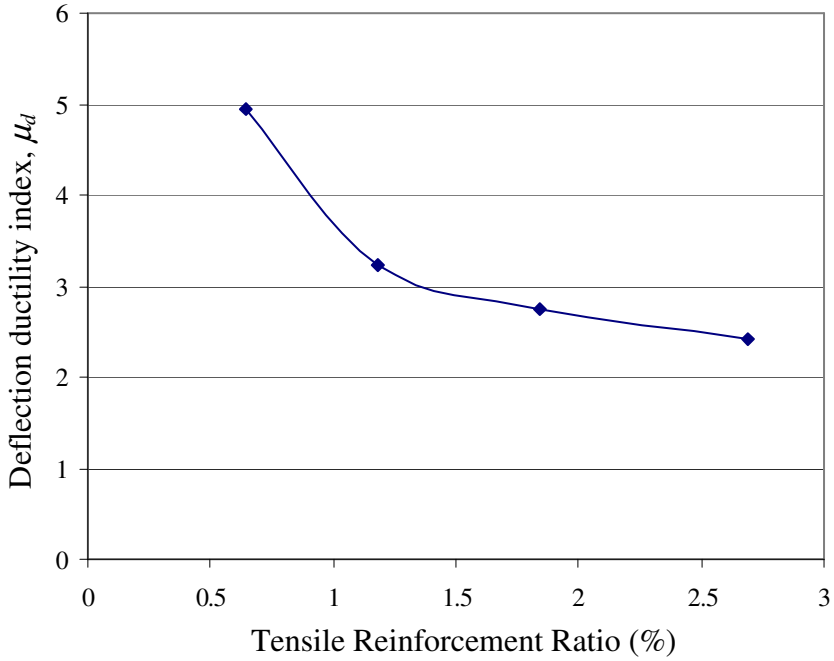


**Figure 4.23 Effect of Tensile Reinforcement Ratio on Ductility (GBIII Series)**

## 4.3 Columns

### 4.3.1 General Behaviour of Columns

All columns were tested under monotonically increasing load with specified load eccentricity until failure. The load eccentricity, concrete compressive strength, and longitudinal reinforcement ratio influenced the load capacity of the test columns. The load capacity increased with the increase of concrete compressive strength and longitudinal reinforcement ratio. The load capacity of test columns decreased when the load eccentricity increased.

### 4.3.2 Crack Patterns and Failure Modes

In all cases, cracks initiated at column mid-height at the tension face. As the load increased, the existing cracks propagated and new cracks formed along the length of the columns. The width of cracks varied depending on the location. The cracks at the mid-height widely opened near failure.

The location of the failure zone varied plus or minus 250 mm from the column mid-height. The failure was due to crushing of the concrete in the compression zone. The longitudinal bars in the compression zone buckled especially in the case of columns subjected to low eccentricity.

Some typical failure modes of test columns are presented in Figure 4.24 to Figure 4.25.

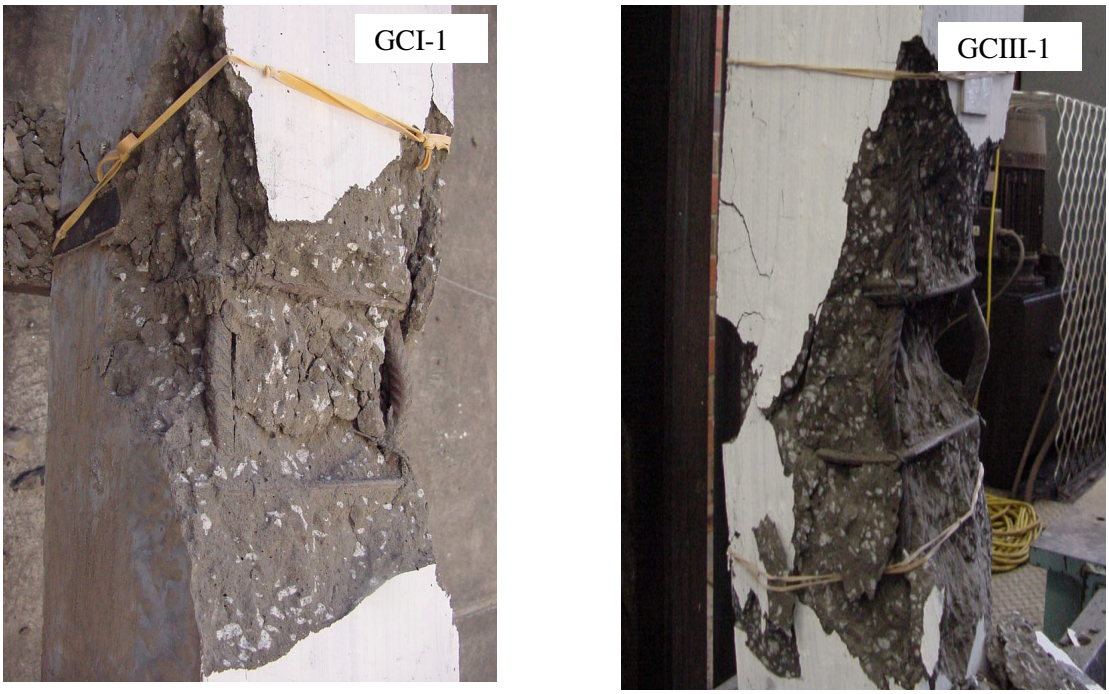


**Figure 4.24 Failure Mode of GCI-1 and GCIII-1**

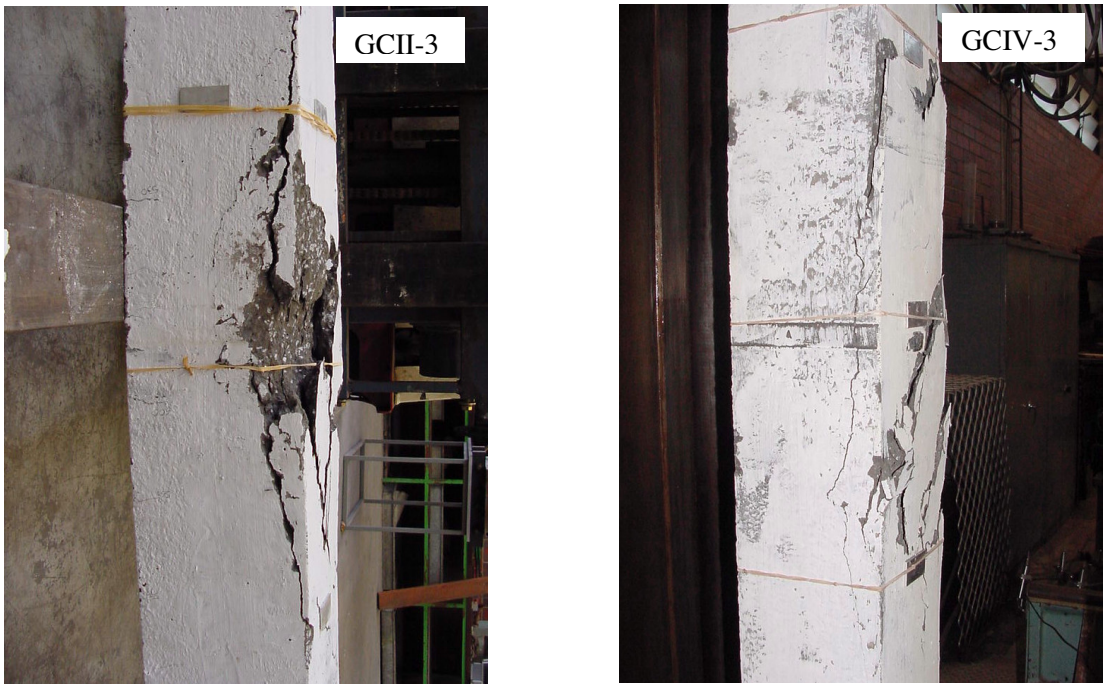


**Figure 4.25 Failure Mode of GCII-3 and GCIV-3**

### 4.3.3 Load-Deflection Relationship

The loads versus mid-height deflection graph of test columns are presented in Figure 4.26 to Figure 4.37. Complete test data are given in Appendix A and Appendix B. As expected, the mid-height deflection of columns at failure increased as the load eccentricity increased (Table 4.5).

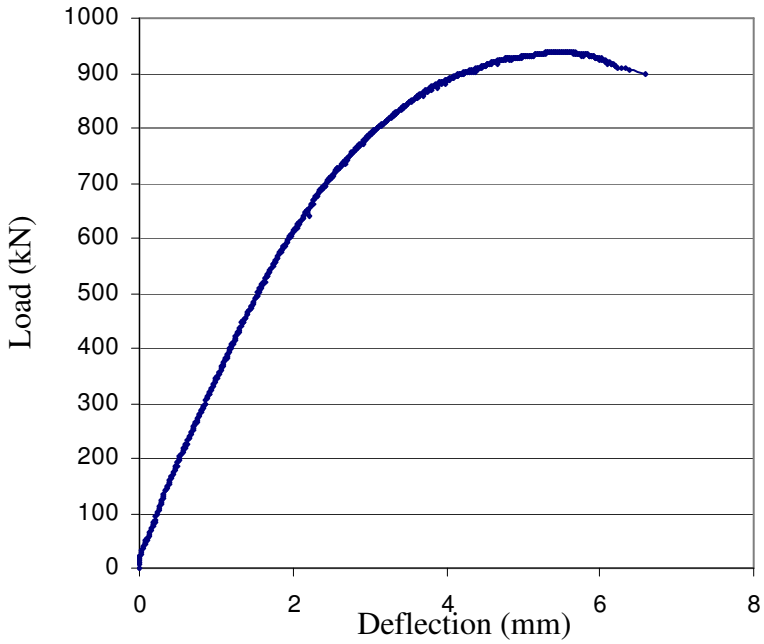


**Figure 4.26 Load versus Mid-height Deflection Curve (GCI-1)**

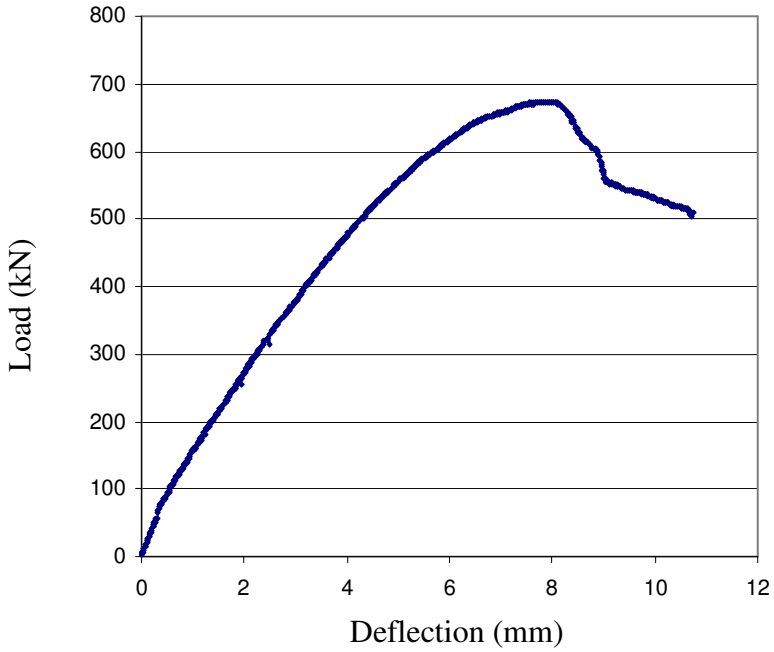


**Figure 4.27 Load versus Mid-height Deflection Curve (GCI-2)**

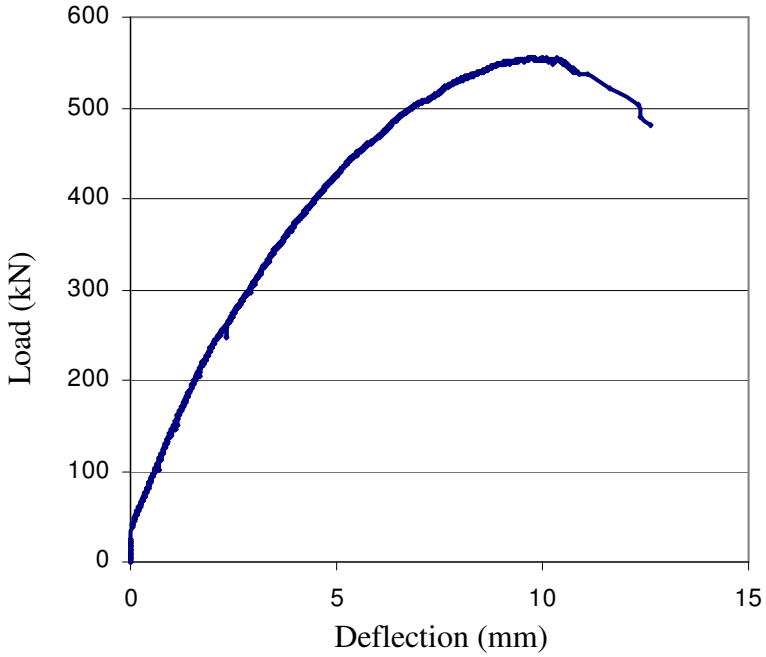


**Figure 4.28 Load versus Mid-height Deflection Curve (GCI-3)**

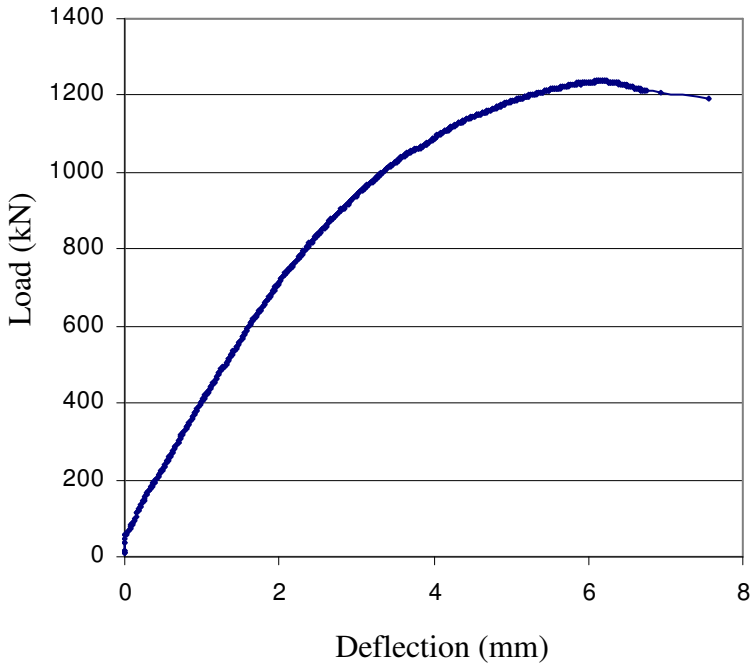


**Figure 4.29 Load versus Mid-height Deflection Curve (GCII-1)**

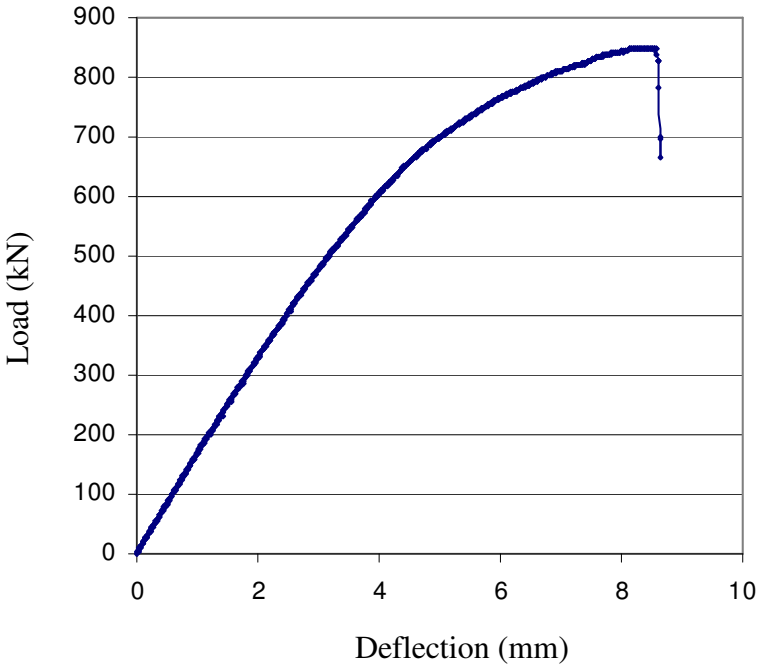


**Figure 4.30 Load versus Mid-height Deflection Curve (GCII-2)**

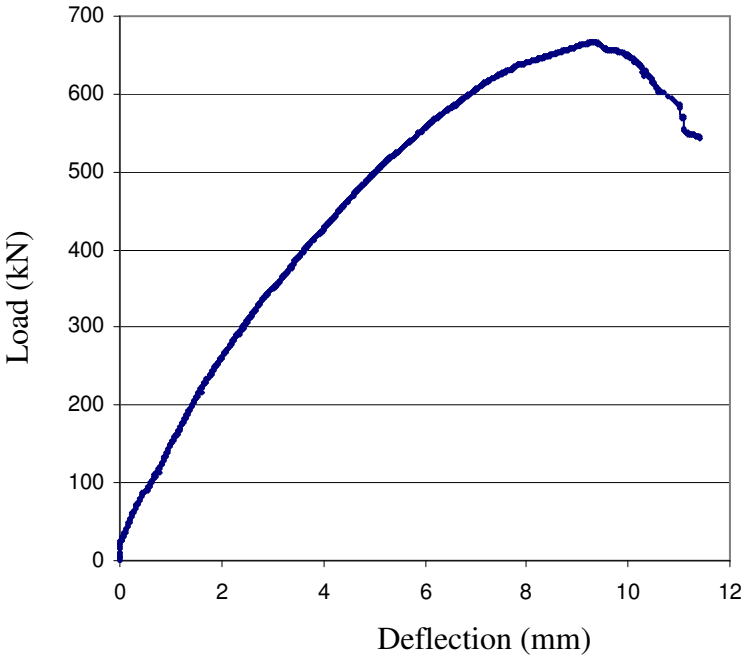


**Figure 4.31 Load versus Mid-height Deflection Curve (GCII-3)**

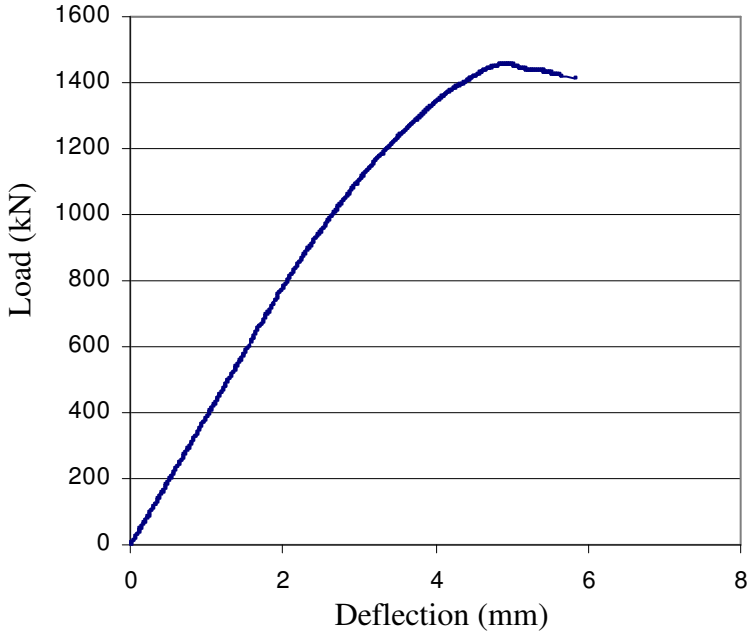


**Figure 4.32 Load versus Mid-height Deflection Curve (GCIII-1)**

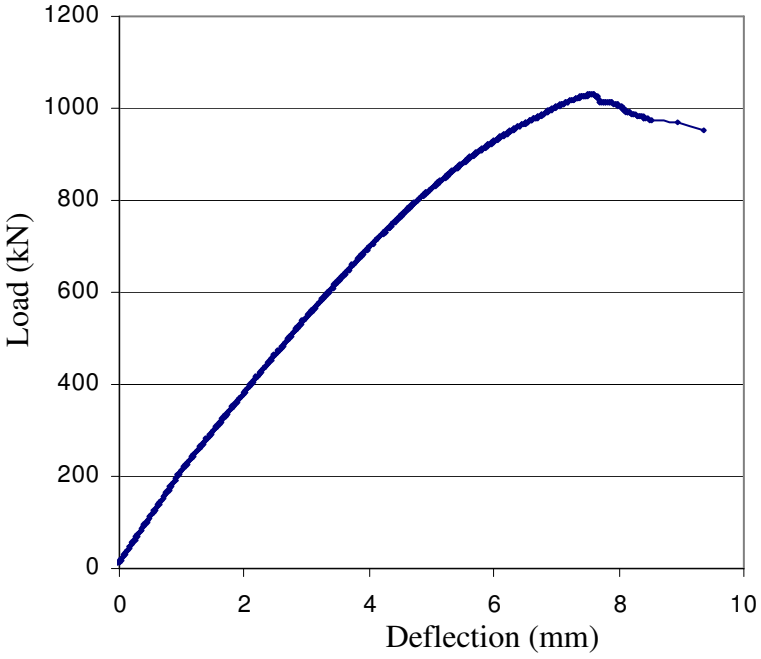


**Figure 4.33 Load versus Mid-height Deflection Curve (GCIII-2)**

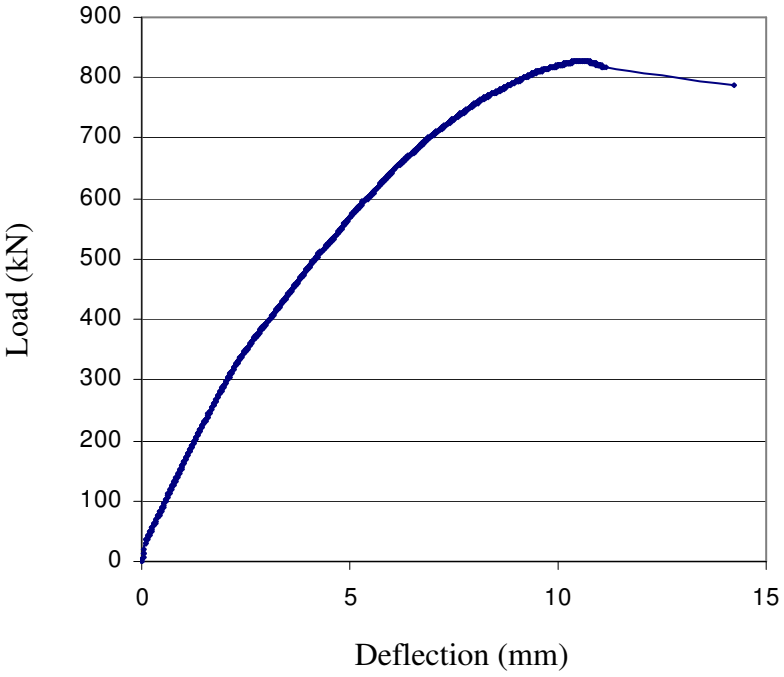


**Figure 4.34 Load versus Mid-height Deflection Curve (GCIII-3)**

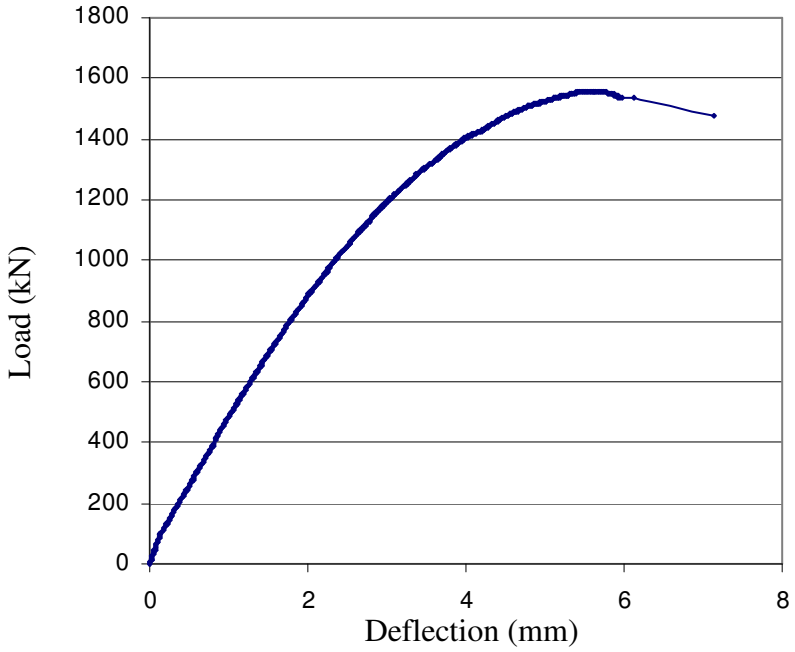


**Figure 4.35 Load versus Mid-height Deflection Curve (GCIV-1)**

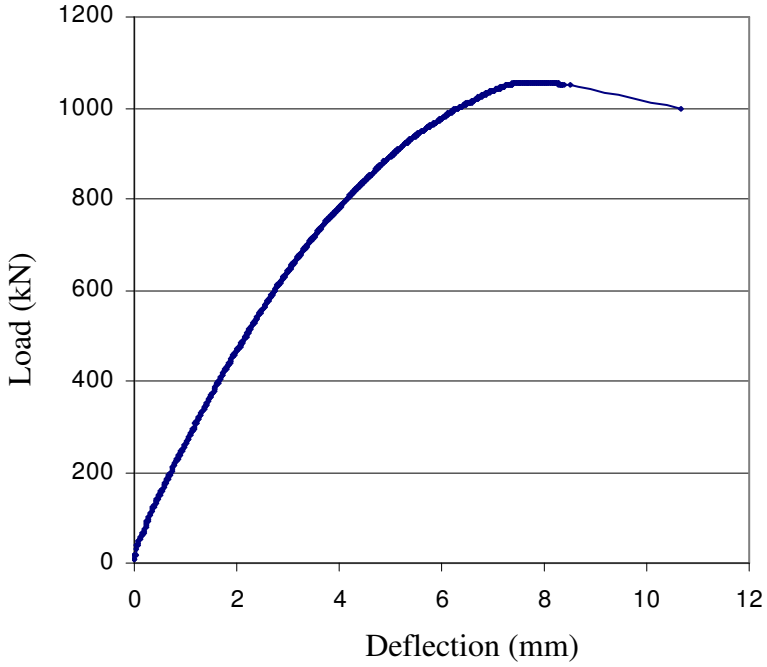


**Figure 4.36 Load versus Mid-height Deflection Curve (GCIV-2)**

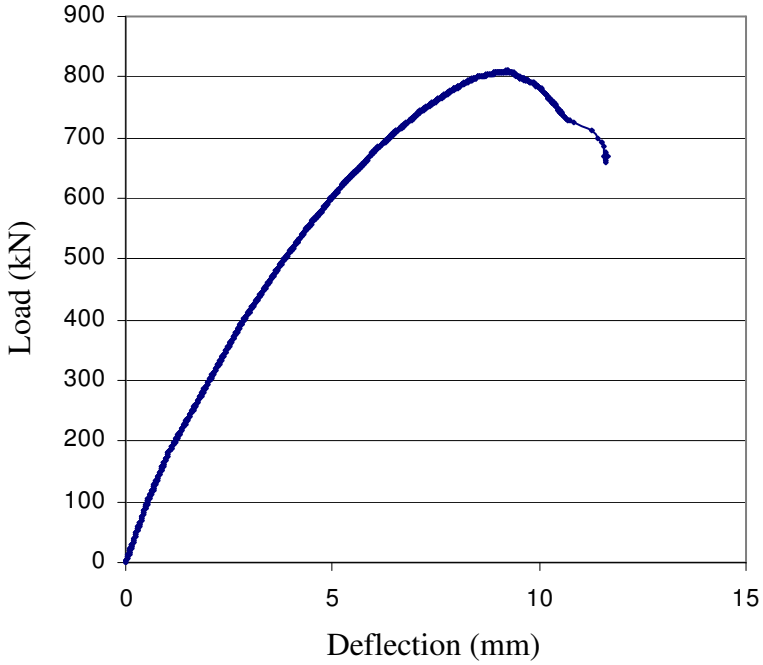


**Figure 4.37 Load versus Mid-height Deflection Curve (GCIV-3)**

### 4.3.4 Load Capacity

The test results are presented in Table 4.5. The load capacity of columns is influenced by load eccentricity, concrete compressive strength, and longitudinal reinforcement ratio. As expected, when the load eccentricity decreased, the load capacity of columns increased. The load capacity also increased when the compressive strength of concrete and the longitudinal reinforcement ratio increased.

**Table 4.5 Summary of Column Test Results**

| Column No. | Concrete Compres-sive Strength (MPa) | Load Eccentricity (mm) | Longitudinal Reinforcement | | At Failure | |
|---|---|---|---|---|---|---|
| | | | Bars | Ratio (%) | Failure Load (kN) | Mid-height deflection at failure load |
| GCI-1 | 42 | 15 | 4Y12 | 1.47 | 940 | 5.44 |
| GCI-2 | 42 | 35 | 4Y12 | 1.47 | 674 | 8.02 |
| GCI-3 | 42 | 50 | 4Y12 | 1.47 | 555 | 10.31 |
| GCII-1 | 43 | 15 | 8Y12 | 2.95 | 1237 | 6.24 |
| GCII-2 | 43 | 35 | 8Y12 | 2.95 | 852 | 9.08 |
| GCII-3 | 43 | 50 | 8Y12 | 2.95 | 666 | 9.40 |
| GCIII-1 | 66 | 15 | 4Y12 | 1.47 | 1455 | 4.94 |
| GCIII-2 | 66 | 35 | 4Y12 | 1.47 | 1030 | 7.59 |
| GCIII-3 | 66 | 50 | 4Y12 | 1.47 | 827 | 10.70 |
| GCIV-1 | 59 | 15 | 8Y12 | 2.95 | 1559 | 5.59 |
| GCIV-2 | 59 | 35 | 8Y12 | 2.95 | 1057 | 7.97 |
| GCIV-3 | 59 | 50 | 8Y12 | 2.95 | 810 | 9.18 |

### 4.3.5 Effect of Load Eccentricity

Figure 4.38 shows a plot of failure load versus load eccentricity of the test columns. As expected, the failure load decreased as the load eccentricity ratio increased.

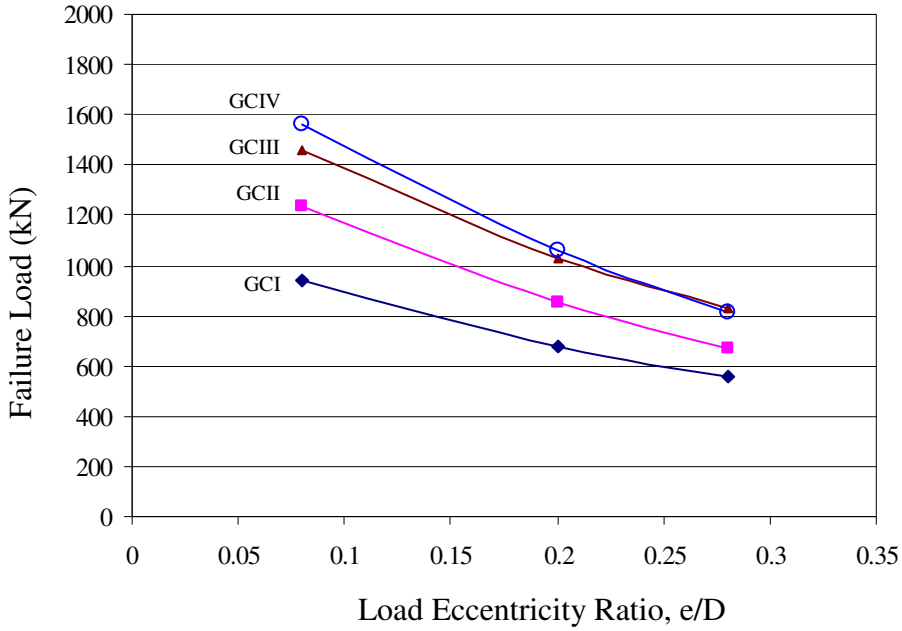


**Figure 4.38 Effect of Load Eccentricity**

### 4.3.6 Effect of Concrete Compressive Strength

The effect of concrete compressive strength on the column strength is shown in Figure 4.39 and Figure 4.40. These Figures show that the load capacity of test columns increased as the concrete compressive strength increased.

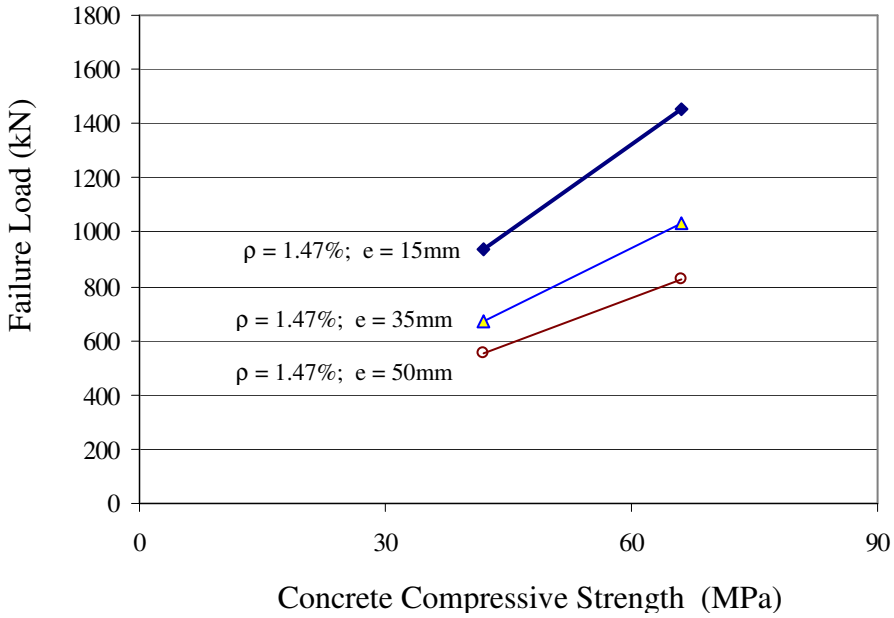


**Figure 4.39 Effect of Concrete Compressive Strength on Load Capacity (GCI and GCI III Series)**

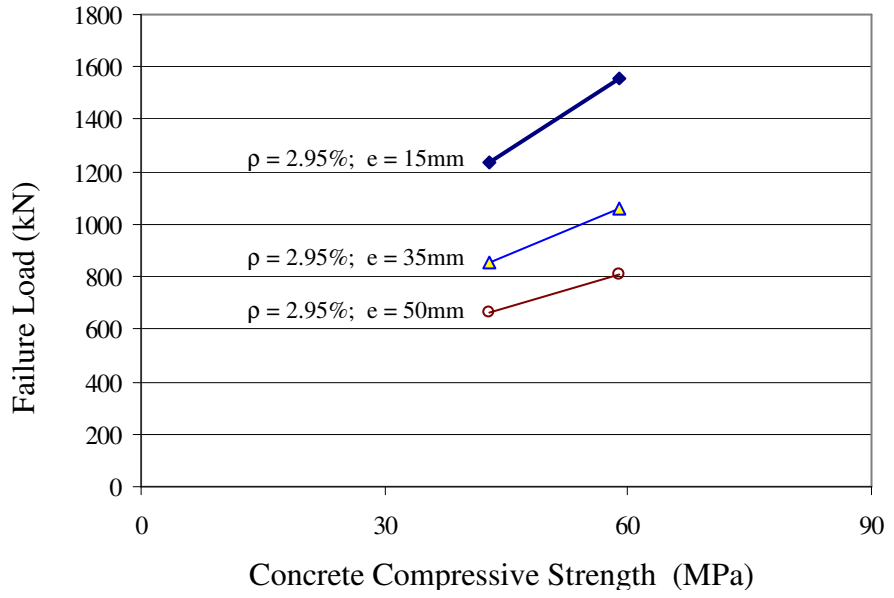


**Figure 4.40 Effect of Concrete Compressive Strength on Load Capacity (GCII and GCI IV Series)**

### 4.3.7 Effect of Longitudinal Reinforcement

The effect of longitudinal reinforcement ratio on the column failure load is demonstrated in Figure 4.41. As expected, an increase in the longitudinal reinforcement ratio increased the failure load of columns.

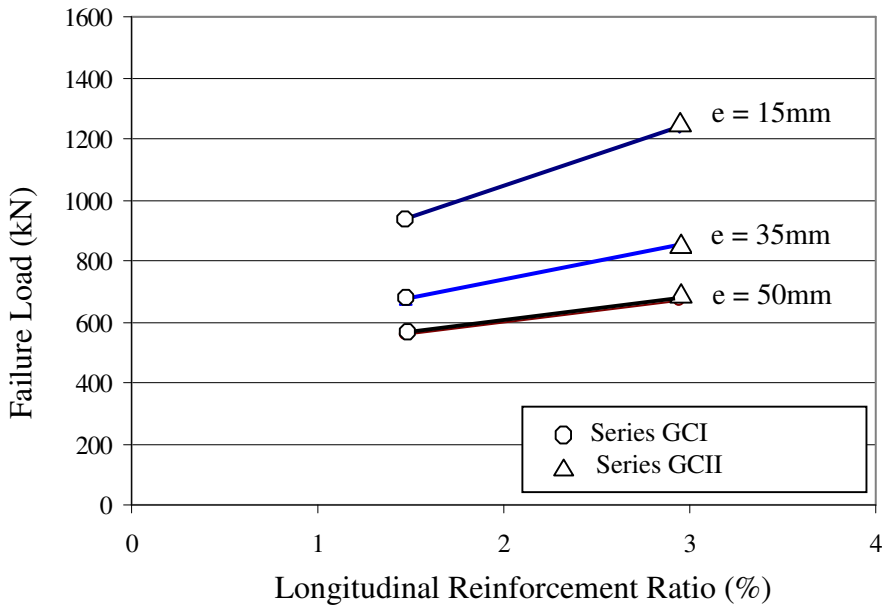


**Figure 4.41 Effect of Longitudinal Reinforcement on Load Capacity**

# CHAPTER 5

# CORRELATION OF TEST AND CALCULATED RESULTS

## 5.1 Introduction

In Section 5.2, the calculated values of cracking moment and ultimate moment of reinforced geopolymer concrete beams are compared with the test values. The calculated values were obtained by using the methods given in the draft Australian Standard for Portland cement concrete, AS 3600 (2005). The measured deflections of beams are also compared with those calculated using the serviceability design provisions given in draft AS 3600 (2005).

In Section 5.3, the failure loads of reinforced geopolymer test columns are compared with the values calculated using the slender column design provisions given in AS 3600 and the American Concrete Institute Building Code ACI 318 (2002). The test values are also compared with those predicted using a simplified stability analysis method developed by Rangan (1990).

In all strength calculations, the strength reduction factor is taken as unity.

## 5.2 Reinforced Geopolymer Concrete Beams

### 5.2.1 Cracking Moment

The theoretical cracking moment $M_{cr}$ was calculated by taking the flexural tensile strength of geopolymer concrete as equal to $0.6\sqrt{f_c'}$ (Clause 6.1.1.2, AS 3600). The drying shrinkage strain needed for the calculations was based on the test data reported by Wallah and Rangan (2006) for heat-cured low-calcium fly ash-based geopolymer concrete. Both these data are given in Table C.1 of Appendix C.

The calculated cracking moments are compared with the test values in Table 5.1. The average test to calculated ratio of cracking moment is 1.35, with a standard deviation of 0.09.

**Table 5.1 Correlation of Test and Calculated Cracking Moment of Beams**

| Beam | Tensile Reinforce-ment ratio (%) | Concrete compressive strength (MPa) | Moment at 1st Crack – $M_{cr}$ (kNm) | Calculated Cracking Moment (kNm) | Ratio Test/Calc. |
|---|---|---|---|---|---|
| GBI-1 | 0.64 | 37 | 13.40 | 10.39 | 1.28 |
| GBI-2 | 1.18 | 42 | 13.55 | 10.86 | 1.24 |
| GBI-3 | 1.84 | 42 | 13.50 | 10.61 | 1.27 |
| GBI-4 | 2.69 | 37 | 14.30 | 9.66 | 1.48 |
| GBII-1 | 0.64 | 46 | 15.00 | 11.65 | 1.28 |
| GBII-2 | 1.18 | 53 | 16.20 | 12.27 | 1.32 |
| GBII-3 | 1.84 | 53 | 16.65 | 12.02 | 1.38 |
| GBII-4 | 2.69 | 46 | 16.05 | 10.91 | 1.47 |
| GBIII-1 | 0.64 | 76 | 19.00 | 15.13 | 1.25 |
| GBIII-2 | 1.18 | 72 | 20.00 | 14.43 | 1.38 |
| GBIII-3 | 1.84 | 72 | 21.00 | 14.18 | 1.48 |
| GBIII-4 | 2.69 | 76 | 19.90 | 14.39 | 1.38 |
| | | | | Average | 1.35 |
| | | | | Standard Deviation | 0.09 |

### 5.2.2 Flexural Capacity

The flexural strength of the beams was calculated using the design provisions contained in the draft Australian Standard for Concrete Structures, AS 3600 (2005), and the usual flexural strength theory for reinforced concrete beams (Warner et al 1988).

The test and the calculated values are compared in Table 5.2 and Figure 5.1. For beams with tensile reinforcement ratio of 1.18%, 1.84%, and 2.69%, the test and calculated values agree well. In the case of beams GBI-1, GBII-1 and GBIII-1, with a tensile steel ratio of 0.64%, the calculated values are conservative due to the neglect of the effect of strain hardening of tensile steel bars on the ultimate bending moment. In all, the average of ratio of test/calculated values is 1.11, with a standard deviation of 0.14.

**Table 5.2 Comparison of Test and Calculated Ultimate Moment of Beams**

| Beam | Tensile Reinforce-ment ratio (%) | Concrete compressive strength (MPa) | Mid-span Deflection at Failure Load (mm) | Ultimate Moment (kNm) | | Ratio Test/Calc. |
|---|---|---|---|---|---|---|
| | | | | *Test* | *Calc.* | |
| GBI-1 | 0.64 | 37 | 56.63 | 56.30 | 45.17 | 1.24 |
| GBI-2 | 1.18 | 42 | 46.01 | 87.65 | 80.56 | 1.09 |
| GBI-3 | 1.84 | 42 | 27.87 | 116.85 | 119.81 | 0.98 |
| GBI-4 | 2.69 | 37 | 29.22 | 160.50 | 155.31 | 1.03 |
| GBII-1 | 0.64 | 46 | 54.27 | 58.35 | 42.40 | 1.28 |
| GBII-2 | 1.18 | 53 | 47.20 | 90.55 | 81.50 | 1.11 |
| GBII-3 | 1.84 | 53 | 30.01 | 119.0 | 122.40 | 0.97 |
| GBII-4 | 2.69 | 46 | 27.47 | 168.7 | 162.31 | 1.04 |
| GBIII-1 | 0.64 | 76 | 69.75 | 64.90 | 45.69 | 1.42 |
| GBIII-2 | 1.18 | 72 | 40.69 | 92.90 | 82.05 | 1.13 |
| GBIII-3 | 1.84 | 72 | 34.02 | 126.80 | 124.17 | 1.02 |
| GBIII-4 | 2.69 | 76 | 35.85 | 179.95 | 170.59 | 1.05 |
| | | | | | Average | 1.11 |
| | | | | | Standard Deviation | 0.14 |

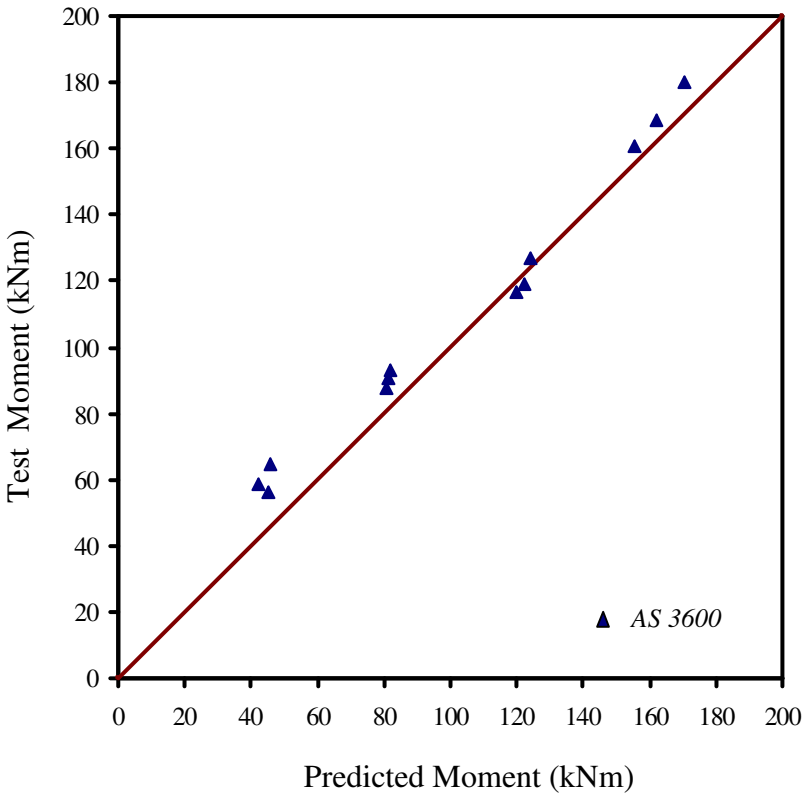


**Figure 5.1 Comparison of Test to Predicted Ultimate Moment of Beams**

### 5.2.3 Deflections

Maximum mid-span deflection at service load for the test beams was calculated using the elastic bending theory and the serviceability design provisions given in draft AS 3600 (2005). According to AS3600, the calculation of short-term deflection of the beams should include the effects of cracking, tension stiffening, and shrinkage properties of the concrete.

In these calculations, the cracking moment was taken as the calculated value given in Table 5.1. The modulus of elasticity of concrete, $E_c$, was interpolated from the measured data reported earlier by Hardjito and Rangan (2005) for geopolymer concrete similar to that used in the present study. The service load,$P_s$ was taken as the test failure load divided by 1.5. All data used in these calculations are given in Table C.1 of Appendix C.

Comparison between the calculated and the corresponding experimental deflection at service load is given in Table 5.3. The average ratio of the test-to-calculated values is 1.15, with the standard deviation of 0.06.

**Table 5.3 Comparison of Test-to-Calculated Deflections of Beams**

| Beam | $P_s$ (kN) | $\Delta_{exp.}$ (mm) | $\Delta_{cal.}$ (mm) | Ratio=$\Delta_{exp.}/\Delta_{cal.}$ |
|---|---|---|---|---|
| GBI-1 | 75 | 13.49 | 11.88 | 1.17 |
| GBI-2 | 117 | 15.27 | 12.49 | 1.25 |
| GBI-3 | 156 | 13.71 | 12.41 | 1.14 |
| GBI-4 | 217 | 15.60 | 14.21 | 1.14 |
| GBII-1 | 78 | 14.25 | 11.91 | 1.21 |
| GBII-2 | 121 | 14.38 | 12.58 | 1.20 |
| GBII-3 | 159 | 13.33 | 12.36 | 1.14 |
| GBII-4 | 225 | 16.16 | 14.18 | 1.17 |
| GBIII-1 | 87 | 14.10 | 12.07 | 1.21 |
| GBIII-2 | 124 | 12.55 | 12.41 | 1.08 |
| GBIII-3 | 169 | 12.38 | 12.59 | 1.05 |
| GBIII-4 | 240 | 14.88 | 14.16 | 1.10 |
| | | | Average | 1.15 |
| | | | Standard deviation | 0.06 |

## 5.3 Reinforced Geopolymer Concrete Columns

The load-carrying capacity of test columns was calculated using both a simplified stability analysis proposed by Rangan (1990) and the moment-magnifier method incorporated in the daft Australian Standard for Concrete Structures AS 3600 (2005) and the American Concrete Institute Building Code ACI 318-02 (2002).

The calculated failure loads are compared with the test values in Table 5.4. The mean value of test-to-calculated failure load by the simplified stability analysis proposed by Rangan (1990) is 1.01 with a standard deviation of 0.07. The mean value of test-to-calculated failure load by AS 3600 is 1.03 with a standard deviation of 0.06. The mean value of test-to-calculated failure load by ACI 318-02 is 1.11 with a standard deviation of 0.08. Figure 5.2 shows the correlation between test and calculated failure loads in the form of a scatter diagram.

These results demonstrate that the methods of calculations used in the case of reinforced Portland cement concrete columns are applicable for reinforced geopolymer concrete columns.

**Table 5.4 Comparison of Test and Calculated Failure Loads of Columns**

| Column | $f_c'$ (MPa) | $e$ (mm) | $\rho$ (%) | Test Failure Load (kN) | Calculated Failure Load (kN) | | | Failure Load Ratio* | | |
|---|---|---|---|---|---|---|---|---|---|---|
| | | | | | Rangan | AS 3600 | ACI 318-02 | 1 | 2 | 3 |
| GCI-1 | 42 | 15 | 1.47 | 940 | 988 | 962 | 926 | 0.95 | 0.98 | 1.01 |
| GCI-2 | 42 | 35 | 1.47 | 674 | 752 | 719 | 678 | 0.90 | 0.94 | 0.99 |
| GCI-3 | 42 | 50 | 1.47 | 555 | 588 | 573 | 541 | 0.94 | 0.97 | 1.03 |
| GCII-1 | 43 | 15 | 2.95 | 1237 | 1149 | 1120 | 1050 | 1.08 | 1.10 | 1.18 |
| GCII-2 | 43 | 35 | 2.95 | 852 | 866 | 832 | 758 | 0.98 | 1.02 | 1.12 |
| GCII-3 | 43 | 50 | 2.95 | 666 | 673 | 665 | 604 | 0.99 | 1.00 | 1.10 |
| GCIII-1 | 66 | 15 | 1.47 | 1455 | 1336 | 1352 | 1272 | 1.09 | 1.08 | 1.14 |
| GCIII-2 | 66 | 35 | 1.47 | 1030 | 1025 | 1010 | 917 | 1.00 | 1.02 | 1.12 |
| GCIII-3 | 66 | 50 | 1.47 | 827 | 773 | 760 | 738 | 1.07 | 1.09 | 1.12 |
| GCIV-1 | 59 | 15 | 2.95 | 1559 | 1395 | 1372 | 1267 | 1.11 | 1.14 | 1.23 |
| GCIV-2 | 59 | 35 | 2.95 | 1057 | 1064 | 1021 | 911 | 0.99 | 1.04 | 1.16 |
| GCIV-3 | 59 | 50 | 2.95 | 810 | 815 | 800 | 723 | 0.99 | 1.01 | 1.12 |
| | | | | | | | Mean | 1.01 | 1.03 | 1.11 |
| | | | | | | | Standard Deviation | 0.07 | 0.06 | 0.08 |

**1 = Test/ Rangan; 2 = Test/AS3600; 3 = Test/ACI318-02*

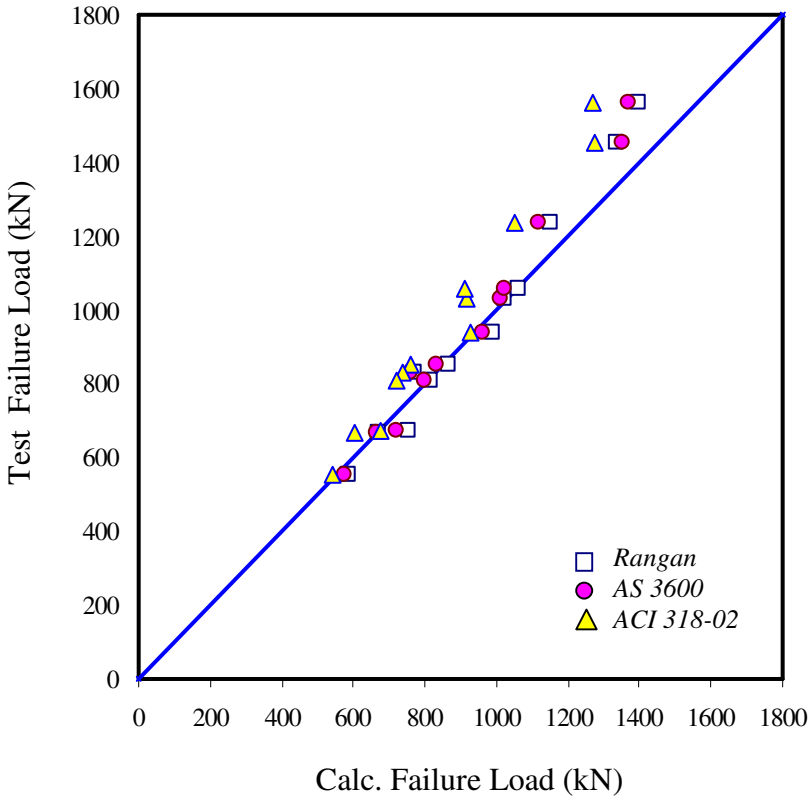


**Figure 5.2 Comparison of Test and Calculated Failure Loads of Columns**

# CHAPTER 6

# CONCLUSIONS

The research reported herein comprised experimental and analytical studies on the behaviour and strength of reinforced fly ash-based geopolymer concrete beams and columns. Low-calcium (ASTM Class F) dry fly ash obtained from a local power station was used as the source material to make geopolymer concrete. Sodium silicate solution and sodium hydroxide solution were mixed together to form the alkaline liquid. The silicon and the aluminium in fly ash reacted with the alkaline liquid to form the geopolymer paste that bound the loose aggregates and other un-reacted materials to produce the geopolymer concrete. The aggregates consisted of 10mm and 7mm granite-type coarse aggregates, and fine sand. The mixture proportions and the manufacturing process used to make the geopolymer concrete were based on earlier research at Curtin (Hardjito and Rangan 2005).

Twelve reinforced geopolymer concrete beams and twelve reinforced geopolymer concrete columns were made and tested. The test results were compared with the predictions of methods of calculations available for reinforced Portland cement concrete and the design provisions given in the Australian Standard for Concrete Structures AS3600 and the American Concrete Institute Building Code ACI318-02. The major conclusions drawn from this research are presented in the following Sections.

## 6.1 Reinforced Geopolymer Concrete Beams

Twelve 200 mm wide by 300 mm deep by 3300 mm long rectangular doubly-reinforced geopolymer concrete beams were manufactured and tested. The beams were simply supported over a span of 3000 mm and loaded with two concentrated loads placed symmetrically over the span. The distance between the concentrated loads was 1000 mm. The test parameters were the tensile reinforcement ratio and the concrete compressive strength. From the experimental and analytical studies the following conclusions are made:

1. The crack patterns observed for reinforced geopolymer concrete beams were similar to those reported in the literature for reinforced Portland cement

concrete beams. All beams failed in flexure in a ductile manner accompanied by crushing of the concrete in the compression zone.

2 As expected, the cracking moment increased as the concrete compressive strength increased.

3. The cracking moments of reinforced geopolymer concrete beams were calculated using the design provisions contained in the draft AS3600 (2005). The mean value of test/calculated cracking moments is 1.35 with a standard deviation of 0.09.
4. As expected, the flexural capacity of the beams was influenced by the longitudinal tensile reinforcement ratio and the concrete compressive strength. As the longitudinal tensile reinforcement ratio increased, the flexural capacity of the beams increased significantly. Because the test beams were under-reinforced, the flexural capacity increased only marginally when the compressive strength of concrete increased.
5. The ductility of reinforced geopolymer concrete beams, as indicated by the ratio of mid-span deflection at ultimate moment-to-mid-span deflection at yield moment, increased as the tensile reinforcement ratio decreased. Test results showed that the ductility increased significantly for beams with tensile reinforcement ratio less than 2%. For beams with tensile reinforcement ratio greater than 2%, the ductility was moderately unaffected. These test trends are comparable to the behaviour of reinforce Portland cement concrete beams.
6. The flexural capacity of test beams were calculated using the flexural design provisions contained in the draft AS3600 (2005). Good correlation is found between the test and calculated ultimate bending moments. In the case of beams with low tensile steel ratio, the test values are conservative due to the neglect of the strain-hardening effect of tensile steel bars on the ultimate bending moment. In all, the mean value of ratio of test/calculated ultimate moments is 1.11 with a standard deviation of 0.14.
7. The measured service load deflections of test beams were compared with the values calculated using the serviceability provisions of draft AS3600 (2005). For the purpose of these calculations, the service load was taken as the failure load/1.5. Good correlation between test and calculated values is found. The mean value of ratio of test/calculated deflections is 1.15 with a standard deviation of 0.06.

8. The study demonstrated that the design provisions contained in the draft Australian Standard for Concrete Structures AS3600 (2005) are applicable to reinforced geopolymer concrete beams.

## 6.2 Reinforced Geopolymer Concrete Columns

Twelve 175 mm wide by 175 mm deep by 1500 mm long square reinforced geopolymer concrete columns were manufactured and tested. The test columns were subjected to eccentric compression in single curvature bending. The columns were pin-ended, and the effective length was 1684 mm. The test parameters were the longitudinal reinforcement ratio, the concrete compressive strength, and the load eccentricity. From the experimental and analytical studies the following conclusions are drawn:

1. The crack patterns and failure modes observed for geopolymer concrete columns were similar to those reported in the literature for reinforced Portland cement concrete columns. Flexural cracks initiated at column mid-height, followed by cracks along the length of the column. Failure of the columns occurred in the region plus or minus 250 mm from the mid-height. The mode of failure was flexural, as indicated by opening of the cracks and the crushing of the concrete in the compression zone in the mid-height region. The longitudinal bars in the compression zone buckled especially when the load-eccentricity was low.
2. As expected, the capacity of test columns was influenced by the longitudinal reinforcement ratio, concrete compressive strength, and the load-eccentricity. The failure load of test columns increased as the load-eccentricity decreased, and as the longitudinal reinforcement ratio and concrete compressive strength increased.
3. The mid-height deflection of test columns decreased as the load-eccentricity decreased. The behaviour of geopolymer test columns was similar to that of reinforced Portland cement columns reported in the literature.
4. The load capacity of test columns were calculated using a simplified stability analysis proposed by Rangan (1990) for reinforced Portland cement concrete columns, and the design provisions contained in Section 10.4 of AS3600 and Rule 10.12 of ACI318-02. Good correlation between test and calculated failure

loads is found. The mean value of test failure load/calculated failure load is 1.01 with a standard deviation of 0.07 in the case of simplified stability analysis. The mean value of test failure load/calculated failure load and the standard deviation are, respectively, 1.03 and 0.06 for AS3600, and 1.11 and 0.08 for ACI318.

5. The study demonstrated that the design provisions contained in the Australian Standard for Concrete Structures AS3600 and the American Concrete Institute Building Code ACI318-02 are applicable to reinforced geopolymer concrete columns.

# REFERENCES


ACI 318-02 (2002) “Building Code Requirements for Structural Concrete.” Reported by ACI Committee 318, American Concrete Institute, Farmington Hills, MI.

ACI 232.2R-03 (2003) “Use of Fly Ash in Concrete.” Reported by ACI Committee 232, American Concrete Institute, Farmington Hills, MI.

Balaguru, P N, Kurtz, S, & Rudolph, J. (1997) “Geopolymer for Repair and Rehabilitation of Reinforced Concrete Beams.” The State University of New Jersey Rutgers, Geopolymer Institute:5.

Bhanumathidas, N. and Kalidas, N. (2004) “Fly ash for Sustainable Development.” Ark communications, Chennai.

Brooke, N.J., Keyte, L.M., South, W., Megget, L.M., and Ingham, J.M. (2005) “Seismic Performance of ‘Green Concrete’ Interior Beam-Column Joints.” In Proceeding of Australian Structural Engineering Conference (ASEC), September 2005, Newcastle.

Cheng, T. W. and Chiu J.P. (2003) "Fire-resistant Geopolymer Produced by Granulated Blast Furnace Slag." Minerals Engineering 16(3): pp. 205-210.

Cross, D., Stephens, J., and Vollmer, J. (2005) “Field Trials 0f 100% Fly Ash Concrete.” Concrete International, Vol.27:9, pp.47- 51

Davidovits, J. & Sawyer, J. L. (1985) Early high-strength mineral, US Patent No.4, 509,985, 1985.

Davidovits, J. (1988) “Soft Mineralurgy and Geopolymers.” In proceeding of Geopolymer 88 International Conference, the Université de Technologie, Compiègne, France.

Davidovits, J. (1994) “High-Alkali Cements for 21$^{st}$ Century Concretes. in Concrete Technology, Past, Present and Future.” In proceedings of V. Mohan Malhotra Symposium. 1994. Editor: P. Kumar Metha, ACI SP- 144. pp. 383-397.

Davidovits, J. (1999) “Chemistry of geopolymer systems, terminology.” In Proceedings of Geopolymer ‘99 International Conferences, France.

Gourley, T. (2000) “Inorganic Polymer.” Personal Communication.

Hardjito, D., Wallah, S. E. & Rangan, B. V. (2002) “Study on Engineering Properties of Fly Ash-Based Geopolymer Concrete.” Journal of the Australasian Ceramic Society, vol. 38, no. 1, pp. 44-47.

Hardjito, D., Wallah, S. E., Sumajouw, D. M. J. & Rangan B. V. (2004a) “Properties of Geopolymer Concrete with Fly Ash as Source Material: Effect of Mixture Composition.” In Proceedings of the Seventh CANMET/ACI International Conference on Recent Advances in Concrete Technology, Las Vegas, SP-222-8, pp. 109-118.

Hardjito, D., Wallah, S. E., Sumajouw, D. M. J. & Rangan B. V. (2004b) “On the development of fly ash based geopolymer concrete.” Technical paper No. 101-M52, ACI Material Journal, Vol. 101, No. 6, November-December, American Concrete Institute.

Hardjito, D., Wallah, S. E., Sumajouw, D. M. J. & Rangan, B. V. (2004c) “The Stress-Strain Behaviour of Fly Ash-Based Geopolymer Concrete.” In *Development in Mechanics of Structures & Materials*, vol. 2, Eds. A.J. Deeks and Hong Hao, A.A. Balkema Publishers - The Netherlands, pp. 831-834.

Hardjito, D., Wallah, S. E., Sumajouw, D. M. J. & Rangan, B. V. (2005) “Effect of Mixing Time and Rest Period on the Engineering Properties of Fly Ash-Based Geopolymer Concrete.” In proceeding of Geopolymer 2005 Fourth International Conference, Saint-Quentin, France.

Hardjito, D. and Rangan, B. V. (2005) “Development and Properties of Low-Calcium Fly Ash-based Geopolymer Concrete.” Research Report GC-1, Faculty of Engineering, Curtin University of Technology.

Kilpatrick. A. E. and Rangan, B.V. (1999) “Test on High-Strength Concrete-Filled Steel Tubular Columns.” ACI Structural Journal, Vol. 96:2, pp.268-274

Malhotra, V. M. (2002) “Introduction: Sustainable development and concrete technology, ACI Board Task Group on Sustainable Development.” ACI Concrete International, 24(7); 22.

Malhotra, V. M. (1999) “Making concrete ‘greener’ with fly ash.” ACI Concrete International, 21, pp. 61-66.

Malhotra, V. M. and Ramezanianpour A.A. (1994). “Fly Ash in Concrete.” Ottawa, Ontario, Canada, CANMET.

Metha, P. K. (2001) “Reducing the environmental impact of concrete.” ACI Concrete International, 23(10); pp. 61-66.

Palomo, A., Fernandez-Jimenez, A., Lopez-Hombrados, C., Lleyda, J.L. (2004) “Precast Elements Made of Alkali-Activated Fly Ash Concrete. Eighth CANMET/ACI International Conference on Fly Ash, Silica Fume, Slag, and Natural Pozzolans in Concrete”, Las Vegas, USA.

Palomo, A., Grutzeck, M. W., & Blanco, M. T. (1999) “Alkali-activated fly ash cement for future.” Cement and Concrete Research, 29(8); pp.1323-1329.

Rangan, B.V. (1990) “Strength of Reinforced Concrete Slender Columns.” ACI Structural Journal, Vol. 87. No.1, pp. 32-38.

Standards Australia (2005) “Concrete Structures.” Draft Australian Standard to be AS3600-200x, Committee-BD-002-Concrete Structures, Standards Australia

Standards Australia (2001) “Concrete Structures, AS3600-2001”, Standards Australia.

Standards Australia (2000). “Methods for Sampling and Testing Aggregate.” Method 5: Particle Density and Water Absorption of Fine Aggregates, Standards Australia: 8.

Standards Australia (2000). “Methods for Sampling and Testing Aggregates.” Method 6.1: Particle Density and Water Absorption of Coarse Aggregate - Weighing in Water Method: 8.

Swanepoel, J. C. & Strydom, C. A. (2002) "Utilisation of fly ash in geopolymeric material." Journal of Applied Geochemistry, 17:pp.1143-1148.

van Jaarsveld, J. G. S., van Deventer, J. S. J., & Schartzman, A.(1999) "The potential use of geopolymer materials to immobilise toxic metals: Part II, Material and leaching characteristics." Mineral Engineering, 12(1),pp.75-91.

van Jaarsveld, J. G. S., van Deventer J. S. J., & Lukey, G. C. (2002) "The effect of composition and temperature on the properties of fly ash and kaolinite-based geopolymers." Chemical Engineering Journal, 4001:1-11.

Wallah, S. E., Hardjito D., Sumajouw, D. M. J., and Rangan, B. V. (2005a) "Sulfate and Acid Resistance of Fly Ash-Based Geopolymer Concrete." In Proceeding of Australian Structural Engineering Conference (ASEC), September 2005, Newcastle.

Wallah, S. E., Hardjito, D., Sumajouw D. M. J., and Rangan, B. V. (2005b) "Creep and Drying Shrinkage Behaviour of Fly Ash-Based Geopolymer Concrete." In proceedings of the 22nd Biennial Conference Concrete 2005, Melbourne.

Wallah, S.E. and Rangan, B.V. (2006) "Low-Calcium Fly Ash-Based Geopolymer Concrete: Long-Term Properties", Research Report GC2, Faculty of Engineering. Curtin University of Technology.

Warner, R.F., Rangan, B.V., Hall, A.S., & Faulkes, K. A. (1998) "Concrete Structures," Melbourne, Longman.

Xu, H and van Deventer J.S.J (2000) "The Geopolymerisation of Alumino-Silicate Minerals." International Journal of Mineral Processing 59(3): 247-226.

# APPENDIX A TEST DATA

## A.1 Beams

### Table A.1.1 Test Data Beam GBI-1

| Total Load P (kN) | Mid-span Deflection (mm) |
|---|---|
| 1.26808 | 0.05652 |
| 4.84453 | 0.16957 |
| 7.26598 | 0.28262 |
| 10.42894 | 0.39567 |
| 13.1384 | 0.50872 |
| 16.29312 | 0.62177 |
| 19.47046 | 0.79135 |
| 22.16735 | 1.01744 |
| 24.62191 | 1.69574 |
| 26.7406 | 2.43056 |
| 28.99707 | 2.82623 |
| 31.67653 | 3.33495 |
| 33.85866 | 3.9002 |
| 34.65616 | 4.18282 |
| 36.84353 | 4.8046 |
| 39.46952 | 5.25679 |
| 42.22905 | 6.04814 |
| 44.90665 | 6.55686 |
| 46.91574 | 6.95253 |
| 49.61722 | 7.63083 |
| 52.43358 | 8.2526 |
| 55.50402 | 8.87437 |
| 58.66466 | 9.60919 |
| 61.48495 | 10.28749 |
| 64.23471 | 11.07883 |
| 67.31746 | 11.87018 |
| 71.25543 | 12.77457 |
| 74.35072 | 13.79202 |
| 79.14042 | 15.60081 |
| 83.65507 | 17.52264 |
| 88.04538 | 19.84015 |
| 92.78078 | 23.34468 |
| 96.00191 | 27.58403 |
| 99.52293 | 33.80175 |
| 102.9841 | 39.96293 |
| 106.5204 | 48.89383 |
| 108.4633 | 56.63771 |
| 106.0878 | 58.16387 |
| 103.1854 | 58.6726 |
| 99.90723 | 59.01174 |
| 93.74011 | 59.74656 |
| 83.25602 | 59.91614 |
| 69.89394 | 61.15968 |

**Table A.1.2 Test Data Beam GBI-2**

| Total Load P (kN) | Mid-span Deflection (mm) |
|---|---|
| 1.69155 | 0.05652 |
| 6.81629 | 0.33915 |
| 11.9101 | 0.56525 |
| 15.38975 | 0.84787 |
| 19.81434 | 1.35659 |
| 24.2657 | 1.86531 |
| 28.85328 | 2.60013 |
| 32.20113 | 2.93928 |
| 36.82648 | 3.56105 |
| 41.58893 | 4.18282 |
| 45.73151 | 4.8046 |
| 50.26197 | 5.42637 |
| 54.78097 | 6.04814 |
| 59.35846 | 6.66991 |
| 64.22453 | 7.23516 |
| 68.79757 | 7.85693 |
| 73.11982 | 8.30912 |
| 77.52289 | 9.04395 |
| 82.04387 | 9.72224 |
| 85.47618 | 10.17444 |
| 89.98622 | 10.85273 |
| 94.29515 | 11.53103 |
| 98.67381 | 12.43542 |
| 103.4624 | 13.17025 |
| 107.5254 | 13.79202 |
| 111.3975 | 14.41379 |
| 115.7272 | 15.26166 |
| 120.382 | 16.22258 |
| 125.3862 | 17.24002 |
| 129.8094 | 18.37051 |
| 133.6075 | 19.38796 |
| 140.6102 | 21.42285 |
| 146.2565 | 23.79688 |
| 151.0943 | 25.83177 |
| 157.0723 | 29.27977 |
| 162.1396 | 33.4626 |
| 165.1509 | 37.41932 |
| 168.0708 | 42.22392 |
| 171.1852 | 46.01107 |
| 170.8942 | 46.18064 |
| 167.6121 | 47.19809 |
| 167.2152 | 47.93291 |
| 165.5045 | 48.66773 |
| 163.0107 | 49.00688 |
| 159.9441 | 50.25042 |
| 162.8118 | 90.04378 |

**Table A.1.3 Test Data Beam GBI-3**

| Total Load P (kN) | Mid-span Deflection (mm) |
|---|---|
| 1.69523 | 0.05652 |
| 8.60178 | 0.33915 |
| 14.56613 | 0.6783 |
| 20.74164 | 1.18702 |
| 26.66542 | 1.75226 |
| 32.25399 | 2.37404 |
| 38.05109 | 2.88276 |
| 43.92188 | 3.448 |
| 49.88509 | 4.01325 |
| 56.15009 | 4.5785 |
| 70.33842 | 5.93509 |
| 76.40172 | 6.50034 |
| 82.46311 | 7.06558 |
| 88.58877 | 7.63083 |
| 95.14021 | 8.2526 |
| 101.3649 | 8.87437 |
| 107.8505 | 9.49614 |
| 113.8728 | 10.00486 |
| 119.2309 | 10.57011 |
| 125.2842 | 11.13536 |
| 130.4609 | 11.64408 |
| 136.6502 | 12.26585 |
| 144.5721 | 13.00067 |
| 150.4005 | 13.62244 |
| 156.2042 | 14.18769 |
| 162.7485 | 14.86598 |
| 169.5216 | 15.43123 |
| 175.146 | 15.99648 |
| 182.5465 | 16.7313 |
| 188.0969 | 17.29655 |
| 194.2278 | 17.69222 |
| 199.8892 | 18.48356 |
| 204.9627 | 19.16186 |
| 209.852 | 20.12278 |
| 214.5034 | 20.80107 |
| 219.5492 | 21.98809 |
| 222.4729 | 22.60986 |
| 226.5843 | 23.40121 |
| 229.3742 | 27.86666 |
| 218.9758 | 28.60148 |
| 212.7581 | 33.2365 |
| 208.7568 | 34.81919 |
| 202.6267 | 35.72358 |
| 197.1503 | 44.9371 |
| 194.9757 | 46.68937 |
| 190.2067 | 48.49816 |

**Table A.1.4 Test Data Beam GBI-4**

| Total Load P (kN) | Mid-span Deflection (mm) |
|---|---|
| 1.90407 | 0.05652 |
| 10.21979 | 0.4522 |
| 19.10043 | 1.01744 |
| 28.48619 | 1.69574 |
| 38.30102 | 2.43056 |
| 46.58322 | 3.10886 |
| 55.7146 | 3.78715 |
| 64.13797 | 4.40892 |
| 72.85799 | 5.03069 |
| 80.52036 | 5.65247 |
| 88.55124 | 6.21771 |
| 96.20696 | 6.78296 |
| 106.00179 | 7.5743 |
| 114.12787 | 8.13955 |
| 122.23866 | 8.7048 |
| 130.44379 | 9.38309 |
| 139.14834 | 10.00486 |
| 147.67432 | 10.62664 |
| 155.90461 | 11.36146 |
| 163.51659 | 11.9267 |
| 181.08471 | 13.28329 |
| 189.94707 | 14.01812 |
| 197.15286 | 14.69641 |
| 212.14868 | 15.88343 |
| 221.68271 | 16.61825 |
| 238.41333 | 18.08789 |
| 247.42456 | 18.93576 |
| 256.55188 | 19.78363 |
| 266.03383 | 20.68802 |
| 274.14871 | 21.59242 |
| 282.11738 | 22.44029 |
| 290.35052 | 23.34468 |
| 298.35025 | 24.58823 |
| 306.72526 | 26.05787 |
| 312.65381 | 26.67964 |
| 316.14517 | 27.41446 |
| 318.06073 | 27.86666 |
| 320.48986 | 29.22325 |
| 308.72736 | 29.78849 |
| 291.08772 | 30.12764 |
| 263.95242 | 32.21906 |
| 259.01874 | 38.15414 |
| 251.61819 | 47.02851 |
| 249.15135 | 48.21553 |
| 246.68451 | 49.5156 |
| 231.88344 | 52.05921 |

**Table A.1.5 Test Data Beam GBII-1**

| Total Load P (kN) | Mid-span Deflection (mm) |
|---|---|
| 0.28948 | 0.02101 |
| 4.04816 | 0.21014 |
| 8.14633 | 0.48331 |
| 12.37534 | 0.71446 |
| 16.14333 | 0.88257 |
| 20.41527 | 1.2398 |
| 24.18712 | 1.66007 |
| 28.77986 | 2.41656 |
| 32.00731 | 3.42521 |
| 36.19535 | 4.09765 |
| 40.18361 | 5.4215 |
| 43.31321 | 5.75772 |
| 47.08457 | 6.74536 |
| 50.70016 | 7.48083 |
| 53.95433 | 8.09023 |
| 57.39927 | 8.90976 |
| 61.33474 | 10.04449 |
| 64.13797 | 10.6749 |
| 70.15707 | 12.10382 |
| 73.51199 | 12.94436 |
| 77.85807 | 14.3943 |
| 81.64774 | 15.73917 |
| 85.05404 | 17.14708 |
| 88.66342 | 18.8912 |
| 91.17326 | 20.84546 |
| 92.13666 | 21.45486 |
| 94.09252 | 23.97649 |
| 97.87571 | 28.11616 |
| 98.30004 | 28.36832 |
| 100.7178 | 33.7478 |
| 103.6075 | 38.01356 |
| 107.5759 | 46.81824 |
| 107.9842 | 47.5327 |
| 108.1712 | 48.73048 |
| 109.8171 | 52.40786 |
| 110.8359 | 54.15198 |
| 111.1233 | 54.27806 |
| 108.8714 | 54.32009 |
| 104.9771 | 54.50921 |
| 99.94976 | 54.59327 |
| 96.70033 | 54.63529 |
| 94 | 55 |
| 92 | 62 |
| 90 | 71 |

**Table A.1.6 Test Data Beam GBII-2**

| Total Load P (kN) | Mid-span Deflection (mm) |
|---|---|
| 4.65122 | 0.05652 |
| 9.14376 | 0.2261 |
| 14.55017 | 0.4522 |
| 20.17666 | 0.73482 |
| 24.96683 | 1.01744 |
| 29.0284 | 1.52617 |
| 32.3094 | 1.80879 |
| 37.8956 | 2.48708 |
| 42.10101 | 3.22191 |
| 46.37893 | 3.78715 |
| 50.36177 | 4.3524 |
| 54.7871 | 4.97417 |
| 59.00647 | 5.59594 |
| 63.52568 | 6.27424 |
| 69.02061 | 6.89601 |
| 73.20778 | 7.46126 |
| 77.90497 | 8.19608 |
| 82.47012 | 8.87437 |
| 86.75148 | 9.55267 |
| 91.78582 | 10.34401 |
| 96.13586 | 11.13536 |
| 100.8064 | 11.75713 |
| 105.4133 | 12.32238 |
| 110.6179 | 13.22677 |
| 115.7511 | 14.07464 |
| 121.3837 | 15.14861 |
| 127.6123 | 16.2791 |
| 132.8786 | 17.1835 |
| 138.4857 | 18.65314 |
| 144.5714 | 20.06625 |
| 150.0085 | 22.04462 |
| 156.6989 | 24.92737 |
| 162.1725 | 28.03623 |
| 166.2376 | 30.86246 |
| 170.9975 | 35.10181 |
| 174.6903 | 38.83244 |
| 179.3666 | 47.19809 |
| 173.6648 | 48.27206 |
| 171.5655 | 55.90289 |
| 170.7908 | 61.55535 |
| 170.0865 | 69.01661 |
| 168.854 | 84.67393 |
| 167.6215 | 88.0089 |
| 154.3104 | 88.34804 |
| 147.197 | 88.40456 |
| 140.5063 | 88.51762 |

**Table A.1.7 Test Data Beam GBII-3**

| Total Load P (kN) | Mid-span Deflection (mm) |
|---|---|
| 0.40564 | 0.05652 |
| 8.21674 | 0.16957 |
| 15.11975 | 1.18702 |
| 22.25007 | 1.46964 |
| 28.58093 | 1.80879 |
| 34.63737 | 2.20446 |
| 40.65446 | 2.76971 |
| 46.66424 | 3.22191 |
| 53.93468 | 4.01325 |
| 60.04794 | 4.63502 |
| 66.5556 | 5.25679 |
| 72.85088 | 5.82204 |
| 79.07791 | 6.38729 |
| 85.21392 | 6.95253 |
| 91.20582 | 7.51778 |
| 105.3886 | 8.81785 |
| 111.2838 | 9.43962 |
| 117.9102 | 10.00486 |
| 123.0236 | 10.51359 |
| 129.7423 | 11.13536 |
| 136.8812 | 11.75713 |
| 142.6105 | 12.3789 |
| 148.6626 | 13.0572 |
| 155.0992 | 13.62244 |
| 162.6915 | 14.41379 |
| 170.3648 | 15.14861 |
| 178.8902 | 15.99648 |
| 186.3483 | 16.7313 |
| 194.3043 | 17.52264 |
| 200.8993 | 18.20094 |
| 206.8612 | 18.93576 |
| 213.0151 | 19.78363 |
| 220.8458 | 21.02717 |
| 226.7025 | 22.10114 |
| 231.3087 | 23.06206 |
| 235.4507 | 26.51007 |
| 239.1071 | 30.46679 |
| 232.5338 | 30.63636 |
| 212.533 | 31.20161 |
| 210.9355 | 31.82338 |
| 206.2402 | 35.61053 |
| 202.1318 | 42.28045 |
| 199.6668 | 54.94197 |
| 186.7254 | 59.12479 |
| 183.0279 | 62.00755 |
| 175.0166 | 70.3732 |

**Table A.1.8 Test Data Beam GBII-4**

| Total Load P (kN) | Mid-span Deflection (mm) |
|---|---|
| 0.70481 | 0.05652 |
| 9.14847 | 0.6783 |
| 18.70529 | 1.18702 |
| 27.60074 | 1.75226 |
| 36.37551 | 2.31751 |
| 45.74876 | 3.05233 |
| 55.7707 | 3.78715 |
| 62.13105 | 4.29587 |
| 70.68927 | 4.91765 |
| 79.02127 | 5.53942 |
| 87.49078 | 6.16119 |
| 96.82367 | 6.83948 |
| 105.9202 | 7.46126 |
| 116.4043 | 8.19608 |
| 125.8817 | 8.98742 |
| 135.3681 | 9.66572 |
| 144.1254 | 10.34401 |
| 155.0258 | 11.13536 |
| 163.3874 | 11.81365 |
| 171.4914 | 12.3789 |
| 181.0664 | 13.11372 |
| 189.4696 | 13.79202 |
| 198.3792 | 14.47031 |
| 206.4095 | 15.09208 |
| 214.8358 | 15.77038 |
| 224.1066 | 16.44868 |
| 232.7571 | 17.1835 |
| 241.2575 | 17.80527 |
| 250.2987 | 18.59661 |
| 258.8966 | 19.33143 |
| 266.0127 | 19.89668 |
| 275.7174 | 20.68802 |
| 283.4629 | 21.53589 |
| 293.7124 | 22.66639 |
| 306.5513 | 24.19255 |
| 315.6376 | 25.04042 |
| 321.6208 | 25.83177 |
| 326.5206 | 26.51007 |
| 330.9871 | 27.47098 |
| 325.393 | 28.82758 |
| 315.0695 | 31.82338 |
| 304.6979 | 34.08437 |
| 297.666 | 36.62798 |
| 278.0487 | 42.95874 |
| 261.4856 | 47.59376 |
| 246.6845 | 48.72425 |
| 160.3449 | 51.83311 |

**Table A.1.9 Test Data Beam GBIII-1**

| Total Load P (kN) | Mid-span Deflection (mm) |
|---|---|
| 8.60174 | 0.05652 |
| 14.50158 | 0.16957 |
| 18.04019 | 0.33915 |
| 21.70236 | 0.4522 |
| 25.06106 | 0.62177 |
| 28.59426 | 0.73482 |
| 31.0972 | 0.84787 |
| 34.89447 | 1.13049 |
| 38.86411 | 1.92184 |
| 42.2223 | 2.82623 |
| 45.64856 | 3.78715 |
| 48.83534 | 4.29587 |
| 52.60039 | 5.59594 |
| 55.91296 | 6.27424 |
| 60.1316 | 6.95253 |
| 63.2132 | 8.2526 |
| 66.45289 | 8.98742 |
| 69.60553 | 9.72224 |
| 72.96465 | 10.45706 |
| 76.29445 | 11.47451 |
| 82.21797 | 13.11372 |
| 85.43247 | 13.84854 |
| 88.61754 | 15.14861 |
| 92.24871 | 16.44868 |
| 96.01463 | 17.97484 |
| 99.72775 | 99.72775 |
| 102.7093 | 21.47937 |
| 105.6387 | 24.19255 |
| 108.2714 | 27.18836 |
| 110.3206 | 29.3363 |
| 113.0315 | 33.97132 |
| 116.0532 | 39.73684 |
| 119.7076 | 44.65448 |
| 120.8309 | 48.8373 |
| 123.3281 | 52.90708 |
| 125.6757 | 58.2204 |
| 127.4078 | 62.5728 |
| 127.0761 | 64.04243 |
| 128.4656 | 67.03825 |
| 129.956 | 69.75143 |
| 130.3504 | 73.93425 |
| 125.7161 | 76.19524 |
| 130.2437 | 75.29085 |
| 130.6462 | 77.15616 |
| 125.7161 | 76.19524 |
| 78.88071 | 79.98239 |

**Table A.1.10 Test Data Beam GBIII-2**

| Total Load P (kN) | Mid-span Deflection (mm) |
|---|---|
| 5.66955 | 0.05652 |
| 9.57775 | 0.28262 |
| 14.9852 | 0.4522 |
| 21.82637 | 0.73482 |
| 26.98818 | 0.96092 |
| 31.32439 | 1.13049 |
| 36.33625 | 1.46964 |
| 41.46293 | 1.86531 |
| 46.57594 | 2.31751 |
| 51.48259 | 2.93928 |
| 56.36127 | 3.448 |
| 61.62555 | 4.46545 |
| 65.28457 | 5.08722 |
| 71.09643 | 5.82204 |
| 77.22242 | 6.55686 |
| 82.73727 | 7.34821 |
| 87.99057 | 7.96998 |
| 91.20582 | 8.59175 |
| 96.24623 | 9.21352 |
| 101.6942 | 10.00486 |
| 107.016 | 10.73969 |
| 112.2234 | 11.58755 |
| 117.569 | 12.26585 |
| 122.4395 | 13.11372 |
| 127.6071 | 14.01812 |
| 132.3887 | 15.09208 |
| 137.425 | 16.10953 |
| 142.0469 | 16.9574 |
| 147.3731 | 18.20094 |
| 152.3931 | 19.50101 |
| 157.1452 | 20.8576 |
| 162.1686 | 22.89249 |
| 165.3619 | 24.7578 |
| 170.0329 | 26.96226 |
| 173.3989 | 28.99715 |
| 177.4816 | 32.04948 |
| 181.2739 | 34.81919 |
| 183.9376 | 37.3628 |
| 185.8542 | 40.92385 |
| 184.3109 | 42.84569 |
| 183.6441 | 44.71101 |
| 183.1049 | 45.05015 |
| 181.7883 | 45.50235 |
| 176.1464 | 47.70681 |
| 169.0301 | 49.34603 |
| 157.7614 | 49.62865 |

**Table A.1.11 Test Data Beam GBIII-3**

| Total Load P (kN) | Mid-span Deflection (mm) |
|---|---|
| 1.7148 | 0.05652 |
| 9.4437 | 0.73482 |
| 15.47125 | 1.01744 |
| 21.86368 | 1.24354 |
| 28.15315 | 1.46964 |
| 34.58655 | 1.69574 |
| 41.31993 | 2.14794 |
| 47.73179 | 2.54361 |
| 53.25079 | 2.88276 |
| 59.90395 | 3.448 |
| 73.6852 | 4.63502 |
| 79.6098 | 5.20027 |
| 85.27547 | 5.70899 |
| 91.37015 | 6.27424 |
| 97.45337 | 6.78296 |
| 103.1201 | 7.29168 |
| 111.096 | 8.0265 |
| 117.4066 | 8.59175 |
| 123.6683 | 9.15699 |
| 131.3572 | 9.77877 |
| 136.4652 | 10.17444 |
| 142.4956 | 10.79621 |
| 148.4027 | 11.36146 |
| 154.0423 | 11.87018 |
| 162.7956 | 12.605 |
| 170.3241 | 13.33982 |
| 176.5187 | 13.84854 |
| 183.3165 | 14.47031 |
| 191.2409 | 15.14861 |
| 198.5911 | 15.77038 |
| 207.1075 | 16.56173 |
| 212.9548 | 17.1835 |
| 220.1429 | 17.97484 |
| 228.4121 | 18.93576 |
| 234.2945 | 19.95321 |
| 237.0858 | 20.34888 |
| 243.3906 | 21.42285 |
| 250.4799 | 35.49749 |
| 239.518 | 35.83663 |
| 226.0004 | 37.02365 |
| 221.0974 | 42.39349 |
| 218.2718 | 48.55468 |
| 218.7857 | 51.66354 |
| 196.3801 | 52.28531 |
| 216.9219 | 52.79403 |
| 194.7367 | 52.85056 |

**Table A.1.12 Test Data Beam GBIII-4**

| Total Load P (kN) | Mid-span Deflection (mm) |
|---|---|
| 2.49097 | 0.05652 |
| 10.71954 | 0.4522 |
| 21.05387 | 0.79135 |
| 30.50154 | 1.13049 |
| 39.82956 | 1.69574 |
| 50.78972 | 2.37404 |
| 58.45027 | 3.10886 |
| 67.37727 | 3.6741 |
| 76.55263 | 4.29587 |
| 85.20127 | 4.91765 |
| 94.05007 | 5.53942 |
| 103.0174 | 6.16119 |
| 112.4429 | 6.78296 |
| 121.1433 | 7.34821 |
| 130.6119 | 8.0265 |
| 139.9947 | 8.64827 |
| 148.6004 | 9.21352 |
| 155.1514 | 9.66572 |
| 164.5696 | 10.28749 |
| 175.6433 | 11.07883 |
| 183.0656 | 11.58755 |
| 194.2692 | 12.3789 |
| 216.3796 | 13.96159 |
| 227.528 | 14.75294 |
| 242.9416 | 15.77038 |
| 258.6561 | 16.90087 |
| 270.9788 | 17.74874 |
| 287.8126 | 18.99228 |
| 298.0291 | 19.89668 |
| 309.0668 | 20.97065 |
| 319.0613 | 21.98809 |
| 337.2561 | 23.96646 |
| 344.8456 | 24.9839 |
| 350.9295 | 25.88829 |
| 351.9087 | 26.96226 |
| 352.1522 | 28.99715 |
| 352.4981 | 30.97551 |
| 358.2699 | 34.14089 |
| 359.5197 | 36.96712 |
| 357.976 | 37.24975 |
| 344.9661 | 38.0411 |
| 338.9405 | 39.39769 |
| 311.0036 | 40.58471 |
| 305.0465 | 44.31533 |
| 300.7327 | 45.05015 |
| 294.8259 | 48.21553 |
| 293.3376 | 50.30695 |

## A.2 Columns

**Table A.2.1 Test Data Column GCI-1**

| Axial Load (kN) | Mid-height Deflection (mm) |
|---|---|
| 6.73166 | 0.00159 |
| 40.38924 | 0.05719 |
| 61.25796 | 0.13344 |
| 84.17885 | 0.20016 |
| 100.8629 | 0.23829 |
| 132.1693 | 0.31454 |
| 161.2835 | 0.40032 |
| 203.4915 | 0.53376 |
| 242.0332 | 0.6672 |
| 260.6827 | 0.72439 |
| 280.2359 | 0.79111 |
| 310.1409 | 0.88643 |
| 330.0932 | 0.95315 |
| 359.182 | 1.05799 |
| 389.422 | 1.15331 |
| 421.7095 | 1.25815 |
| 450.0311 | 1.363 |
| 481.624 | 1.47738 |
| 508.0971 | 1.57269 |
| 532.4514 | 1.66801 |
| 560.0337 | 1.78238 |
| 581.2061 | 1.86817 |
| 600.8381 | 1.95395 |
| 627.0011 | 2.07786 |
| 640.7261 | 2.14458 |
| 658.7224 | 2.23036 |
| 676.9698 | 2.30662 |
| 691.7169 | 2.38287 |
| 731.3425 | 2.63069 |
| 750.8696 | 2.74506 |
| 789.0548 | 3.01194 |
| 800.3415 | 3.10726 |
| 842.0458 | 3.47899 |
| 866.7514 | 3.7268 |
| 881.4809 | 3.89837 |
| 903.311 | 4.29869 |
| 920.564 | 4.64183 |
| 930.0706 | 4.98496 |
| 939.8707 | 5.44247 |
| 935.3521 | 5.72841 |
| 932.8874 | 5.8142 |
| 930.4227 | 5.89045 |
| 898.3817 | 6.59578 |

**Table A.2.2 Test Data Column GCI-2**

| Axial Load (kN) | Mid-height Deflection (mm) |
|---|---|
| 3.193988 | 0.005766 |
| 30.34285 | 0.149297 |
| 55.89472 | 0.284385 |
| 84.10775 | 0.427916 |
| 121.0782 | 0.706535 |
| 153.6738 | 0.976711 |
| 190.3097 | 1.272216 |
| 210.7315 | 1.466405 |
| 250.1666 | 1.812568 |
| 270.295 | 1.972985 |
| 290.218 | 2.141845 |
| 315.7549 | 2.38287 |
| 330.68 | 2.51631 |
| 357.2269 | 2.81178 |
| 375.9688 | 2.97382 |
| 395.7206 | 3.15492 |
| 410.3529 | 3.30742 |
| 425.8942 | 3.45992 |
| 440.6592 | 3.6029 |
| 453.6294 | 3.74587 |
| 470.1551 | 3.9365 |
| 483.4765 | 4.089 |
| 496.5242 | 4.23197 |
| 505.2627 | 4.34635 |
| 515.7226 | 4.46073 |
| 530.7569 | 4.65136 |
| 543.1172 | 4.83246 |
| 560.7526 | 5.09934 |
| 579.7929 | 5.34715 |
| 600.4958 | 5.69982 |
| 615.7889 | 5.9667 |
| 632.0576 | 6.27171 |
| 641.6782 | 6.47187 |
| 655.2218 | 6.89125 |
| 665.5064 | 7.30111 |
| 670.7054 | 7.64424 |
| 673.3902 | 8.0255 |
| 665.8787 | 8.19706 |
| 660.8466 | 8.26378 |
| 653.7606 | 8.3305 |
| 643.9018 | 8.41629 |
| 629.1136 | 8.5116 |
| 510.1921 | 10.74197 |

**Table A.2.3 Test Data Column GCI-3**

| Axial Load (kN) | Mid-height Deflection (mm) |
|---|---|
| 0.905411 | 0.000352 |
| 10.86479 | 0.004235 |
| 22.63496 | 0.008824 |
| 39.94861 | 0.02859 |
| 43.50188 | 0.05719 |
| 56.48262 | 0.1811 |
| 69.78171 | 0.30501 |
| 81.95114 | 0.42892 |
| 95.87667 | 0.54329 |
| 108.0358 | 0.65767 |
| 122.0025 | 0.78158 |
| 135.2502 | 0.91502 |
| 148.4979 | 1.03893 |
| 161.7457 | 1.16284 |
| 174.9934 | 1.30581 |
| 191.6301 | 1.46785 |
| 204.8779 | 204.8779 |
| 216.4825 | 1.73473 |
| 228.7546 | 1.8777 |
| 241.2664 | 2.0302 |
| 254.5483 | 2.23036 |
| 267.8303 | 2.44006 |
| 280.2711 | 2.59256 |
| 293.7096 | 2.79272 |
| 305.1088 | 2.95476 |
| 318.2196 | 3.14539 |
| 332.5286 | 3.33601 |
| 345.3313 | 3.52664 |
| 358.6133 | 3.7554 |
| 372.7853 | 3.98415 |
| 397.8723 | 4.44166 |
| 410.3308 | 4.68948 |
| 414.0337 | 4.7562 |
| 428.7846 | 5.05168 |
| 441.2366 | 5.28997 |
| 456.3795 | 5.65216 |
| 470.3461 | 6.07155 |
| 493.573 | 6.6339 |
| 506.0373 | 7.03422 |
| 520.3589 | 7.58705 |
| 534.2229 | 8.13988 |
| 554.0284 | 10.34164 |
| 546.5463 | 10.59899 |
| 539.7684 | 10.7515 |
| 504.0303 | 12.31466 |
| 481.8481 | 12.61013 |

**Table A.2.4 Test Data Column GCII-1**

| Axial Load (kN) | Mid-height Deflection (mm) |
|---|---|
| 14.78818 | 0.001058 |
| 56.91907 | 0.00953 |
| 93.00984 | 0.12391 |
| 131.8612 | 0.20969 |
| 173.9665 | 0.31454 |
| 213.4137 | 0.44798 |
| 254.6339 | 0.57189 |
| 296.5477 | 0.68627 |
| 336.431 | 0.80064 |
| 375.8661 | 0.91502 |
| 412.9393 | 1.0294 |
| 455.0885 | 1.16284 |
| 496.6362 | 1.30581 |
| 537.7967 | 1.42972 |
| 581.6683 | 1.55363 |
| 620.9088 | 1.67754 |
| 660.4088 | 1.82051 |
| 700.5214 | 1.95395 |
| 740.6411 | 2.09692 |
| 782.695 | 2.26849 |
| 824.4911 | 2.44006 |
| 865.2124 | 2.62115 |
| 900.5446 | 2.79272 |
| 930.0462 | 2.94522 |
| 960.2852 | 3.11679 |
| 990.3538 | 3.28836 |
| 1020.261 | 3.45992 |
| 1059.569 | 3.7554 |
| 1094.202 | 4.04134 |
| 1114.892 | 4.21291 |
| 1155.251 | 4.65136 |
| 1165.631 | 4.77527 |
| 1181.635 | 4.9659 |
| 1190.53 | 5.09934 |
| 1199.339 | 5.23278 |
| 1204.796 | 5.32809 |
| 1216.83 | 5.54732 |
| 1222.046 | 5.67122 |
| 1226.298 | 5.75701 |
| 1231.239 | 5.87139 |
| 1236.524 | 6.23358 |
| 1230.91 | 6.38608 |
| 1226.578 | 6.49093 |
| 1225.099 | 6.51953 |
| 1218.616 | 6.62437 |
| 1215.403 | 6.67203 |
| 1194.145 | 7.54892 |

**Table A.2.5 Test Data Column GCII-2**

| Axial Load (kN) | Mid-height Deflection (mm) |
|---|---|
| 3.236493 | 0.009624 |
| 24.27373 | 0.135191 |
| 43.69272 | 0.251099 |
| 63.11171 | 0.367007 |
| 84.14894 | 0.492574 |
| 103.5679 | 0.608482 |
| 124.6052 | 0.73392 |
| 144.0242 | 0.8483 |
| 165.0614 | 0.97221 |
| 184.4804 | 1.08659 |
| 205.9782 | 1.22956 |
| 223.231 | 1.33441 |
| 245.8534 | 1.45831 |
| 265.1191 | 1.58222 |
| 284.6724 | 1.71566 |
| 303.7738 | 1.83004 |
| 325.8328 | 1.97301 |
| 363.8948 | 2.22083 |
| 383.8764 | 2.3638 |
| 405.4425 | 2.49725 |
| 424.6671 | 2.62115 |
| 445.7308 | 2.76413 |
| 465.4168 | 2.9071 |
| 485.3911 | 3.05007 |
| 503.8021 | 3.19304 |
| 524.9063 | 3.35508 |
| 543.5603 | 3.49805 |
| 564.631 | 3.66962 |
| 605.0196 | 3.99369 |
| 624.4954 | 4.17478 |
| 644.7473 | 4.36541 |
| 664.8842 | 4.56557 |
| 684.9261 | 4.80386 |
| 704.458 | 5.07074 |
| 724.8671 | 5.37575 |
| 738.9789 | 5.57591 |
| 750.612 | 5.75701 |
| 770.2859 | 6.09061 |
| 805.3394 | 6.8436 |
| 825.5124 | 7.41548 |
| 849.0421 | 8.36863 |
| 838.9356 | 8.56879 |
| 826.0957 | 8.59739 |
| 783.8681 | 8.62598 |
| 699.6791 | 8.65457 |

**Table A.2.6 Test Data Column GCII-3**

| Axial Load (kN) | Mid-height Deflection (mm) |
|---|---|
| 2.136789 | 0.000537 |
| 16.46865 | 0.006356 |
| 32.86261 | 0.07625 |
| 49.74794 | 0.1811 |
| 65.53851 | 0.28594 |
| 83.25195 | 0.41938 |
| 95.87667 | 0.57189 |
| 121.5095 | 0.80064 |
| 138.177 | 0.92455 |
| 152.107 | 1.01987 |
| 168.4209 | 1.16284 |
| 184.236 | 1.29628 |
| 200.3446 | 1.42019 |
| 217.263 | 1.56316 |
| 233.2219 | 1.7252 |
| 250.6596 | 1.89676 |
| 266.6493 | 2.04927 |
| 282.2077 | 2.23036 |
| 297.612 | 2.3924 |
| 314.6595 | 2.5735 |
| 330.6801 | 2.73553 |
| 346.5979 | 2.94522 |
| 362.0259 | 3.17398 |
| 378.6389 | 3.36461 |
| 394.1973 | 3.55524 |
| 410.6457 | 3.76493 |
| 444.6916 | 4.2415 |
| 460.8981 | 4.4512 |
| 492.8878 | 4.91824 |
| 508.9597 | 5.15653 |
| 524.4814 | 5.44247 |
| 540.1135 | 5.71888 |
| 556.0628 | 5.98576 |
| 574.1445 | 6.3289 |
| 590.3507 | 6.67203 |
| 609.6928 | 7.08188 |
| 625.5557 | 7.50127 |
| 635.4707 | 7.78721 |
| 647.2084 | 8.3305 |
| 666.2895 | 9.37897 |
| 649.9403 | 9.98898 |
| 634.3511 | 10.26539 |
| 602.6182 | 10.68478 |
| 570.1663 | 11.05651 |
| 554.3431 | 11.10416 |
| 544.0816 | 11.4187 |

**Table A.2.7 Test Data Column GCIII-1**

| Axial Load (kN) | Mid-height Deflection (mm) |
|---|---|
| 4.587462 | 0.01175 |
| 41.287158 | 0.10572 |
| 77.986854 | 0.1997 |
| 114.68655 | 0.29368 |
| 151.38625 | 0.38765 |
| 188.08594 | 0.48163 |
| 224.78564 | 0.5756 |
| 261.48533 | 0.66958 |
| 298.18503 | 0.76355 |
| 334.88473 | 0.85753 |
| 371.58442 | 0.95151 |
| 408.28412 | 1.04548 |
| 444.98381 | 1.13946 |
| 481.68351 | 1.23344 |
| 527.55813 | 1.35091 |
| 564.25783 | 1.44488 |
| 600.95752 | 1.53886 |
| 637.29194 | 1.62323 |
| 673.56619 | 1.72014 |
| 711.20977 | 1.81705 |
| 746.16205 | 1.90184 |
| 786.23802 | 2.01087 |
| 824.7929 | 2.11989 |
| 859.28263 | 2.2168 |
| 897.24413 | 2.32582 |
| 932.58765 | 2.43484 |
| 972.47659 | 2.55598 |
| 1007.2275 | 2.665 |
| 1044.1791 | 2.78614 |
| 1079.655 | 2.90728 |
| 1117.539 | 3.04053 |
| 1154.9727 | 3.17378 |
| 1192.8786 | 3.33125 |
| 1228.0347 | 1228.0347 |
| 1264.9744 | 3.63409 |
| 1304.5635 | 3.82791 |
| 1341.0757 | 3.9975 |
| 1374.3564 | 4.17921 |
| 1401.7846 | 4.38514 |
| 1425.557 | 4.55473 |
| 1455.1291 | 4.93025 |
| 1447.6568 | 5.05139 |
| 1440.7597 | 5.12407 |
| 1430.1398 | 5.48748 |
| 1423.3619 | 5.57228 |
| 1414.7355 | 5.82666 |

**Table A.2.8 Test Data Column GCIII-2**

| Axial Load (kN) | Mid-height Deflection (mm) |
|---|---|
| 16.926224 | 0.01211 |
| 41.106544 | 0.13325 |
| 67.704896 | 0.2665 |
| 91.885216 | 0.38764 |
| 116.06554 | 0.50877 |
| 142.66389 | 0.64202 |
| 169.26224 | 0.77527 |
| 193.44256 | 0.89641 |
| 217.38619 | 1.01755 |
| 242.2444 | 1.16291 |
| 267.933 | 1.32039 |
| 290.34119 | 1.45364 |
| 315.68647 | 1.599 |
| 339.20378 | 1.74437 |
| 366.16139 | 1.90184 |
| 392.06272 | 2.05932 |
| 417.76596 | 2.20468 |
| 442.56696 | 2.36216 |
| 468.06402 | 2.51964 |
| 492.24599 | 2.665 |
| 519.08256 | 2.82248 |
| 543.67084 | 2.97996 |
| 567.90704 | 3.13743 |
| 592.93543 | 3.29491 |
| 617.58238 | 3.45239 |
| 642.72548 | 3.62198 |
| 668.98572 | 3.80369 |
| 693.28106 | 3.96116 |
| 718.43604 | 4.14287 |
| 743.14907 | 4.33669 |
| 768.40898 | 4.51839 |
| 794.36029 | 4.72432 |
| 815.28349 | 4.90603 |
| 843.23412 | 5.16041 |
| 868.10878 | 5.37846 |
| 894.06845 | 5.62073 |
| 917.37432 | 5.87512 |
| 942.69971 | 6.16585 |
| 968.6255 | 6.51714 |
| 994.6542 | 6.88055 |
| 1016.6871 | 7.23185 |
| 1029.1369 | 7.59526 |
| 1011.5112 | 7.8981 |
| 992.16334 | 8.12826 |
| 977.25195 | 8.45533 |
| 953.83734 | 9.36385 |

**Table A.2.9 Test Data Column GCIII-3**

| Axial Load (kN) | Mid-height Deflection (mm) |
|---|---|
| 2.6662123 | 0.01211 |
| 21.044711 | 0.06057 |
| 44.090673 | 0.16959 |
| 64.355948 | 0.31495 |
| 84.374757 | 0.46032 |
| 103.86933 | 0.59357 |
| 125.17135 | 0.73893 |
| 145.94521 | 0.89641 |
| 165.7508 | 1.02966 |
| 185.02825 | 1.17502 |
| 204.44653 | 1.30827 |
| 223.95124 | 1.45364 |
| 244.49783 | 1.61112 |
| 264.54402 | 1.76859 |
| 285.35701 | 1.92607 |
| 304.6638 | 2.08355 |
| 324.63566 | 2.25314 |
| 344.56449 | 2.44696 |
| 364.92904 | 2.665 |
| 384.49256 | 2.88305 |
| 403.79935 | 3.11321 |
| 424.74927 | 3.33125 |
| 463.979 | 3.76734 |
| 484.31275 | 3.98539 |
| 506.18693 | 4.22766 |
| 524.98022 | 4.48205 |
| 544.69781 | 4.72432 |
| 566.88007 | 4.9666 |
| 586.84411 | 5.22098 |
| 606.56166 | 5.4996 |
| 626.44357 | 5.7661 |
| 650.37165 | 6.09316 |
| 670.89023 | 6.42023 |
| 692.98008 | 6.77153 |
| 712.62575 | 7.13494 |
| 732.69935 | 7.52257 |
| 752.38085 | 7.91021 |
| 774.31576 | 8.45533 |
| 789.93506 | 8.90353 |
| 807.35598 | 9.40019 |
| 826.68145 | 10.72058 |
| 825.10438 | 10.79326 |
| 822.59226 | 10.9144 |
| 819.51141 | 10.98708 |
| 817.04669 | 817.04669 |
| 788.7027 | 14.22142 |

**Table A.2.10 Test Data Column GCIV-1**

| Axial Load (kN) | Mid-height Deflection (mm) |
|---|---|
| 5.36603 | 0.00727 |
| 37.56221 | 0.05088 |
| 75.12442 | 0.10175 |
| 112.68663 | 0.16959 |
| 150.24884 | 0.25439 |
| 193.17708 | 0.3513 |
| 230.73929 | 0.43609 |
| 268.3015 | 0.52089 |
| 305.86371 | 0.60568 |
| 348.79195 | 0.70259 |
| 386.35416 | 0.78739 |
| 424.38625 | 0.86007 |
| 463.16825 | 0.94486 |
| 503.19232 | 1.04177 |
| 543.05466 | 1.13868 |
| 584.09045 | 1.23559 |
| 624.38964 | 1.3325 |
| 663.25995 | 1.42941 |
| 703.11054 | 1.52632 |
| 747.18205 | 1.63534 |
| 783.58372 | 1.73225 |
| 824.50926 | 1.84127 |
| 866.66493 | 1.9503 |
| 908.63257 | 2.07143 |
| 948.11924 | 2.19257 |
| 986.94641 | 2.30159 |
| 1014.4715 | 2.38639 |
| 1054.6018 | 2.51964 |
| 1091.8222 | 2.64078 |
| 1130.2014 | 2.77403 |
| 1172.139 | 2.91939 |
| 1212.3261 | 3.07687 |
| 1249.1104 | 3.23434 |
| 1294.1006 | 3.42816 |
| 1329.0113 | 3.60987 |
| 1371.4764 | 3.8158 |
| 1410.4118 | 4.04596 |
| 1449.6607 | 4.33669 |
| 1481.309 | 4.55473 |
| 1510.7783 | 4.82123 |
| 1533.3695 | 5.11196 |
| 1558.0986 | 5.59651 |
| 1554.551 | 5.74187 |
| 1549.8829 | 5.82666 |
| 1533.0409 | 6.12951 |
| 1473.8882 | 7.13494 |

**Table A.2.11 Test Data Column GCIV-2**

| Axial Load (kN) | Mid-height Deflection (mm) |
|---|---|
| 8.9345225 | 0.002422 |
| 32.258521 | 0.03634 |
| 59.694934 | 0.14536 |
| 85.820712 | 0.24227 |
| 114.66704 | 0.33918 |
| 140.04755 | 0.4482 |
| 167.26323 | 0.56934 |
| 195.06308 | 0.69048 |
| 211.47091 | 0.76316 |
| 237.84315 | 0.8843 |
| 265.87907 | 1.01755 |
| 290.58766 | 1.13868 |
| 316.71343 | 1.24771 |
| 344.16117 | 1.38096 |
| 371.4969 | 1.51421 |
| 396.69281 | 1.63534 |
| 423.83291 | 1.76859 |
| 449.22709 | 1.90184 |
| 476.80663 | 2.05932 |
| 503.48261 | 2.20468 |
| 529.90963 | 2.35005 |
| 556.40512 | 2.49541 |
| 583.78083 | 2.65289 |
| 609.32762 | 2.79825 |
| 636.15562 | 2.96784 |
| 662.81363 | 3.13743 |
| 682.85769 | 3.27068 |
| 708.18931 | 3.44028 |
| 735.14296 | 3.63409 |
| 761.80854 | 3.84003 |
| 787.69041 | 4.04596 |
| 810.23637 | 4.23978 |
| 840.02769 | 4.49416 |
| 866.60008 | 4.74855 |
| 892.75709 | 4.99082 |
| 928.60353 | 5.36635 |
| 954.48976 | 5.69341 |
| 980.40981 | 6.04471 |
| 1006.7256 | 6.44446 |
| 1030.551 | 6.84421 |
| 1044.3176 | 7.14705 |
| 1056.533 | 7.97078 |
| 1053.4814 | 8.23728 |
| 1051.1929 | 8.30996 |
| 1048.7281 | 8.49167 |
| 996.96948 | 10.68424 |

**Table A.2.12 Test Data Column GCIV-3**

| Axial Load (kN) | Mid-height Deflection (mm) |
|---|---|
| 1.720623 | 0.009111 |
| 22.368099 | 0.118443 |
| 43.015575 | 0.227775 |
| 63.663051 | 0.337107 |
| 84.310527 | 0.446439 |
| 104.18126 | 0.555771 |
| 126.10691 | 0.692436 |
| 146.57085 | 0.81999 |
| 167.03479 | 0.947544 |
| 187.49873 | 1.09023 |
| 207.96267 | 1.25982 |
| 228.42661 | 1.42941 |
| 248.89055 | 1.599 |
| 269.35449 | 269.35449 |
| 289.81843 | 1.93818 |
| 310.28237 | 2.10777 |
| 330.74631 | 2.27737 |
| 351.21025 | 2.44696 |
| 371.67419 | 2.61655 |
| 414.86114 | 3.00418 |
| 433.5811 | 3.18589 |
| 453.68011 | 3.37971 |
| 473.39767 | 3.57353 |
| 493.46733 | 3.76734 |
| 514.50528 | 3.9975 |
| 535.02863 | 4.21555 |
| 555.37815 | 4.44571 |
| 576.73883 | 4.68798 |
| 597.14106 | 4.94237 |
| 617.89925 | 5.19675 |
| 637.61259 | 5.45114 |
| 657.17455 | 5.75398 |
| 676.12407 | 5.99626 |
| 696.96443 | 6.32332 |
| 716.51408 | 6.66251 |
| 736.71708 | 7.02592 |
| 758.04186 | 7.44989 |
| 778.36468 | 7.8981 |
| 798.08444 | 8.45533 |
| 809.36826 | 9.18215 |
| 795.31847 | 9.66669 |
| 770.21747 | 10.15124 |
| 741.87347 | 10.51465 |
| 725.85297 | 10.84171 |
| 699.97363 | 11.41106 |
| 669.16498 | 11.64122 |

# APPENDIX B LOAD-DEFLECTION GRAPHS

## B.1 Beams

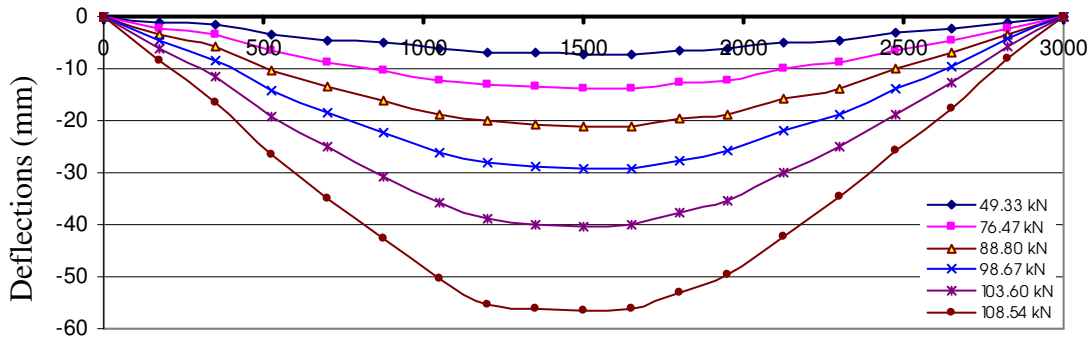


**Figure B.1.1 Beam Deflections along the Span (GBI-1)**

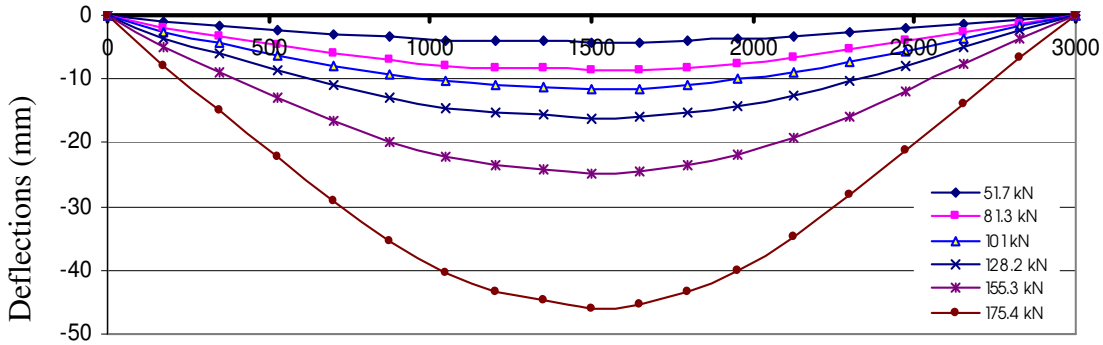


**Figure B.1.2 Beam Deflections along the Span (GBI-2)**

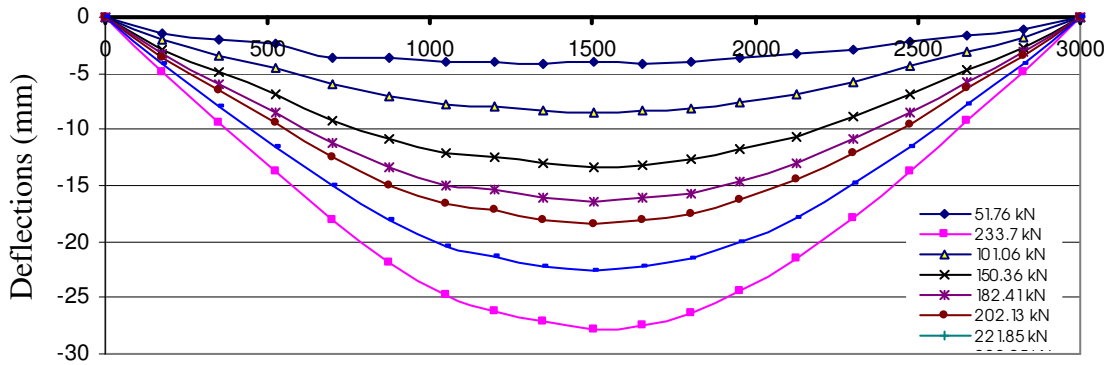


**Figure B.1.3 Beam Deflections along the Span (GBI-3)**

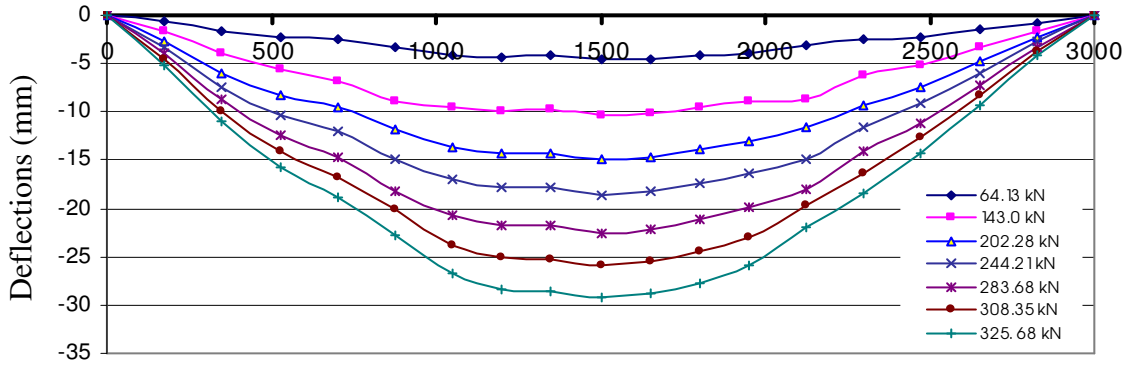


**Figure B.1.4 Beam Deflections along the Span (GBI-4)**

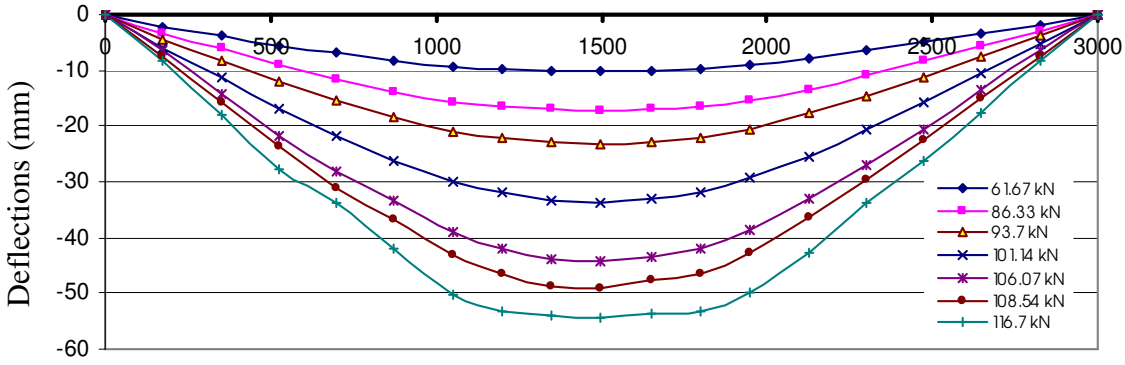


**Figure B.1.5 Beam Deflections along the Span (GBII-1)**

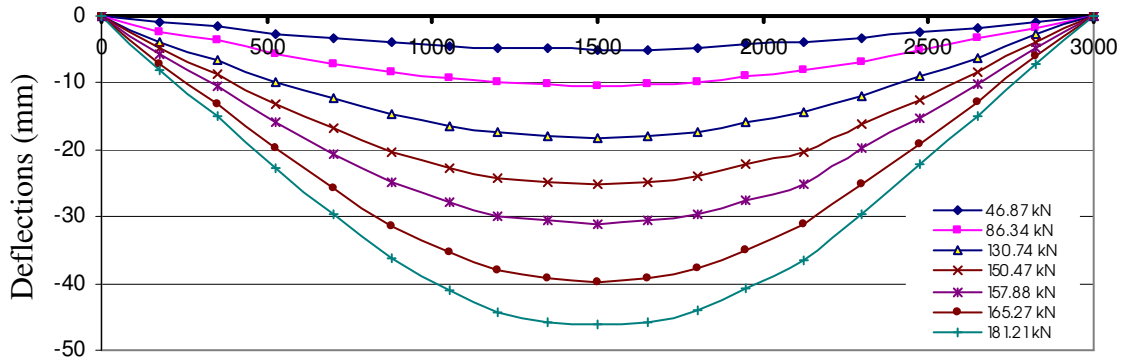


**Figure B.1.6 Beam Deflections along the Span (GBII-2)**

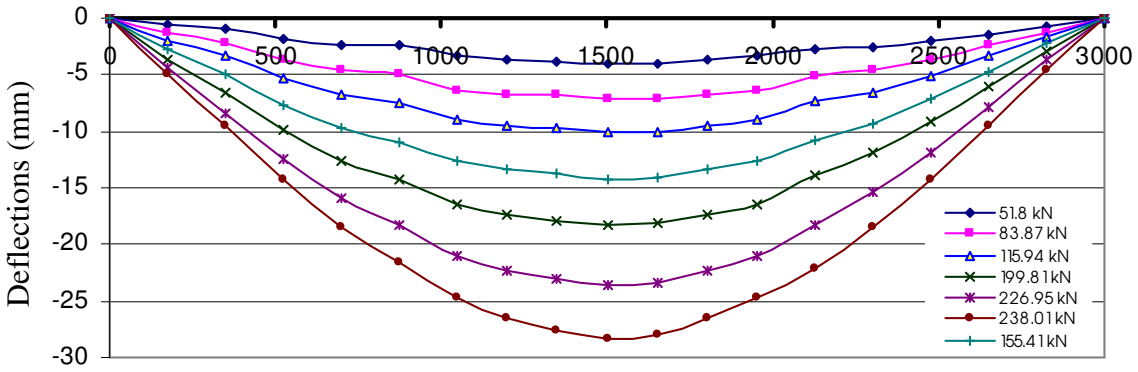


**Figure B.1.7 Beam Deflections along the Span (GBII-3)**

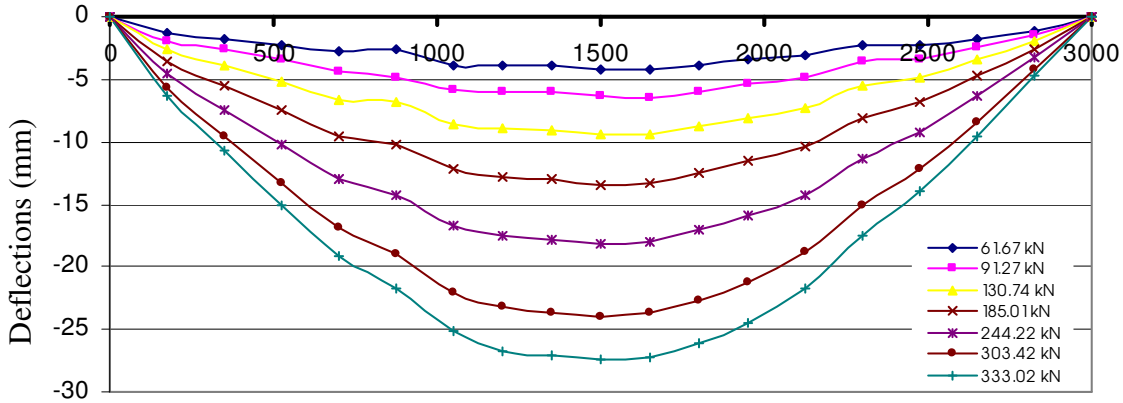


**Figure B.1.8 Beam Deflections along the Span (GBII-4)**

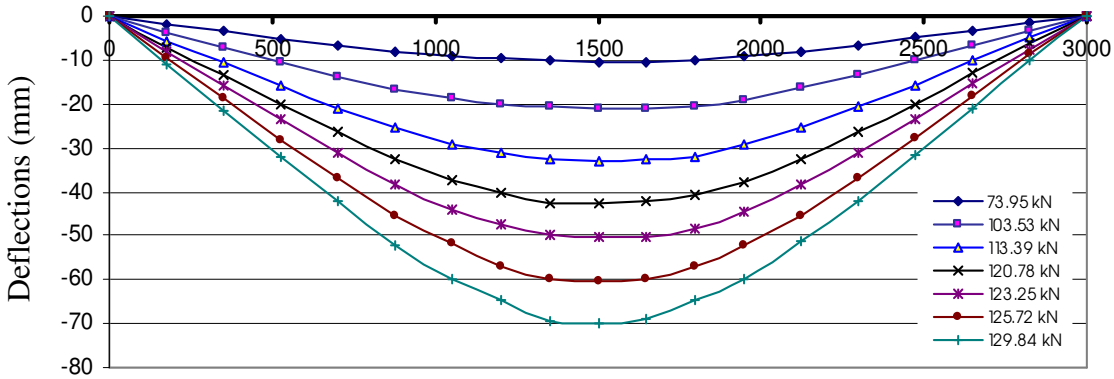


**Figure B.1.9 Beam Deflections along the Span (GBIII-1)**

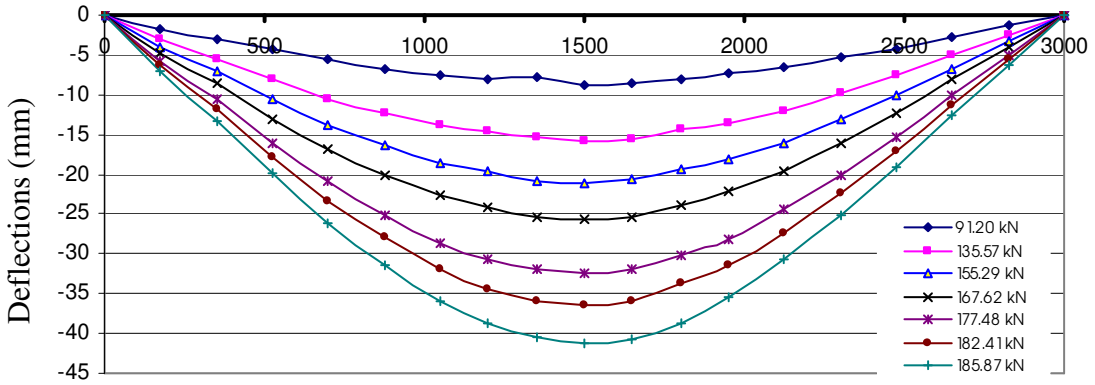


**Figure B.1.10 Beam Deflections along the Span (GBIII-2)**

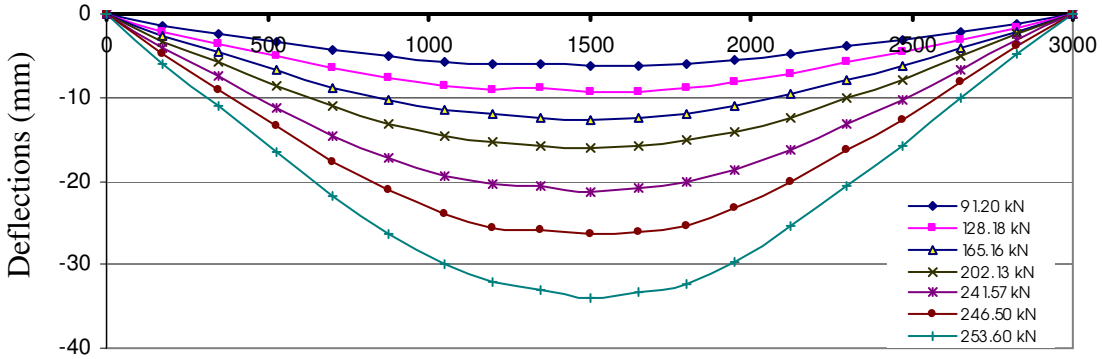


**Figure B.1.11 Beam Deflections along the Span (GBIII-3)**

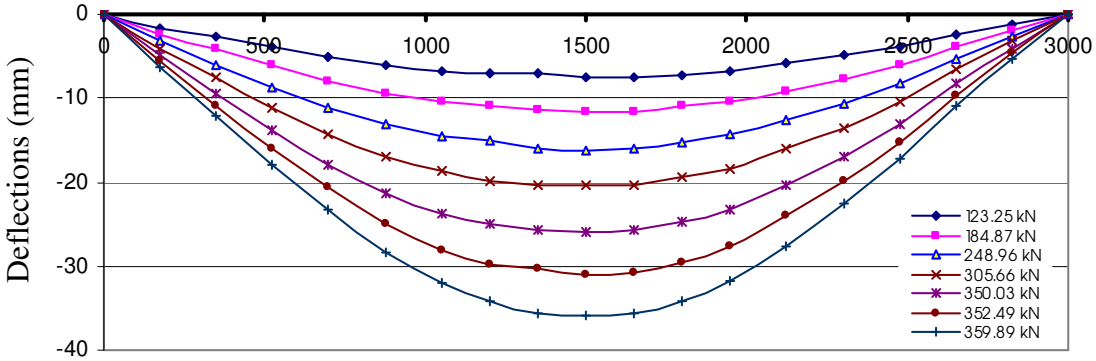


**Figure B.1.12 Beam Deflections along the Span (GBIII-4)**

## B.2 Columns

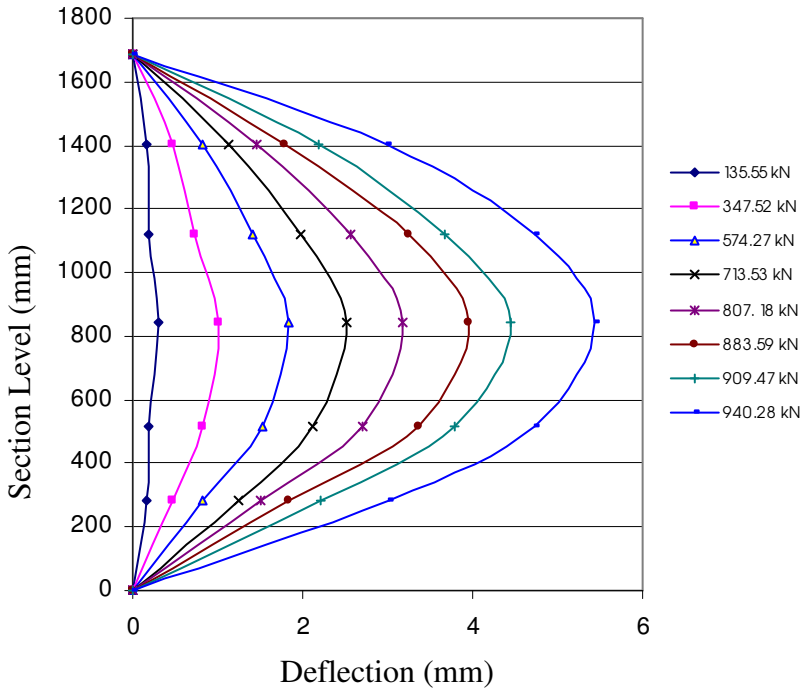


**Figure B.2.1 Deflected Shape of Column GCI-1**

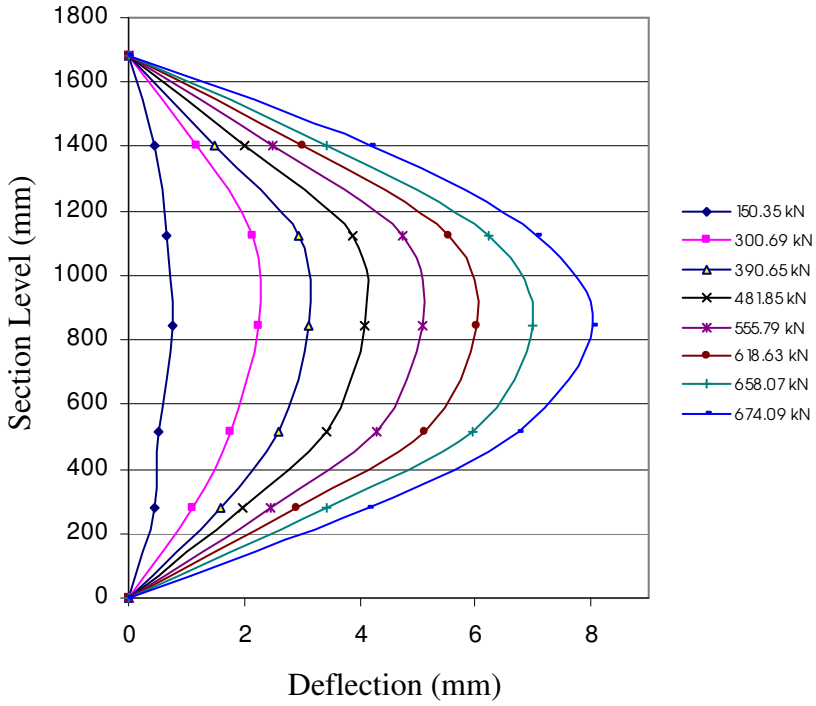


**Figure B.2.2 Deflected Shape of Column GCI-2**

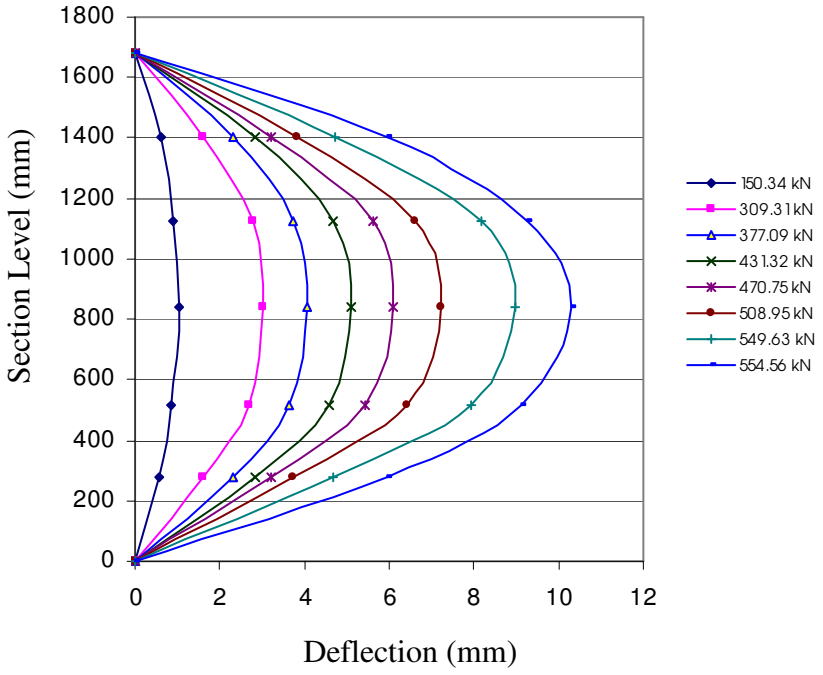


**Figure B.2.3 Deflected Shape of Column GCI-3**

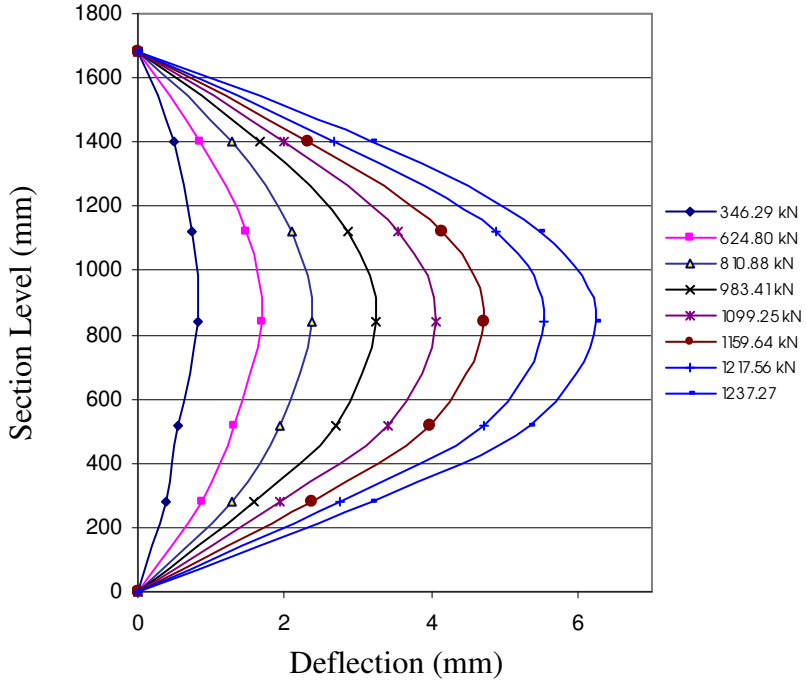


**Figure B.2.4 Deflected Shape of Column GCII-1**

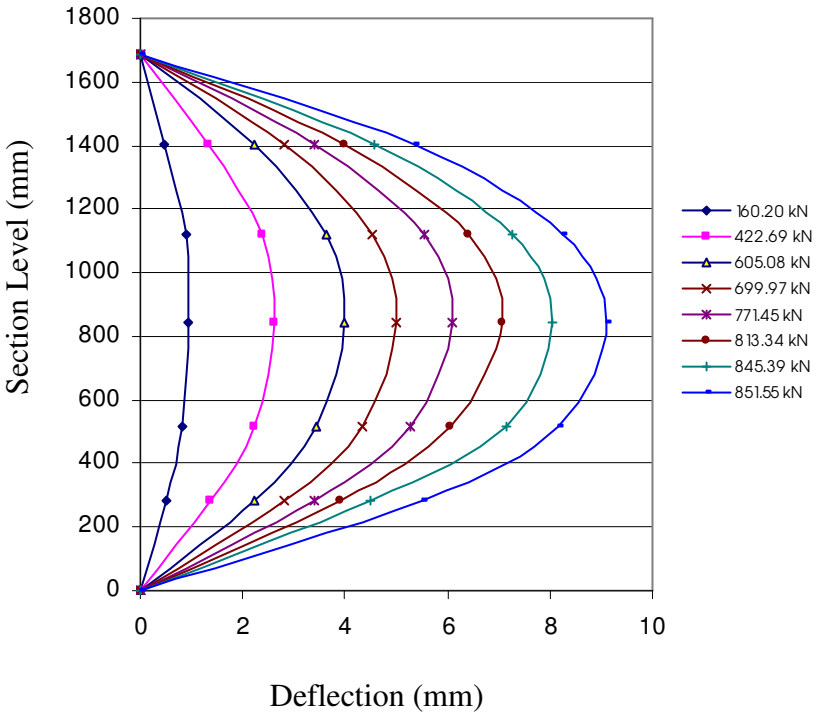


**Figure B.2.5 Deflected Shape of Column GCII-2**

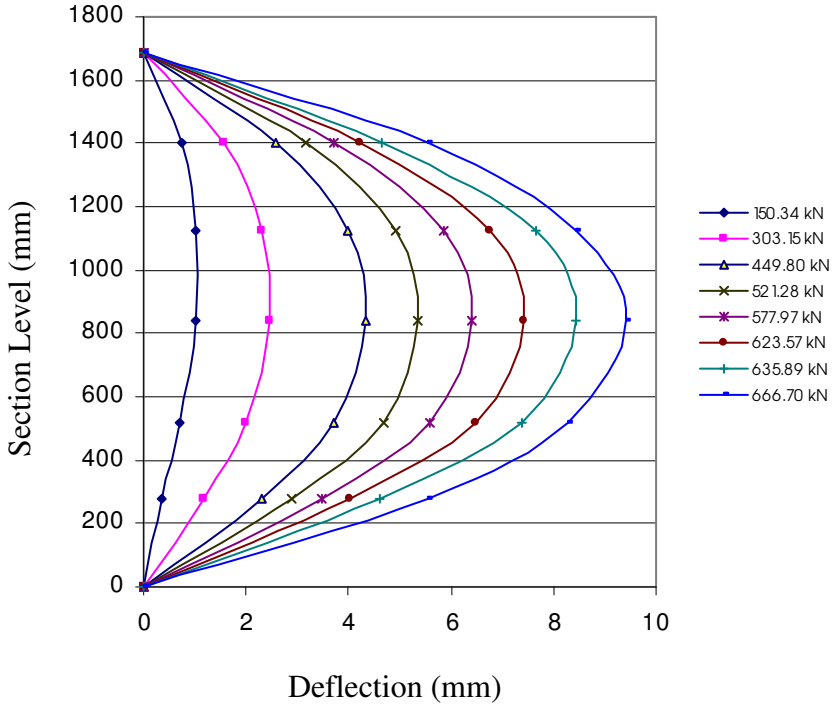


**Figure B.2.6 Deflected Shape of Column GCII-3**

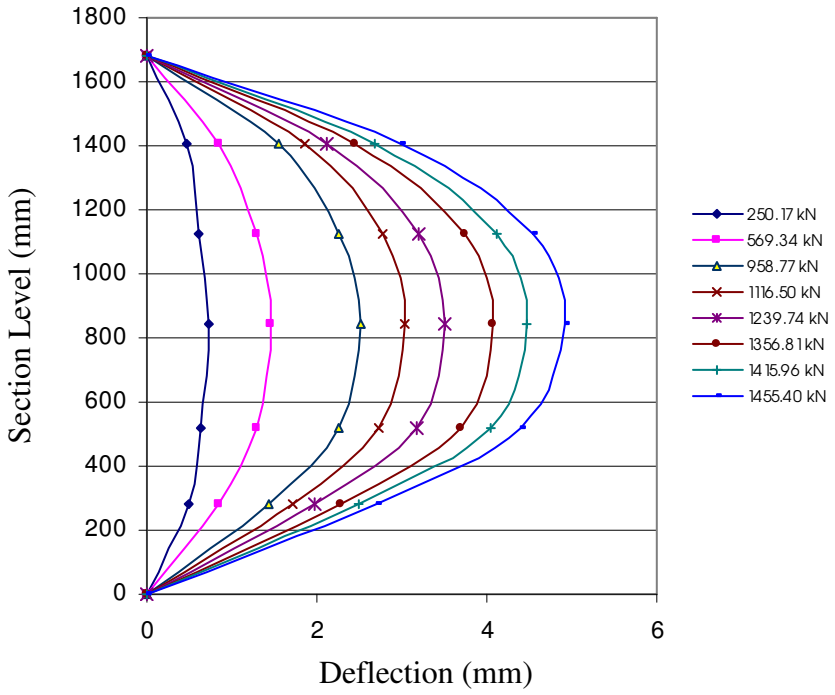


**Figure B.2.7 Deflected Shape of Column GCIII-1**

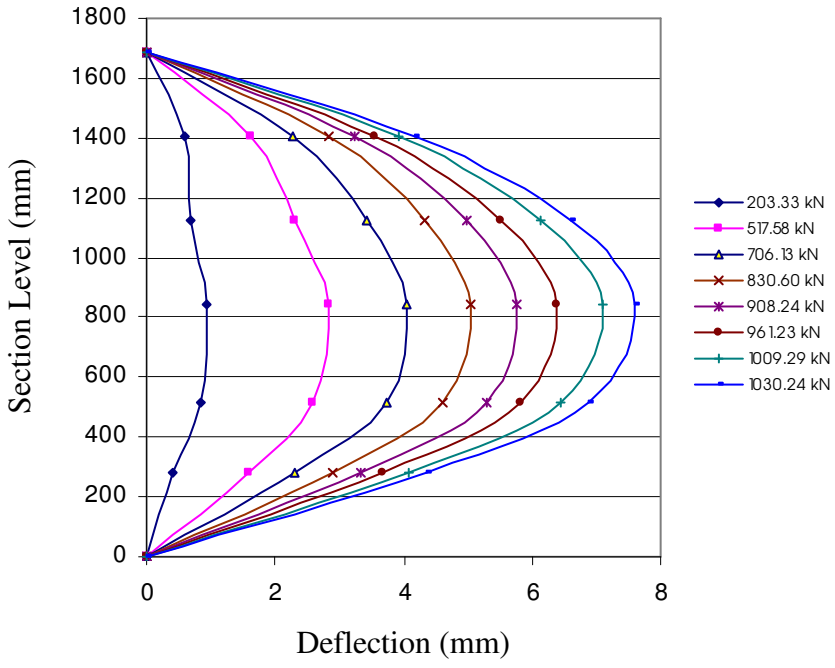


**Figure B.2.8 Deflected Shape of Column GCIII-2**

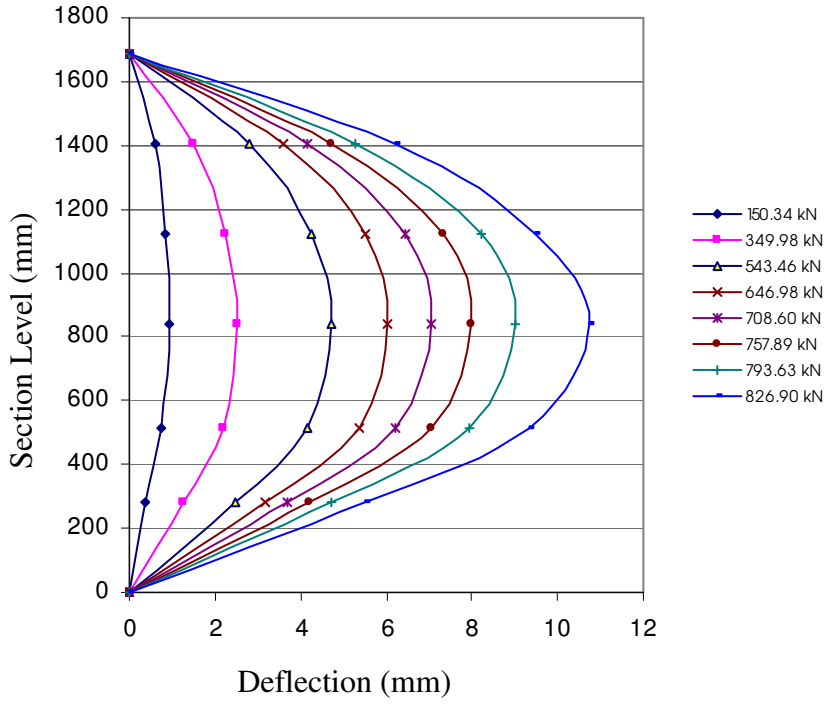


**Figure B.2.9 Deflected Shape of Column GCIII-3**

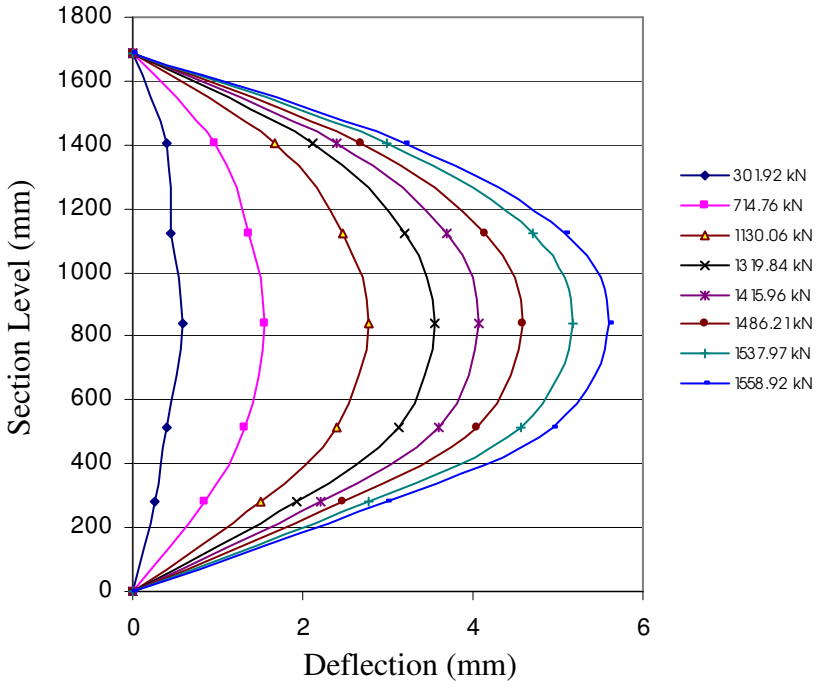


**Figure B.2.10 Deflected Shape of Column GCIV-1**

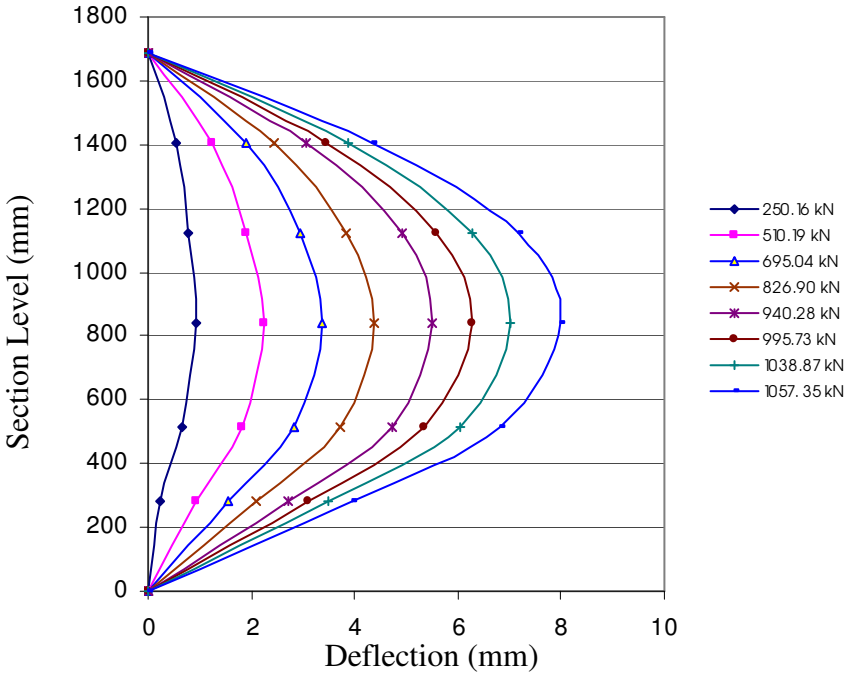


**Figure B.2.11 Deflected Shape of Column GCIV-2**

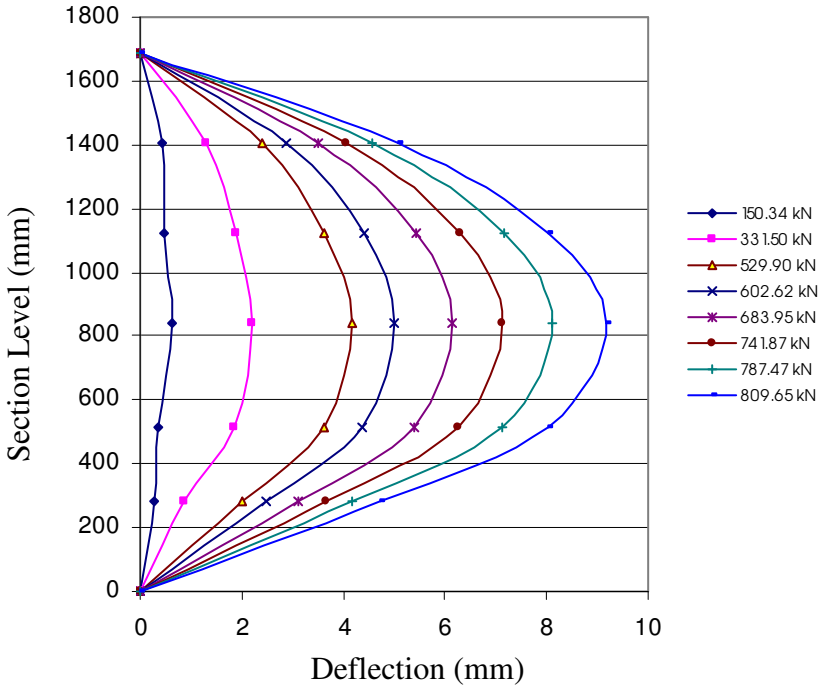


**Figure B.2.12 Deflected Shape of Column GCIV-3**

# APPENDIX C DATA USED IN CALCULATIONS

## C.1 Beams

### Table C.1.1 Beam Data

| Beam | ρ (%) | $A_{sc}$ ($mm^2$) | $A_{st}$ ($mm^2$) | $d_{sc}$ (mm) | $d_{st}$ (mm) | $f_{sy}$ (MPa) | $f_c'$ (MPa) | $E_c$ (GPa) | $\varepsilon_{cs}$ (mm/mm) x $10^{-6}$ | Modulus of Rupture (MPa) $f_r'=0.6\sqrt{f_c'}$ | Failure Load (kN) | Mid-span Deflection at Failure Load (mm) |
|---|---|---|---|---|---|---|---|---|---|---|---|---|
| 1 | 2 | 3 | 4 | 5 | 6 | 7 | 8 | 9 | 10 | 12 | 13 | 14 |
| GBI-1 | 0.64 | 226 | 339 | 43 | 257 | 550 | 37 | 21.0 | 62.5 | 3.65 | 112.6 | 56.63 |
| GBI-2 | 1.18 | 226 | 603 | 43 | 255 | 560 | 42 | 22.5 | 67.5 | 3.90 | 175.3 | 46.01 |
| GBI-3 | 1.84 | 226 | 942 | 43 | 253 | 560 | 42 | 22.5 | 67.5 | 3.90 | 233.7 | 27.87 |
| GBI-4 | 2.69 | 226 | 1356 | 43 | 251 | 557 | 37 | 21.0 | 62.5 | 3.65 | 325.0 | 29.22 |
| GBII-1 | 0.64 | 226 | 339 | 43 | 257 | 550 | 46 | 23.5 | 72.0 | 4.07 | 116.7 | 54.27 |
| GBII-2 | 1.18 | 226 | 603 | 43 | 255 | 560 | 53 | 24.4 | 79.0 | 4.37 | 181.1 | 47.20 |
| GBII-3 | 1.84 | 226 | 942 | 43 | 253 | 560 | 53 | 24.4 | 79.0 | 4.37 | 238.0 | 30.01 |
| GBII-4 | 2.69 | 226 | 1356 | 43 | 251 | 557 | 46 | 23.5 | 72.0 | 4.07 | 337.4 | 27.47 |
| GBIII-1 | 0.64 | 226 | 339 | 43 | 257 | 550 | 76 | 28.6 | 104.0 | 5.23 | 129.8 | 69.75 |
| GBIII-2 | 1.18 | 226 | 603 | 43 | 255 | 560 | 72 | 27.9 | 99.0 | 5.09 | 185.8 | 40.69 |
| GBIII-3 | 1.84 | 226 | 942 | 43 | 253 | 560 | 72 | 27.9 | 99.0 | 5.09 | 253.6 | 34.02 |
| GBIII-4 | 2.69 | 226 | 1356 | 43 | 251 | 557 | 76 | 28.6 | 104.0 | 5.23 | 359.89 | 35.85 |

*Note:*

*Column-9 : Modulus of Elasticity of concrete, $E_c$, was taken from Hardjito and Rangan (2005) measured data; Interpolation was made as necessary to suit the given compressive strength*

*Column-10 : Shrinkage strain, $\varepsilon_{cs}$, was taken from test data reported by Wallah and Rangan (2006); Interpolation was made as necessary*

## C.2 Columns

### Table C.2.1 Column Data

| **Column** | ρ (%) | **e (mm)** | **$A_{st}$= $A_{sc}$ ($mm^2$)** | **$d_{sc}$ (mm)** | **$d_{st}$ (mm)** | **$f_{sy}$ (MPa)** | **$f_c'$ (MPa)** | **Mid-height Deflection at Failure Load (mm)** | **Failure Load (kN)** |
|---|---|---|---|---|---|---|---|---|---|
| 1 | 2 | 3 | 4 | 5 | 6 | 7 | 8 | 10 | 11 |
| GCI-1 | 1.47 | 15 | 226 | 21 | 154 | 519 | 42 | 5.44 | 940 |
| GCI-2 | 1.47 | 35 | 226 | 21 | 154 | 519 | 42 | 8.02 | 674 |
| GCI-3 | 1.47 | 50 | 226 | 21 | 154 | 519 | 42 | 10.31 | 555 |
| GCII-1 | 2.95 | 15 | 339 | 21 | 154 | 519 | 43 | 6.24 | 1237 |
| GCII-2 | 2.95 | 35 | 339 | 21 | 154 | 519 | 43 | 9.08 | 852 |
| GCII-3 | 2.95 | 50 | 339 | 21 | 154 | 519 | 43 | 9.40 | 666 |
| GCIII-1 | 1.47 | 15 | 226 | 21 | 154 | 519 | 66 | 4.94 | 1455 |
| GCIII-2 | 1.47 | 35 | 226 | 21 | 154 | 519 | 66 | 7.59 | 1030 |
| GCIII-3 | 1.47 | 50 | 226 | 21 | 154 | 519 | 66 | 10.70 | 827 |
| GCIV-1 | 2.95 | 15 | 339 | 21 | 154 | 519 | 59 | 5.59 | 1559 |
| GCIV-2 | 2.95 | 35 | 339 | 21 | 154 | 519 | 59 | 7.97 | 1057 |
| GCIV-3 | 2.95 | 50 | 339 | 21 | 154 | 519 | 59 | 9.18 | 810 |